**GROWTH OF ALIGNED CARBON NANOTUBES ON COPPER SUBSTRATES**

by

**Gowtam Atthipalli**

B.E. (Hons.), Birla Institute of Science and Technology (India), 2005

M.S., University of Cincinnati, 2007

Submitted to the Graduate Faculty of

Swanson School of Engineering in partial fulfillment

of the requirements for the degree of

Doctor of Philosophy

University of Pittsburgh

2011

UNIVERSITY OF PITTSBURGH

SWANSON SCHOOL OF ENGINEERING

This dissertation was presented

by

Gowtam Atthipalli

It was defended on

August 19, 2011

and approved by

John A. Barnard, Ph.D., Professor, Department of Mechanical Engineering and
Materials Science

Jung-Kun Lee, Ph.D., Assistant Professor, Department of Mechanical Engineering and
Materials Science

Dr. Alexander Star, Ph.D., Assistant Professor, Department of Chemistry

Dr. Judith C. Yang, Ph.D., Professor, Department of Chemical and Petroleum
Engineering

Dissertation Director: Dr. Jennifer L. Gray, Ph.D., Assistant Professor, Department of

Mechanical Engineering and Materials Science

**GROWTH OF ALIGNED CARBON NANOTUBES ON COPPER SUBSTRATES**

Gowtam Atthipalli, PhD

University of Pittsburgh, 2011

Since the discovery of carbon nanotubes (CNTs) in the early 1990s, there has been enormous interest in trying to synthesize and understand their growth mechanism. This is required in order to successfully integrate them into new devices and applications that exploit their remarkable physical properties, including high mechanical strength, high aspect ratio, and excellent conductivity. Depending on the alignment of CNTs, random "spaghetti-like" or preferentially aligned CNTs on suitable substrates are of interest for potential applications such as energy storage, sensing, supercapacitors, and nanoelectronic devices via a variety of chemical vapor deposition (CVD) techniques such as thermal, plasma enhanced, water assisted growth. For many of the envisioned applications, dense, aligned CNTs grown using an economically viable technique and good contact with a conductive metallic substrate such as copper is required. The primary objective of the experiments described in this dissertation is to achieve vertical growth of carbon nanotubes on copper substrates using thermal CVD. The second goal is to understand and comprehensively determine how the processing conditions can be tailored to improve the density and degree of vertical alignment of the CNTs. The final goal is to measure properties to establish feasibility of use in device structures using aligned carbon nanotubes on copper. Since copper itself is not a good catalyst for carbon nanotube growth, the technique discusses the use of sputtered thin films of nickel or Inconel deposited on copper substrates with additional catalyst supply of iron from ferrocene decomposition during the CVD growth. Thus

the growth studies discussed in the dissertation includes the use of a combination of sputtered thin films and iron as catalysts on copper to promote the dense vertical growth of carbon nanotubes that is desired.

# TABLE OF CONTENTS

# LIST OF TABLES

# LIST OF FIGURES

**PREFACE**

I would first like to thank my dissertation advisor Dr. Jennifer L. Gray for giving me the opportunity to work with her research group over the last four years. It has been a real pleasure and privilege working with Dr. Gray during the course of my doctoral program. I sincerely appreciate all the advice, encouragement, support and the freedom to pursue and explore research from different vantage points. She also provided me with the opportunity to attend various conferences, present our work, which also allowed me to interact with experts and other workers in the field. These interactions later proved to be quite invaluable in problem solving as I carried out my research. The day to day interactions and the constructive feedback, be it the design of experiments, publishing or presenting work during the progression of my program were enjoyable and in the end proved to be very successful. It was a fulfilling experience as she was also my mentor in my capacity as a teaching assistant the last four years. I sincerely appreciate the time she was willing to spend to help me in completing my program in a timely fashion. The knowledge gained through collaborations with other highly respected research groups has been an insightful experience.

I would also like to acknowledge my committee members: Dr. Alexander Star, Dr. Jung-Kun Lee, Dr. Judith C. Yang, Dr. John Barnard, along with Dr. Prashant N. Kumta who have helped in the form of collaborations and/or lending their profound technical expertise on the subject. I am also grateful to a number of people who have assisted me in the completion of the

project, including Dr. Susheng Tan, Albert Stewart, Michael L. McDonald, Cole Van Ormer, RJ Lee Group Inc.

Finally, I would like to thank my family and friends, as they have been supportive in my interest and pursuit of an advanced degree. I consider myself quite fortunate to have found wonderful friends both within and outside the University of Pittsburgh who have helped in various ways, professional and otherwise. These include my co-workers Rigved Epur, Samuel D. Stranks, Florian Nitze, Yifan Tang, Dr. Brett L. Allen, Hao Wang, Mengjin Yang, Bo Ding, Dave Perello, Yannick Heintz, Dr. Harindra Vedala and Dr. Cary L. Pint. A special note of thanks to Heather Meloy-Gorr, Korrinn Strunk, Kai Zweiacker, Robby Armstrong, Tommy Liakos, Oleg Butov for the delightful interactions and keeping my sanity intact as I successfully finish my doctoral work.

# 1.0     INTRODUCTION

There has been tremendous interest in trying to synthesize and understand the growth of carbon nanotubes over the last two decades after the landmark publication by Iijima[1] in 1991 that brought CNTs into the forefront of nanotechnology studies. The fundamental understanding of CNT growth and synthesis is required in order to successfully integrate them into new devices and applications that exploit their excellent physical properties, high aspect ratio, and range of conductivity[2,3].

There have been extensive publications in recent years to demonstrate the growth of nanotubes under different growth conditions on a variety of substrates[4-10] for a number of applications such as field emitters[4,11], high surface area electrodes[12], transistor and logic circuits[13], sensors[14-17]. However for device applications where the nanotubes serve as electrical conductors, direct carbon nanotube growth on a conducting substrate is preferred. For use in applications such as electrodes, where the nanotubes might serve as an electrically conducting array or conducting support structure, vertically aligned CNT growth directly on a common conducting substrate such as copper would be ideal. CNTs are classified into random "spaghetti"[18,19] type CNTs and aligned CNTs, similar to the bristles of a hairbrush on the basis of orientation of the nanotubes with respect to the substrate.  Schematics of the two types of CNTs are shown in figure 1.1.
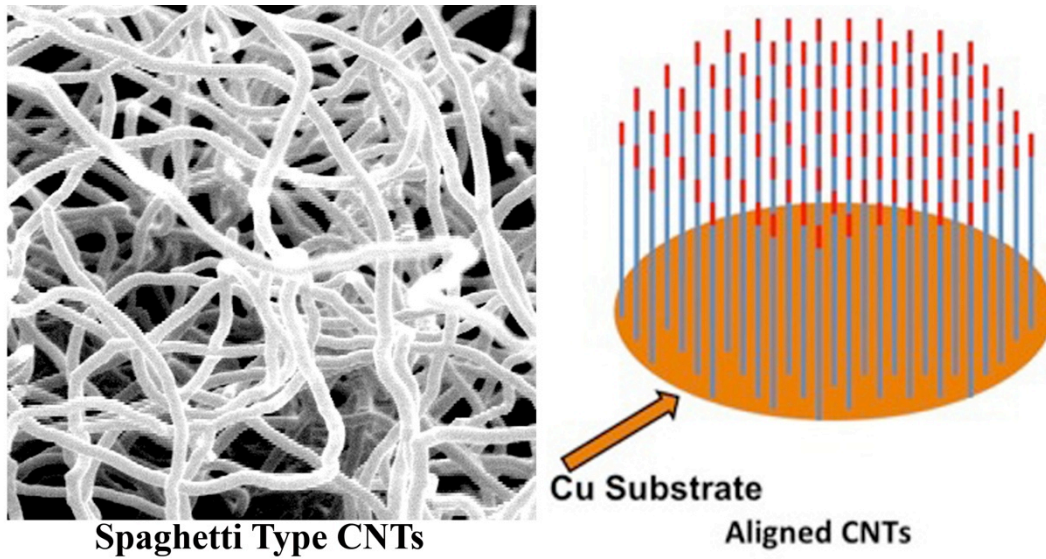
Figure 1.1: Schematics of randomly oriented "spaghetti" type CNTs and vertically aligned CNTs on copper substrates.

For the envisaged application of energy storage, suitable structures with high quality, aligned CNT-metal contacts are required. Aligned CNTs are advantageous over random CNTs, in that the number of CNTs that can be packed per unit area of the substrate with access to the conductive surface area of CNTs is substantially large. The availability of surface area of the CNTs will ultimately dictate the amount of charge that can be stored. Thus the motivation to pursue the goal of achieving aligned CNTs on copper is twofold. The first is to understand the scientific aspects of aligned CNT growth mechanisms and utilize the as grown CNT-Cu system for engineering applications such as energy storage.

**Goals**

✓ Try to achieve vertical growth of carbon nanotubes (CNTs) on copper substrates by exploring the use of transition metal catalysts as a mechanism for supporting nanotube growth on copper. Attempt to understand how the catalyst changes the substrate morphology and leads to the resulting nanotube network that in turn influences the electrical properties.

✓ Understand the effect of native oxides of copper on CNT growth, surface roughness, diffusion and solubility issues of the metal catalysts and carbon during the growth process.

✓ Understand and determine how the processing conditions (thermal CVD) improve the density and degree of vertical alignment of the CNTs.

**Engineering**

➢ Test the CNT-Cu system for prospective charge storage applications such as double layer capacitors in an effort to improve the charge storage capacity.

Thus the primary objective of the experiments described in this dissertation is to achieve vertical growth of carbon nanotubes on copper substrates using thermal chemical vapor deposition. The second goal is to understand and comprehensively determine how the processing conditions can be tailored to improve the density and degree of vertical alignment of

the CNTs. The final goal is to engineer aligned carbon nanotubes on copper for energy storage applications.

## 1.1     GROWTH AND PROPERTIES OF CNTS

Carbon nanotubes may be broadly classified into single walled carbon nanotubes (SWCNTs) and multiwalled carbon nanotubes (MWCNTs) based on their structure. Some of the important factors that help in determining whether the nanotubes will be single walled or multiwalled are the size of the catalyst and the carbon supply during the CVD growth process. Larger sized catalyst particles[20] with a greater supply of carbon[21] tend to form MWCNTs where the CNT growth is primarily driven by the bulk diffusion of carbon into the catalyst particle. The catalyst particle (typically a transition metal such as Fe, Co or Ni) has a solubility limit at the growth temperatures. Once the solubility limit is reached, the excessive carbon simply precipitates out as graphitic cylindrical tube[22]. For SWCNT growth, Hafner et al.[21] and Dai et al.[23] have proposed mechanism that is primarily driven by the large difference in the surface energies of the basal graphite plane and the surface of the metal catalyst. The basal plane of graphite has surface energy that is 10-20 times smaller than the typical metal catalysts (Fe, Co or Ni) used for SWCNT growth. Here the rate-limiting step is the amount of carbon supply during the growth process. Dai et al.[23] termed this type of SWCNT growth as the "yarmulke" mechanism that begins formation of the first graphene cap with extremely low surface energy on a much higher surface energy metal catalyst. The electronic properties (metallic or semiconducting nature) of SWCNTs and MWCNTs are determined by an array of factors such as chirality, diameter of CNTs and the wrapping vectors that have been reported by Wilder et al.[24] .

CNTs are grown using a variety of techniques of which the most common ones are arc discharge[25], laser ablation[26] and chemical vapor deposition[27,28]. The two major CVD techniques that have been widely used to grow CNTs are thermal CVD and plasma enhanced CVD (PECVD) [29]. There are inherent advantages to both the techniques. PECVD uses electric fields that are widely known to aid in the alignment of CNTs during the growth process. Bower et al.[30] have proposed that the alignment of CNTs is primarily due to the electric field bias imposed on the substrate surface by the microwave-induced plasma during PECVD growth. They concluded, that regardless of the orientation of the substrate, the electrostatic force causes CNTs to grow in a direction perpendicular to the substrate and align with the direction of the applied field for the most thermodynamically stable configuration[31]. The disadvantages with the use of PECVD are the inferior quality and limitation on the length of CNTs that can be produced[32]. In addition, the initial equipment cost is a prohibitive factor in using PECVD for commercial CNT production.

Thermal CVDs are essentially furnaces that are very economical from a financial standpoint (despite the lack of electric fields) and stand the best chance of being used for large scale CNT production. The alignment in CNTs using thermal CVD is mainly due to van der Waals interactions between growing nanotubes and steric hindrance between neighboring CNTs[30]. These types of interactional constraints that induce vertical orientation in thermal CVD can only be forced upon by increasing the catalyst density on the substrate, in other words promote the "crowding" effect[33]. Both the CVD techniques have been used to demonstrate CNT growth using metal thin films that are deposited on top of a semiconducting or insulating substrate such as $SiO_2/Si$ and aluminum oxide[4,34-37]. These low surface energy, non-conducting substrates facilitate the formation of small islands or nanoparticles of the catalyst metal on their

surfaces, which are necessary for the formation of the CNTs. The growth of aligned CNTs using thermal CVD on conductive substrates still remains a challenge.

In theory, CNT growth using thin films and thermal CVD involves three relatively simple steps: deposition of thin films on suitable substrates (Cu for example), heating the as deposited film in a furnace (CVD chamber) to the desired growth temperature which causes the film to break up islands. Each island then serves as a nucleation site for CNT growth (figure 1.2). The precise CNT growth mechanism via thermal CVD remains an issue of considerable debate however studies[4,35,38-41] have shown that CNT growth involves three principal stages: dewetting of a higher surface energy catalyst film on a relatively low surface energy substrate to produce catalytically active nanoparticles, reduction of the nanoparticles, and nucleation and growth of the CNTs. To satisfy these broad based conditions, typically high surface energy catalyst metal films such as Fe, Co, Ni and their alloys[42,43] are grown on low surface energy substrates like $Si/SiO_2$[4] or quartz[44] that leads to the breakup of the film into islands or nanoparticles on annealing at the CNT growth temperature. Thermal CVD is carried out by flowing hydrogen gas that ensures the presence of a reducing atmosphere during CNT growth.
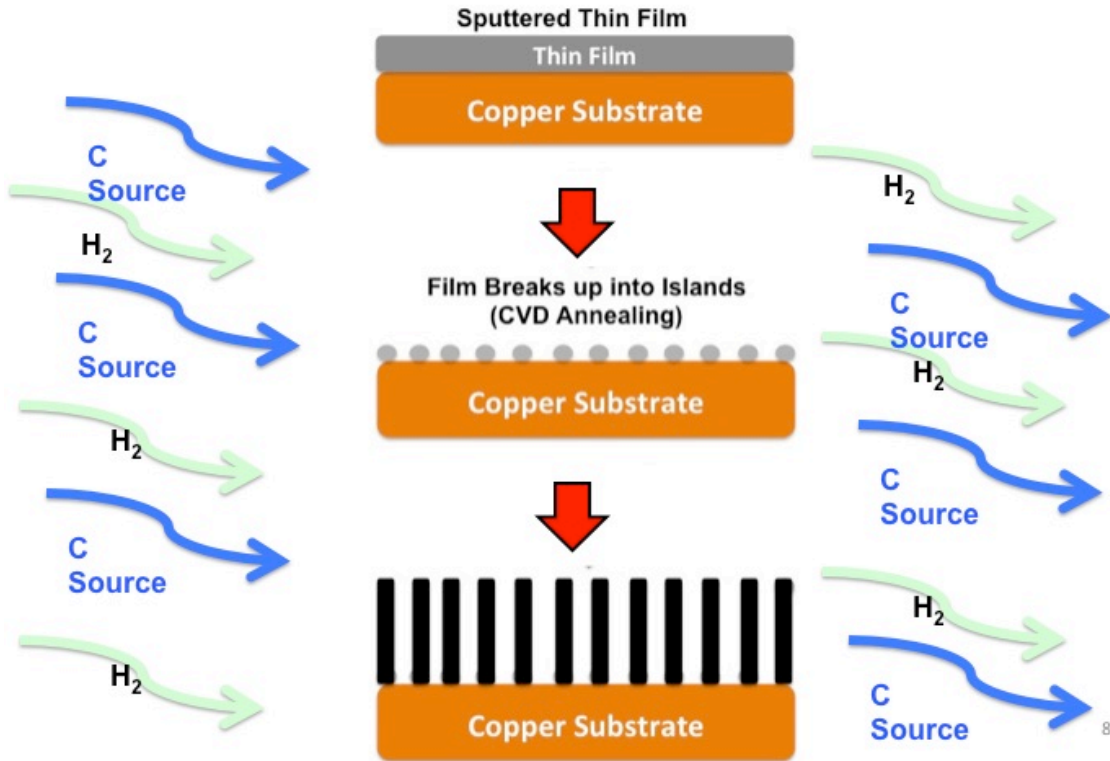
Figure 1.2: Sequence of steps involved in the growth of CNTs using metallic thin films. The sputtered film breaks up into islands on heating and each island acts as a nucleation site for growth.

## 1.2　　GROWTH OF CNTS ON BULK METALS OR ALLOY SUBSTRATES

Research groups have reported the growth of aligned MWCNTs on bulk metallic/alloy substrates such as Inconel [45-47] but there is very little research data available in growing aligned CNTs directly on bulk copper without the use of barrier layers that affect the overall electrical properties of the system. Copper is a poor catalyst for CNT growth as carbon shows very little solubility in copper[43,48]. Although it has been demonstrated that Cu nanoparticles may act as a catalyst for random carbon nanotube growth[49,50], it is difficult to grow CNTs directly on bulk Cu without the aid of an additional catalyst. Deck and Vecchio[48] have reported that for transition metals to act as successful catalysts for multiwalled CNT growth about 1 wt % carbon solubility in the solid solution is required. The solid-state solubility requires the carbon (released from dehydrogenation of hydrocarbons, typically used as carbon feedstocks) to form metastable carbides. The three metals that have been widely studied and shown to catalyze CNT growth are Co, Ni, Fe [51-54]. Following the solid-state solubility in carbon hypothesis, by Deck and Vecchio[48], phase diagrams of the ferromagnetic metals and carbon are shown in figure 1.3. These phase diagrams determine the likely advantages for Fe, Co and Ni as potential catalysts for the CNT growth in the temperature range of 750˚ C -1000˚ C. The other reasons for poor CNT growth on copper could also be attributed to diffusion of the metal catalyst into the substrate and heterogeneous nucleation[45] resulting from the surface roughness of commercially available metallic substrates.
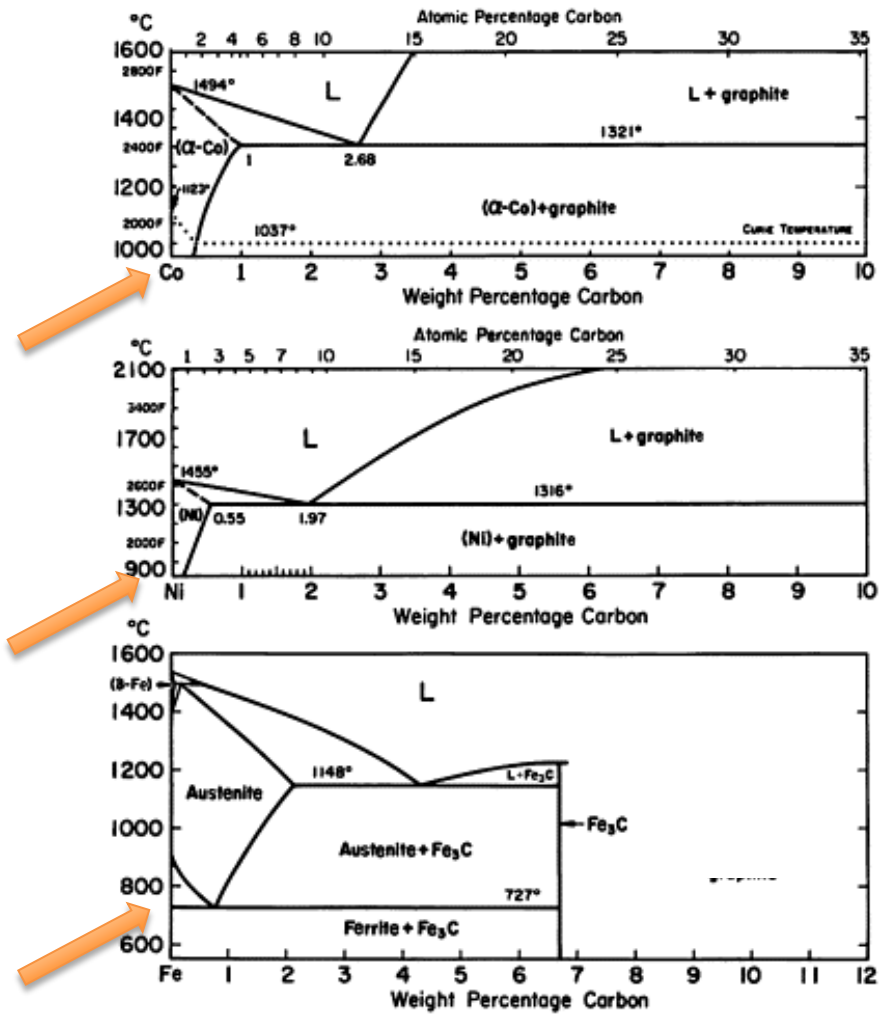
Figure 1.3: Phase diagrams of Co-C, Ni-C and Fe-C. The arrows indicate the solid state solubility of the metals in carbon at the suitable CNT growth temperatures. (Metallography, structures and phase diagrams, American Society for Metals, Metals Park, OH (1973)

In order to achieve growth of CNTs on copper, some success has been achieved by first depositing barrier layers such as TiN, $Al_2O_3$, Ni, Ta on the copper followed by catalyst layers before the nanotube growth. The most recent studies on the growth of aligned MWCNTs (figure 1.4) on copper, using a thermal CVD technique were reported by Li et al.[45]. Their technique consisted of multiple barrier layers: an intermediate Ti buffer layer, an alumina layer (15nm) (to improve catalyst density), and finally a metal catalyst layer (2 nm). Other workers[55] have used a multilayer structure consisting of titanium nitride as a barrier layer and a second layer of iron as the catalyst. However, the presence of such barrier layers could contribute to an undesirable increase in the overall resistance of the CNT-metal system at the interface for potential applications as charge storage and for interconnects.
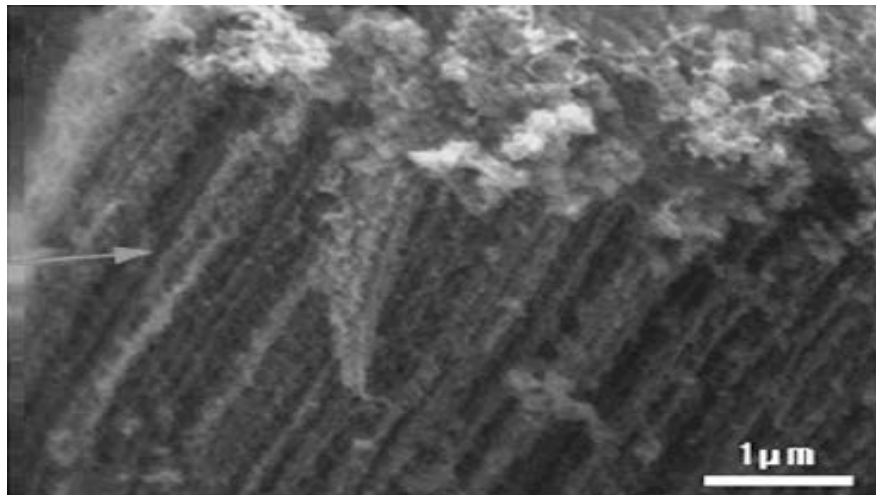


Figure 1.4: MWCNTs on copper using multiple layers of Ti, alumina and iron catalyst[13].

Related reports in the area include a report by Wang et al. [56] who have also demonstrated the growth of CNTs on copper by using a layer of chromium (12nm) for adhesion) and gold (20 nm) as catalyst via water assisted CVD. In this case, the addition of chromium as barrier layer and the high cost of gold are detrimental to replicating the technique on an industrial scale. The thermal resistance of the CNT-Cr-Au-CNT system was reported to be 12 $mm^2$K/W under 0.3 MPa pressure.

A number of researchers have also reported CNT growth on other conductive substrates such as stainless steel. Soneda and Makino[8] reported random CNT growth on stainless steel substrates, grown using a mix of CO gas and hydrogen in a furnace at ~ 80 kPa. Park et al.[9] have reported the growth of aligned CNTs on stainless steel using a combination of PECVD for catalyst pretreatment and thermal CVD for CNT growth. They also reported specific capacitance results in the range of 30-80 $Fg^{-1}$. In the two techniques reported on stainless steel, the lack of alignment and the use of two stage CVD procedures remain big disadvantages for potential large-scale CNT growth.

## 1.3     APPLICATIONS OF THE CNT-CU SYSTEM FOR CHARGE STORAGE (CAPACITORS)

The ballistic mechanism of electrical conduction in CNTs due to their one-dimensional nature with large aspect ratios permit high current densities, three orders of magnitude higher than copper[57,58]. Aligned MWCNTs on conductive substrates are typically attractive for

electrochemical devices due to the availability of high surface area of the porous nanotube structures[59,60]. This property combined with their high mechanical strength makes CNTs ideal for use in electrochemical charge injection via the double layer arrangement. The envisioned mechanism for charge storage on an aligned mat of CNTs is shown as a schematic in figure 1.5. The surface charge storage mechanism in the absence of Faradic reactions (typical in batteries) allows for an extremely fast energy uptake and delivery.
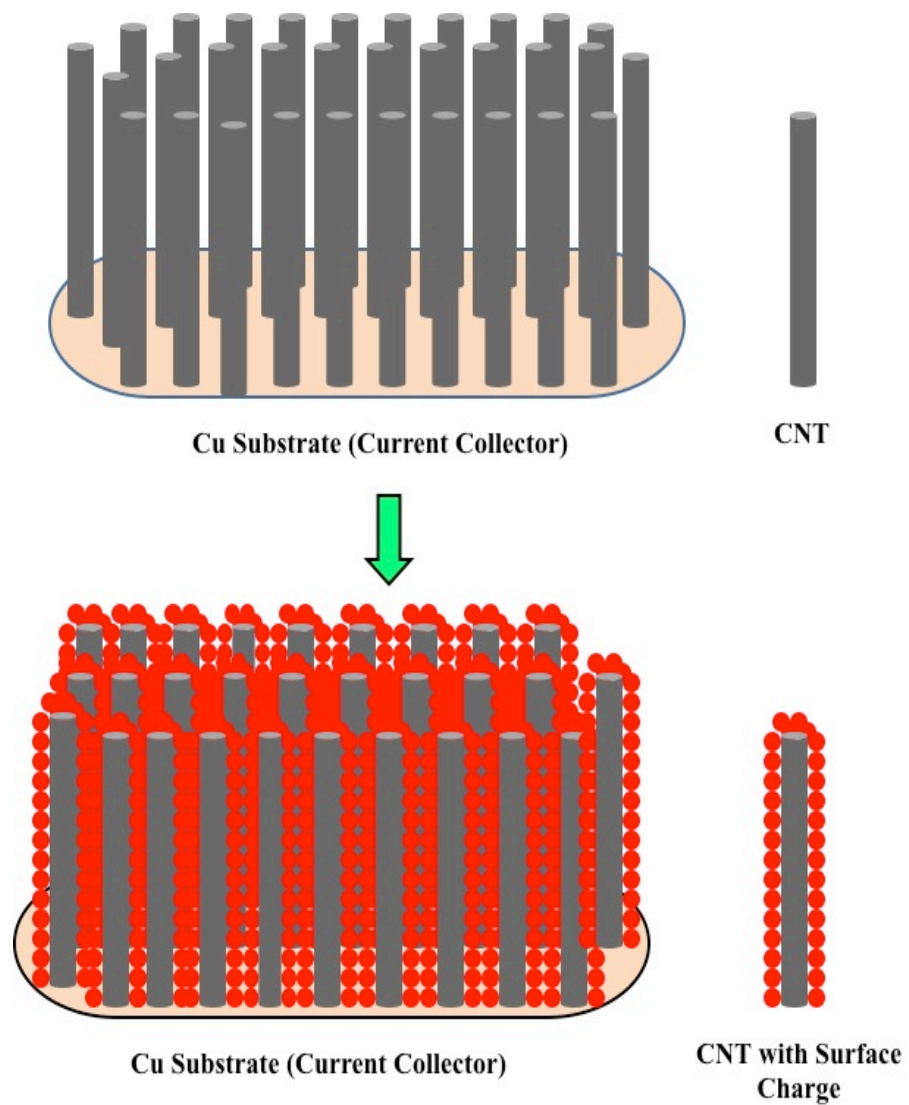
Figure 1.5: Schematic of the basic mechanism of charge storage in aligned CNTs on a conductive current collector.

There have been a number of reports in recent years that have demonstrated the use of CNTs as electrical double layer capacitors (DLCs) with reported specific capacitances and power densities ranging from about 20-200 Fg$^{-1}$ and 5-20 kWkg$^{-1}$ [7,61,62] respectively. One of the major drawbacks in the mechanisms reported is the basic construction of a DLC. DLC assembly using CNTs typically involves initial CNT growth on non-conductive substrates such as quartz. The CNT electrodes are then scraped off and mixed with a binder and a solvent. The resulting slurry is then coated on a Cu foil, which is then tested for capacitance (figure 1.6). The problem with this technique is, once the solvent evaporates, the binder is left behind that drastically affects the composition of the CNT surface. The growth of CNTs directly on copper substrates eliminates the use of binders that affect the overall surface morphology of CNTs and hence the charge storage capability[47,63].
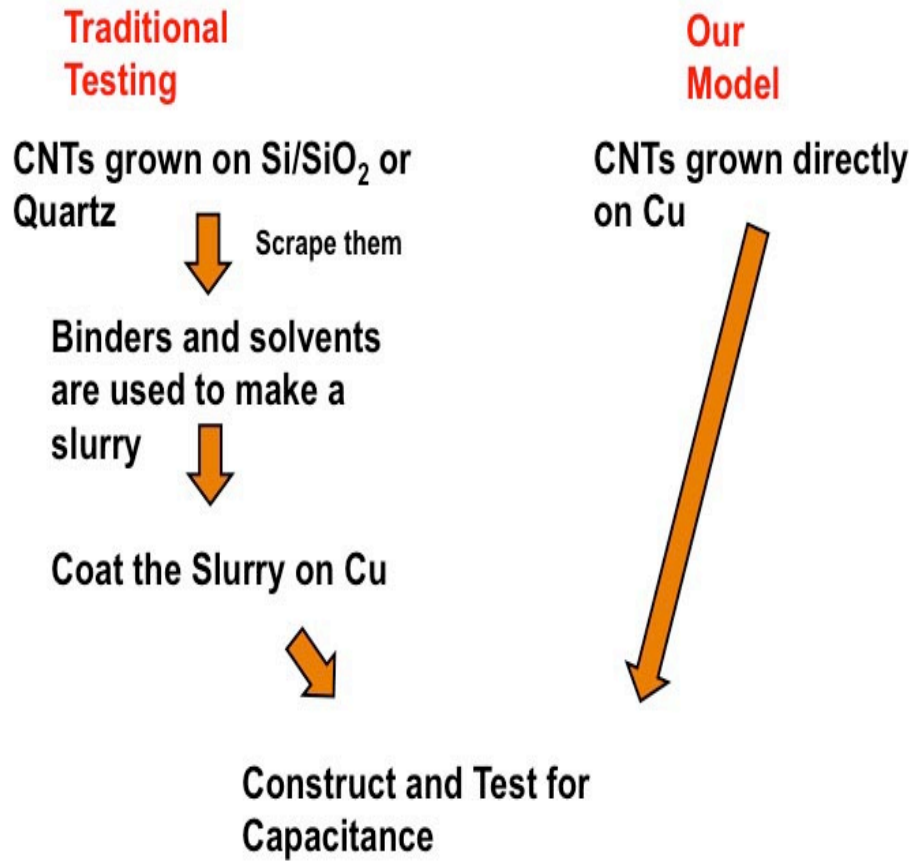
Figure 1.6: Flowchart indicating the advantages of capacitance testing of CNTs grown directly on copper substrates compared to traditional techniques.

## 1.4    EXPERIMENTAL GOALS

In the experiments described in the dissertation, the goal was to find thermal CVD growth conditions under which a single thin film catalyst layer could be used to promote the vertical growth of dense nanotubes on copper substrates. The metallic catalyst nickel and its alloy Inconel were specifically chosen for the experiments described here due to their demonstrated superior capabilities for attaining directed carbon nanotube growth [42,43,55]. Two approaches are used to identify the most suitable conditions for CNT growth. In the first approach, the metal (nickel) thin film serves directly as the primary catalyst for CNT growth (figure 1.7).  In the second method, an additional vapor delivered catalyst (iron from ferrocene decomposition) is supplied during the actual CVD growth (figure 1.8a). This additional supply of catalyst in combination with the thin film is used in order to promote the dense vertical growth of carbon nanotubes that is desired. In the studies conducted, the use of a thin catalyst layer, 60 nm or less, deposited on copper substrates and then exposed to different CVD reaction conditions for growth of nanotubes was explored. Our studies also include the effect of native copper oxide layer and the influence of surface roughness of the copper substrates on the growth of nanotubes. In order to achieve direct CNT growth on pristine, atomically smooth copper surface, Si wafers were used as support substrates. Figure 1.8b summarizes the second approach used in the experiments discussed.
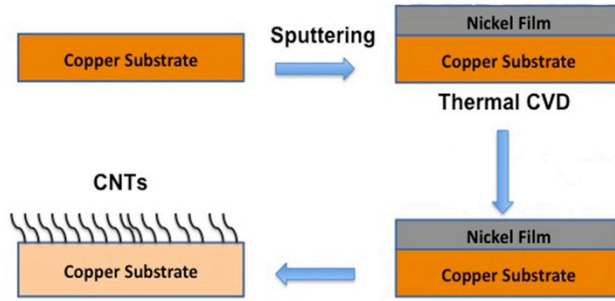
Figure 1.7: Sequence of operations for CNT growth using just a thin film catalyst (no ferrocene)
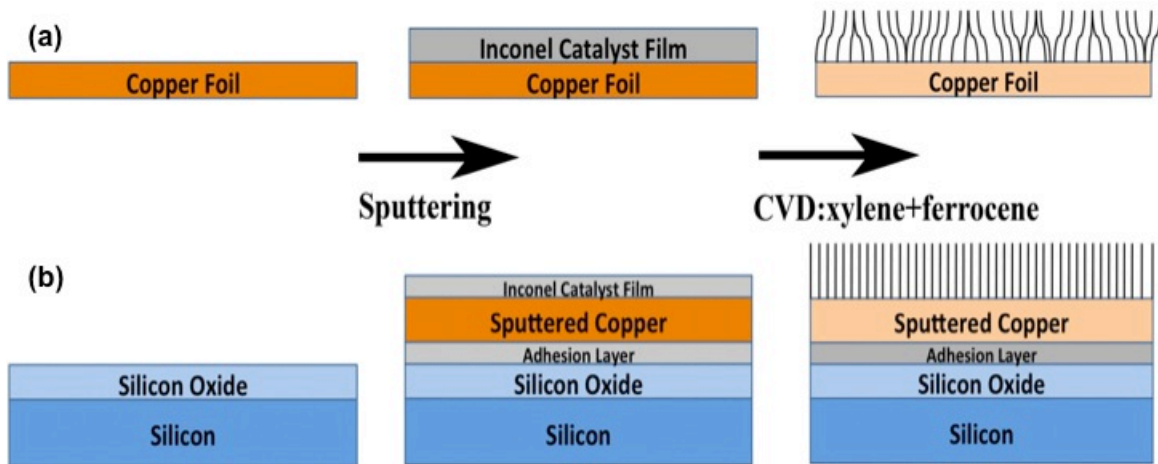


Figure 1.8: Schematic of the general sequence of operations-sputtering and thermal CVD (with ferrocene) for CNT growth on (a) the oxidized copper foil (b) oxide free sputtered copper.

17

Reported studies include the growth of vertically aligned CNTs on bulk copper using a cost effective thermal CVD technique without the aid of any intermediate barrier layers that might otherwise affect the overall thermal/electrical properties of the CNT-metal contact. The aligned CNTs on the conductive copper substrates were then tested as double layer capacitors. The power densities and the specific capacitance values of the CNTs grown using this technique are also reported.

In the context of aligned CNT growth on copper substrates using transition metal catalysts via thermal CVD technique, the following growth and synthesis parameters were optimized to achieve the desired goal:

- Catalyst thin film: the kind of transition metal or alloy catalyst to be used (nickel, Inconel)
- Catalyst film thickness (5 to 60 nm)
- Copper substrate morphology: surface roughness and native oxide layer
- The type of carbon feedstock (methane, acetylene, xylene)
- CNT growth time and temperature (30 – 90 minutes, 650 °C – 900 °C)
- Quality of the CNTs grown ($I_d/I_g$ ratios: 0.6-1.9)
- Qualitative alignment of the CNTs with respect to the substrate
- Electrochemical testing for maximum power density and specific capacitance values (2.5 - 12 $kWkg^{-1}$, and 20-80 $Fg^{-1}$)

## 2.0    EXPERIMENTAL TECHNIQUES

## 2.1    PHYSICAL VAPOR DEPOSITION (SPUTTERING)

Sputtering is a physical vapor deposition process used for depositing thin films of metals, alloys, semiconductors and dielectric materials in a vacuum environment. A basic sputtering system consists of an evacuated chamber with a pair of metallic electrodes. The cathode is usually the target (source) and is connected to the negative terminal of a DC power supply. On the opposite side of the cathode is the substrate, which acts as the anode. The anode could be grounded, biased negative/positive, heated or a combination of all these processes. Vacuum pumps are used to evacuate the chamber and a working gas which is typically a noble gas (argon, neon) is used to initiate a self-sustaining plasma in the presence of an electrical discharge. The gas pressure range to "strike" the plasma ranges from a few to a few hundred millitorr[64,65].

The basic mechanism of deposition in conventional sputtering happens when positively charged inert gas atoms from the plasma sputter or physically remove atoms from the target through momentum transfer, hence sputtering falls under the category of physical vapor deposition. The atoms that have been ejected from the target enter the plasma discharge region to eventually deposit onto the substrate. During the process of sputtering, other particles such as secondary electrons, negative ions, as well as radiation such as x-rays are also emitted from the

target. The secondary electrons in turn, help in increasing the ionization of neutral argon atoms (in the plasma) that take part in the sputtering process. In order to increase the ionization rate, ring magnets are placed directly beneath the targets; this configuration is called magnetron sputtering. The electrons sense the magnetic field and the Lorentzian force traps them from being lost to the sidewalls of the chamber. In this way, magnetron sputtering serves to increase the dwell time of the electrons in the plasma and thus leads to a higher ionization probability. This in turn leads to lower plasma strike pressure in comparison to conventional sputtering. The lower pressure means a higher mean free path for the sputtered atoms on their way to the substrate. Thus magnetron sputtering serves a dual purpose: increases deposition rate and increases the mean free path of sputtered atoms.

The sputtering system set up used for deposition of thin films in all our studies is shown as a schematic in figure 2.1. The nickel and Inconel thin film depositions were done using an AJA Orion® RF magnetron sputtering system with a base pressure of $1.3 \times 10^{-9}$ torr and a process pressure of $3.0 \times 10^{-3}$ torr. The sputter rate for nickel was 1.02 Å /s at 180 W RF power. The sputter rate for Inconel was 0.09 Å/s at 150 W RF power. The deposition rates were chosen for the sake of consistency throughout the experimental studies discussed in the dissertation. The sputter rates for nickel and Inconel were calibrated using the KLA Tencor 'Alpha-Step IQ' Surface Profiler® at the University of Pittsburgh's Nanoscale Fabrication and Characterization (NFCF) Facility. The substrate-target distance **w**as maintained at 6 inches for all the samples. The nickel and Inconel 600 (Ni-72%, Cr-14-17%, Fe-6-10%, trace amounts of Si and Carbon (<1%)) targets used were 2 inches in diameter, 0.125 inch thick, 99.999% pure and were purchased from Kurt J. Lesker Company®. The argon gas used was 99.999% pure, purchased

from Valley National Gas®. All the sputtering processes were carried out at room temperature. For CNT growth substrates, oxygen free Cu foils (~ 18 µm thick), that were cold rolled and electropolished on one side were purchased from Insulectro®. The Si/SiO$_2$ wafers were purchased from Virginia Semiconductor. The 2" wafers had 300 nm thermally grown SiO$_2$ layer on the surface.
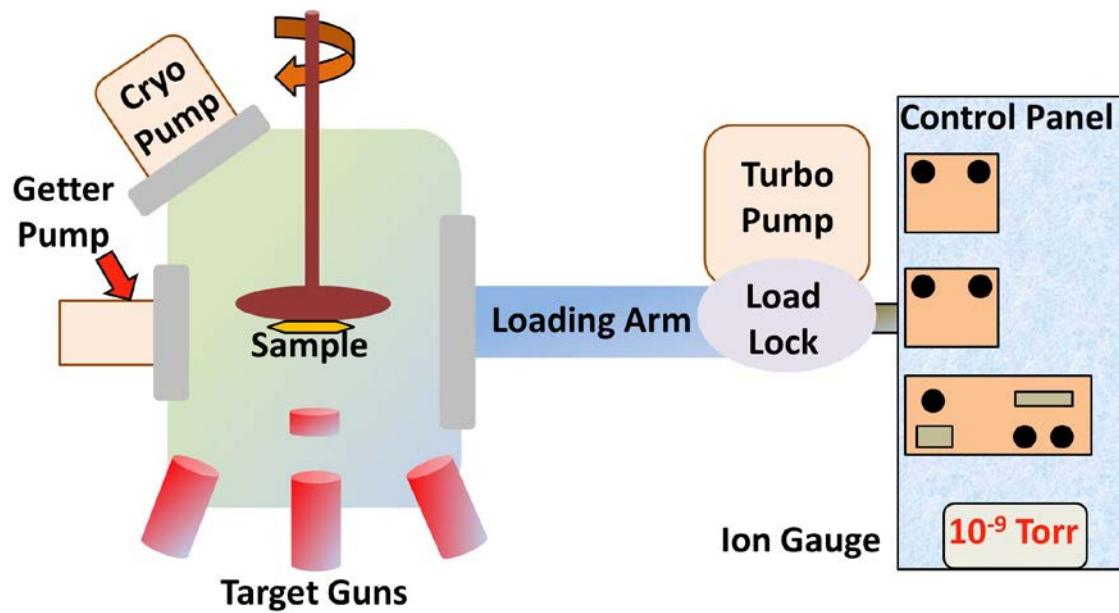
Figure 2.1: Schematic of AJA Orion® magnetron sputtering system that operates in ultra high vacuum conditions.

The samples used in the experiments, Si wafers and the copper foils were cleaned ultrasonically in acetone followed by Iso-Propyl Alcohol (IPA) for 10 minutes. The cleaned samples were then placed on the loading arm in the loadlock of the sputtering system. The loadlock was then pumped down to a crossover pressure of $\sim 10^{-6}$ torr before the gate valve is opened and the sample is transferred to the substrate holder in the main chamber

Copper foils were used as the substrates for the initial CNT growth studies. The growth of CNTs on copper is a two-step process:

1.     Depositing thin metal films of nickel or Inconel using sputtering.

2.     CNT growth using a thermal chemical vapor deposition (CVD).

## 2.2     CHEMICAL VAPOR DEPOSITION

Chemical vapor deposition (CVD), as name suggests involves chemically reacting volatile materials at elevated temperatures that are to be deposited with a mixture of gases in a furnace. This results in a non-volatile solid that deposits on the substrate placed within the furnace. CVD differs from PVD, in that, there is no physical transfer of material from sputter target sources. CVD processes also possess other advantages over PVD since the necessity of high vacuum during depositing is not a requirement[64]. The use of thermal CVD in growing CNTs

is the focus of the research studies discussed here. The set-up of the CVD system used in our studies is shown as a schematic in figure 2.2.
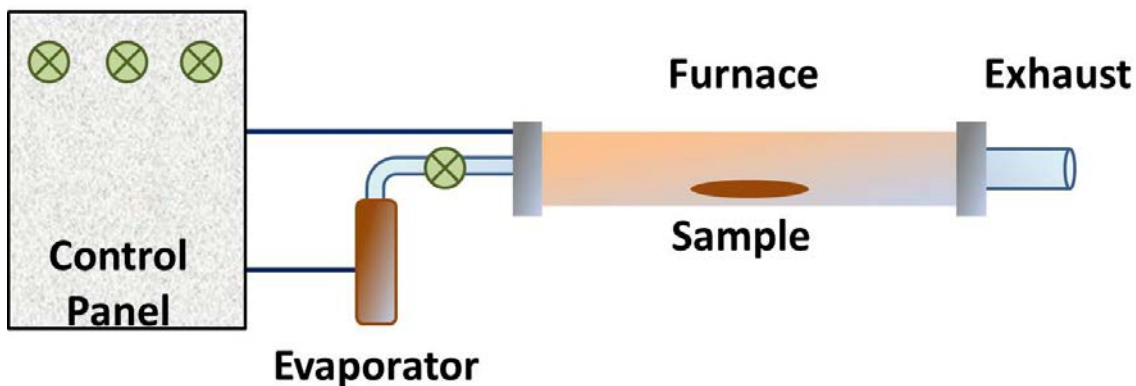


Figure 2.2: Schematic of the CVD set up used for experiments in growing aligned CNTs on copper.

For the CVD growth of the carbon nanotubes, different carbon feedstocks were investigated including methane, acetylene and xylene. The different carbon sources were studied as the different carbon feedstocks have different carbon decomposition temperatures. CVD growth studies on methane and acetylene were conducted using the sputtered metal thin film as the catalyst. In the case of xylene, ferrocene was also used as an additional catalyst during growth. Ferrocene has been demonstrated to work well with a variety of hydrocarbons such as ethylene[56], xylene[9], toluene[66], acetylene[67], benzene[68,69] and anthracene[70]. CNT growth

24

mechanism is initiated by the breakdown of ferrocene into iron nanoparticles[66,67,70]. The temperature and flow conditions were varied according to the carbon feedstock to obtain the best results. In all three cases the copper substrate was placed on a quartz plate situated in the middle of a sealed quartz tube (3 inch I.D.), placed within the CVD furnace.

When using methane ($CH_4$) as the feedstock, the copper substrates were first heated in argon at 800 $^\circ$C for 5 minutes. Hydrogen gas was turned on at a flow rate of approximately 420 sccm and argon was turned off. The temperature of the furnace was then raised from 800 $^\circ$C to 900 $^\circ$C. Once the temperature reached 900$^\circ$C, the $CH_4$ supply was turned on at a flow rate of 690 sccm for 30 minutes. After 30 minutes, $H_2$, $CH_4$, and the furnace were all turned off. Argon was then used at 250 sccm while the system cooled to room temperature. The CVD system used in this case was a Lindberg/Blue Tube furnace with a split hinge and maximum attainable temperature of 1200 $^\circ$C.

For the experiments where acetylene was used as a feedstock, it was introduced at 650 $^\circ$C. The Ar flow rate was fixed at 300 sccm and the $H_2$ gas flow rate at 65 sccm. The growth temperature was maintained at 650 $^\circ$C for 30 minutes. The temperatures and flow conditions were chosen based on similar studies performed on glass substrates[4].

For the m-xylene/ferrocene feedstock, a mixture with a concentration of 0.01g/ml was introduced into a sub-chamber at 200 $^\circ$C, with a 0.11 ml/min feed rate (for the sake of simplicity "m-xylene" will be simply referred to as "xylene"). For the CVD nanotube growth, flow rates of Ar (85%) and $H_2$ (15%) were set at 85 sccm and 15 sccm respectively. After the sample is

introduced into the CVD system, the chamber is heated to 770 °C over one hour. Ferrocene then decomposes into iron nanoparticles[66,67,70] on the substrate that act as the metal catalyst. The deposition time was maintained at 30 minutes at 770 °C[9,71,72]. The bulk of the studies reported were done using the thermal CVD set up shown in figure 2.2 using a combination of xylene-ferrocene mixture and thin film deposited on copper substrates.

## 2.3    ELECTRON MICROSCOPY

### 2.3.1    Scanning Electron Microscopy

Scanning electron microscopy (SEM) was used to study the surface morphology of the CNTs using a Philips XL30 SEM operating at 5 – 10 kV. The SEM is part of the materials micro-characterization lab (MMCL) at the University of Pittsburgh (figure 2.3). SEM images were used in order to qualitatively determine the alignment of the CNTs with respect to the substrate. SEM images of the CNT forests were taken by tilting the sample stage to 60° in order to get a better view of the alignment. SEM imaging was also used in order to get an idea of the catalyst island distribution post annealing an as deposited thin film on copper in a CVD chamber without the carbon feedstock. Sample images of the island distribution and the CNT forests obtained by tilting the stage to 60°.

Figure 2.3: Philips XL30 SEM located in the materials micro-characterization lab, University of

Pittsburgh

The Philips SEM was also used in the energy dispersive spectroscopy (EDS) mode to obtain elemental information of the substrate surface with thin films on them. In this technique, the electron beam is focused on to very small region on the sample surface. When the rastering electron beam interacts with the surface of the substrate, electrons from the inner energy levels of atoms are ejected. This creates a vacant energy and electrons from higher energy levels jump down to fill the vacant energy levels. During this process, characteristic x-rays are emitted with energies that are equal to the difference in energy of the electronic levels. The characteristic x-rays emitted are specific to each element in the periodic table.

### 2.3.2   Transmission Electron Microscopy

Transmission electron microscopy (TEM) analysis of the nanotubes was done using a JEOL JEM-2100F (Schottky field-emission electron gun (FEG) at 120kV up to 200kV). The TEM (figure 2.4) is part of the nano fabrication and characterization facility (NFCF) at the University of Pittsburgh. In a TEM, a high-energy electron beam is scattered, as it is "transmitted" through the sample. The exiting beam has two major components: a transmitted beam and diffracted beams due to scattering from interacting with the sample. A bright field image is formed when only the transmitted beam is used. A dark field image is formed when one of the diffracted beams is selected by using a selected area diffraction aperture. TEM images used for all our research studies were obtained from the bright field-imaging mode.

Figure 2.4: The JEOL JEM-2100F TEM located in the nano fabrication and characterization facility (NFCF), University of Pittsburgh

TEM samples of the CNTs were made, by sonicating copper substrates with the as grown CNTs still present on the surface. The sonication process was carried out for 10 minutes in acetone, during which time the CNTs are detached from the Cu surface and get dispersed in the acetone solution. Using a micropipette, the CNT rich acetone solution is cast on to the TEM copper grids. Acetone is then allowed to evaporate from the grids leaving the CNTs behind. The CNT samples are then examined using TEM in the bright field imaging mode.

The JEOL JEM 2100 F is also equipped with x-ray energy dispersive spectroscopy (XEDS) similar to the SEM –EDS technique described in section 2.3.1. XEDS technique was sometimes used in order to determine the chemical composition of the catalyst particle trapped within CNTs. The x-rays emitted are specific to each element in the periodic table. The JEOL JEM-2100F is a modern computer-controlled high-resolution transmission electron microscope (HR-TEM) with excellent analytical performance for daily use in a multi-user environment. The JEM-2100F HR-TEM offers large sample tilt (about 30° X and Y-tilt) combined with superior XEDS sensitivity. The TEM is equipped with a high-resolution pole-piece (spatial resolution of 2.3 Å), an interactive wave function reconstruction software package for thru-focal HREM.

## 2.4    RAMAN SPECTROSCOPY

Raman measurements on the nanotubes were done using a Renishaw inVia Raman microscope (633 nm wavelength) to evaluate the graphitic quality of the CNTs. The Raman microscope

(figure 2.5) used is part of NFCF, University of Pittsburgh. Raman spectroscopy relies on inelastic or Raman scattering of a monochromatic wavelength of light (usually a laser beam) on interaction with the sample. The scattered laser beam carries the signature of the chemical bonding present within the sample. These signatures are essentially reported as peaks at particular wavenumbers ($cm^{-1}$), which are characteristic of the specific type of bonding present in the sample. In the case of carbon nanotubes, there are there distinct peaks that are observed: the D peak (~1350 $cm^{-1}$), the G peak (~1580 $cm^{-1}$) and the G' peak (~2700 $cm^{-1}$). The D peak corresponds to the disorder peak, which arises due to dangling sp2 bonds on the CNT sidewalls or from amorphous carbon. The G peak or the order peak is due to the graphitic crystallinity of the pristine carbon atoms that make up the CNTs. The G' peak is indicative of the long-range order present within the CNTs which arises due to an inelastic phonon created from a second order scattering process[73].

Figure 2.5: The Renishaw inVia Raman microscope located in the nano fabrication and characterization facility (NFCF), University of Pittsburgh

Intensity ratios (arb. units) are calculated from the peak heights obtained from wavenumbers that correspond to the D peak ($I_d$) and the G peak ($I_g$) in a Raman spectrum. The intensity ratio ($I_d/I_g$) is indicative of the "purity" of the CNTs that are grown on substrates. Purity in this context refers to the degree or index of crystallinity in the carbon nanotubes; a smaller intensity ratio corresponds to a greater degree of graphitic crystallinity, less defects and amount of disordered amorphous carbon. This intensity ratio may be thought of as an "entropic" value with the degree of crystallinity pertaining to the degree of order. A sample Raman spectrum image is shown in figure 2.6 with an estimated $I_d/I_g$ ratio of 0.72. There is a sharp G' peak indicating a very good long range order [74,75] for the CNTs.
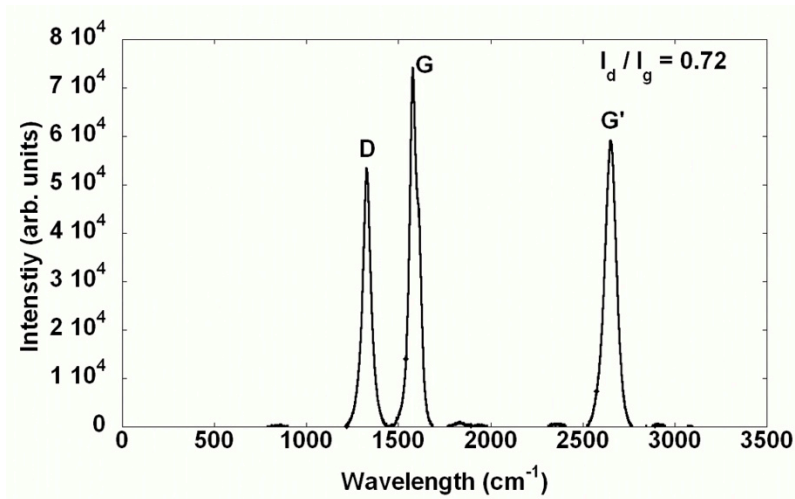


Figure 2.6: Sample Raman spectrum from the CNTs grown using 20 nm Ni film using a xylene-ferrocene mixture on copper

## 2.5    X-RAY PHOTOFLUORESCENCE SPECTROSCOPY (XPS)

X-ray photoelectron Spectroscopy (XPS) measurements were done using Thermo Scientific K-Alpha XPS and the X-ray spot size in all cases was 400 µm. The samples were sent to RJ Lee Group Inc., Monroeville, PA for analysis. XPS is a useful quantitative spectroscopic technique that is capable of measuring the elemental composition, the chemical state of the elements that exist within a material. XPS requires ultra high vacuum (UHV) conditions.

In our experiments, XPS was used to determine the amount and the chemical composition of the islands post annealing a catalyst thin film on copper substrates (without the carbon source). XPS spectra are typically obtained by irradiating a portion of the sample with a beam of high energy x-rays and measuring the kinetic energy and the number of secondary electrons emitted during the process. A typical XPS spectrum is a plot of the count of number of electrons vs the binding energy. Each element in the periodic table produces a set of XPS peaks at specific binding energy values on the surface of the material being analyzed. These characteristic peaks correspond to the electron configuration of the electrons within the atoms. From the area under each peak, corresponding to the specific element, it is possible to evaluate the quantity of the element present on the surface irradiated by the beam. Typical depth profiling of the order of 1000 nm is possible using XPS technique.

## 2.6    X-RAY DIFFRACTION (XRD)

A Philips PW3710 based X'Pert diffractometer (figure 2.7) with copper anode in parallel beam geometry was used for the glancing angle X-Ray Diffraction (XRD) analysis to assess changes in the surface composition of copper substrates due to possible Cu-Ni solid solution formation. X-ray scattering techniques belong to a class of non-destructive analytical techniques, which reveal information about the crystallographic structure, chemical composition, and the physical properties of materials and thin films. The technique involves the measurement of the scattered intensity of an x-ray beam irradiating a sample. The scattered intensity is then measured as a function of the incident angle, the scattered angle, and the wavelength (energy).  For the case of crystalline materials, the chemical composition of the material can be distinguished based on the signature Bragg scattering angles that are well documented in the form of a database. The observed peak intensities can be compared with those available in the database to deduce the actual composition of the material. The sample is held stationary in the horizontal position while the x-Ray tube and the detector both move simultaneously over an angle range $\theta$. Typical scans are recorded in the range of $2\theta = 10\text{-}90°$. A sample XRD spectrum for a Cu foil is shown in figure 2.8.

Figure 2.7: The Philips PW3710 based X'Pert diffractometer located in the materials micro-characterization lab, University of Pittsburgh
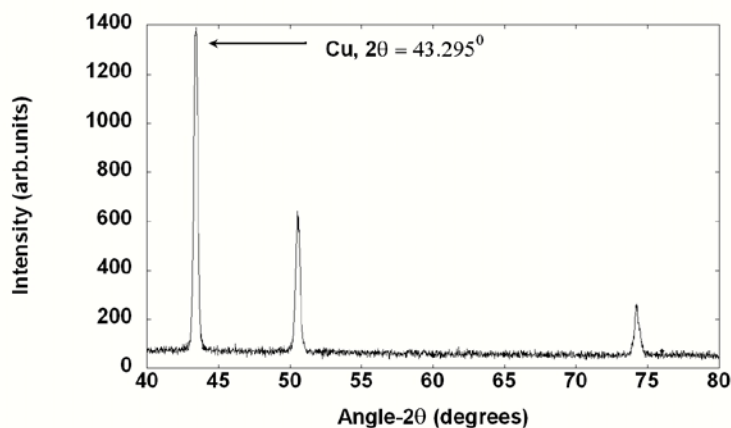
Figure 2.8: Sample XRD spectrum from a Cu foil.

## 2.7 ELECTROCHEMICAL TESTING OF CNTS

Aligned CNTs on copper with greater packing density offer potential to be used as supercapacitors in the energy storage industry due to the surface area of CNTs available for charge storage. The electrochemical testing involving the measurement of specific capacitance and power density of the electrodes (CNTs) was investigated using a double electrode set up with a standard 1M $LiPF_6$ in dimethyl carbonate/ethyl carbonate as the electrolyte (2:1)[44]. The electrodes were set up in a "Swagelok" type arrangement and the voltage was cycled between a specified range with about 30s rest between charge and discharge cycles using a CHI Arbin®

potentiostat. The Swagelok type arrangement involves the use of Whatman® filter paper immersed in the electrolyte as a separator with the electrodes (CNTs) sandwiched onto the filter paper[47]. Copper wires leading to the potentiostat were attached to the outer side of the copper foil using non-conductive vacuum tape. The entire arrangement is shown in figure 2.9. Low resistance between the CNTs and copper (which is the expectation for pursuing this application) would result in cyclic voltammograms that are rectangular in shape (figure 2.10). The power density values are calculated from the area enclosed by the CV curve (figure 2.10) divided by the mass of the CNT electrodes. The mass of the CNT electrodes was calculated using a microbalance with 0.01 mg accuracy. Ideal capacitive behavior is expected to be observed at high scan rates (typically at $1000mVs^{-1}$)[63,76]. Low contact resistance between nanotubes and collector electrodes (copper) is highly desirable in CNT based supercapacitors. Since the nanotubes are directly grown on the collector electrode (copper), high specific capacitance values can be achieved, as copper is an excellent conductor.
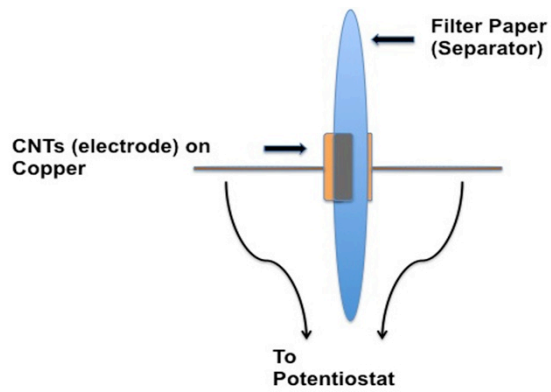
Figure 2.9: Swagelok type arrangement for electrochemical testing of CNTs.
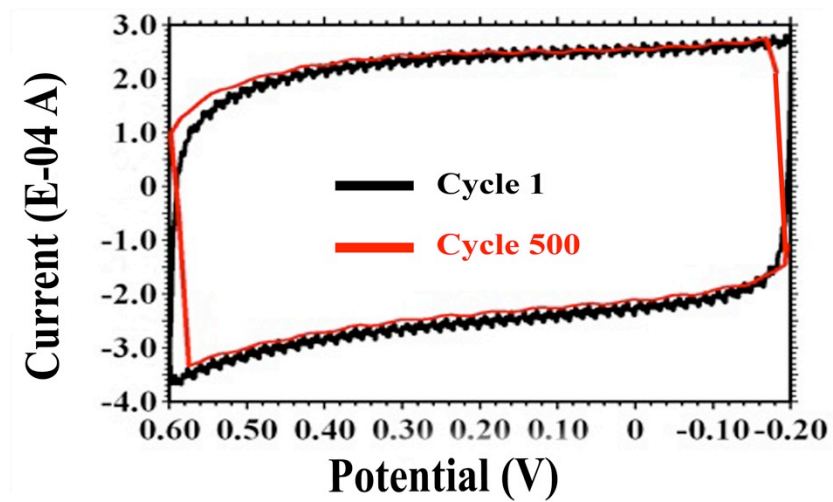


Figure 2.10: Sample CV curve after cycle 1 and cycle 500 obtained using the Swagelok type arrangement for electrochemical testing.

CNTs grown on bulk Inconel and stainless steel have been reported to have specific capacitance values of 18 Fg$^{-1}$ [46] and 30-80 Fg$^{-19}$ respectively. The specific capacitance ($C_{sp}$ in Fg$^{-1}$) values are calculated using the formula

$$C_{sp} = \frac{I}{m \left(\frac{dv}{dt}\right)}$$

where

I = applied constant current (A)

m = mass of the CNT electrodes (kg)

dv/dt = charge-discharge slope calculated from figure 2.11 (mVs$^{-1}$)
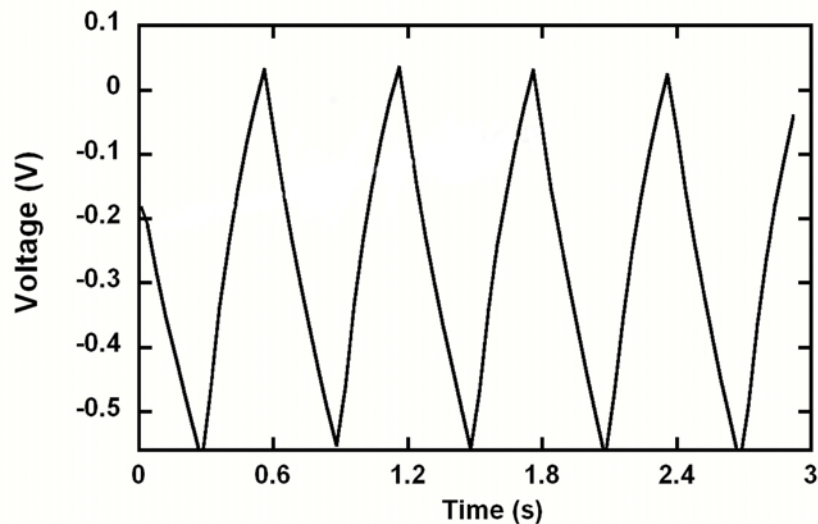
Figure 2.11: Sample charge–discharge cycle data obtained at a constant current of 1 mA. The discharge slope was used to calculate the specific capacitance of the device.

Vertical growth of CNTs on Cu is the ultimate goal of the dissertation; however the initial experimental results yielded only random CNT growth. Chapter 3 details the random CNT growth results that provided the initial data point in course of optimizing the desired CNT growth; the subsequent chapters 4 through 7 describe aligned CNT growth and their applications.

# 3.0    RANDOM CNT GROWTH ON COPPER USING NI THIN FILMS

For the experiments described in this section, the thickness of the nickel film was varied between 20 nm and 60 nm to study the effect of film thickness on the diameter and quality of CNTs for the two carbon feedstocks used: methane and acetylene. The results obtained using different nickel film thicknesses for each of the conditions are discussed below. In these experiments, we have explored the use of a thin nickel layer, deposited on copper substrates and then exposed to different CVD reaction conditions for growth of nanotubes. The results of the effect of catalyst film thickness and growth temperature on CNT growth and diameter are presented below. In addition to showing random CNT growth on copper, it is also demonstrated that temperature driven diffusion of the metal catalyst plays a key role in CNT growth and density.

## 3.1    GROWTH OF CNTS ON A NI CATALYST FILM USING METHANE CARBON FEEDSTOCK

The growth temperature for methane feedstock was 900 °C and growth time was 30 minutes. The results from using methane with four different nickel film thicknesses of 20 nm, 30 nm, 45 nm, 60 nm are shown below in figure 3.1. It is observed that in the thickness range of 20-45 nm,

CNTs form on the surface, but are randomly oriented and the coverage is poor. Although not apparent from the magnification of the images in figure 3.1, the overall coverage of CNTs on the surface is only about 30%. The majority of the substrate surface is bare, meaning no carbon structures have formed. Additionally, as the nickel film thickness increases, the coverage tends to vary. The best CNT coverage was observed for the case of the 45 nm Ni film. For the case of the 60 nm thick nickel film, interestingly, no growth of CNTs is observed although other forms of carbon deposits are visible. Similar to the case of 20-45 nm thin films, the carbonaceous deposits were also sparse with only about 15% of the copper surface covered by them.

Figure 3.1: SEM images of the CNTs grown using different nickel film thicknesses with methane as the carbon source: (a) 20 nm (b) 30 nm (c) 45 nm (d) 60 nm.

The fact that more Ni results in less CNTs may be explained by the diffusion model that is widely used to interpret CNT growth[77-80]. This model is based on the requirement for having small catalyst islands present in order to grow the nanotube structure. Y.Y. Wei et al.[81] had observed that if the catalyst island size is larger than the diffusion length of carbon atoms for a given temperature, CNT growth is not observed. In other words, the Ni regions are not small enough to act as nucleation sites for catalyzing CNT growth.

However the result that there was poor coverage on the substrate surface for thinner Ni films warranted a more thorough investigation. A 45 nm Ni film was chosen to understand what exactly happened to the as sputtered nickel catalyst film during the CVD process. The Ni film on the copper substrate was heated in the CVD furnace to 900 $^0$C to replicate all conditions (Ar and $H_2$ flow rates) that were used during the actual CVD growth without the carbon feedstock. The samples were then examined using SEM and XRD to understand the near surface phenomenon that resulted in poor CNT growth. It is found from the SEM images that the substrate surface was devoid of any islands other than a few sporadic clusters as seen in figure 3.2a. It is assumed that these clusters acted as the catalyst resulting in the CNT growth regions observed in figure 3.1c. The remainder of the sample surface (figure 3.2b) did not reveal any islands, which explains the poor CNT coverage. Our theory for the absence of catalyst islands is that the nickel could be diffusing into the oxide layer on the copper substrate. Copper is known to have two oxidation states: cuprous oxide $Cu_2O$ and cupric oxide $CuO$. Upon exposure to air, a mixture of these copper oxides[82,83] are known to form on the surface. For the 45 nm thin films, it is possible that the nickel is present on the surface without breaking up into islands that are needed to catalyze CNT growth. For the 60 nm Ni film, it is likely that the portion of the film that did break up into

islands were too large to catalyze CNT growth. The reminder of the Ni that did not break up into islands could have diffused into the underlying oxide layer.
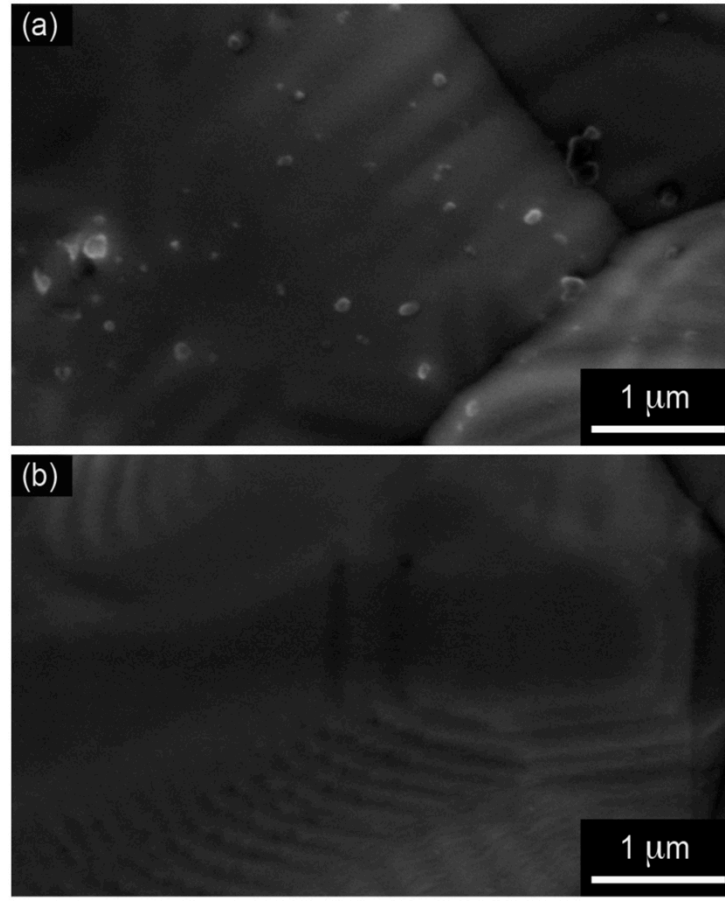
Figure 3.2: SEM images of the 45 nm Ni sample post 900 0C anneal (a) region showing catalyst islands (b) sample image representative of the remainder of the substrate surface.

To further ascertain if nickel is still present on the copper surface, SEM-EDX and glancing angle XRD analysis was performed. Figure 3.3a shows the EDX spectrum for just the copper foil and figure 3.3b shows the EDX spectrum for the nickel film on copper prior to CVD heating. The EDX technique could not detect the nickel in the sample area (after annealing the sample to 900 $^\circ$C for 30 minutes without the carbon feedstock) shown in figure 3.2b. Hence glancing angle XRD analysis was used. The XRD analysis of the region in figure 3.2b is shown in figure 3.3c. The incident angle for X rays used in this case was $1^\circ$. The analysis revealed a peak at $44.505^\circ$ that corresponds to the 111 peak for nickel. This XRD pattern (figure 3.3c) confirms that nickel is still present and is likely to change the surface composition of the copper foil. Hence nickel films may not be the best choice as a catalyst film on copper at elevated temperature as the nickel does not appear to be breaking up into islands which would then act as catalytic sites for CNT growth.
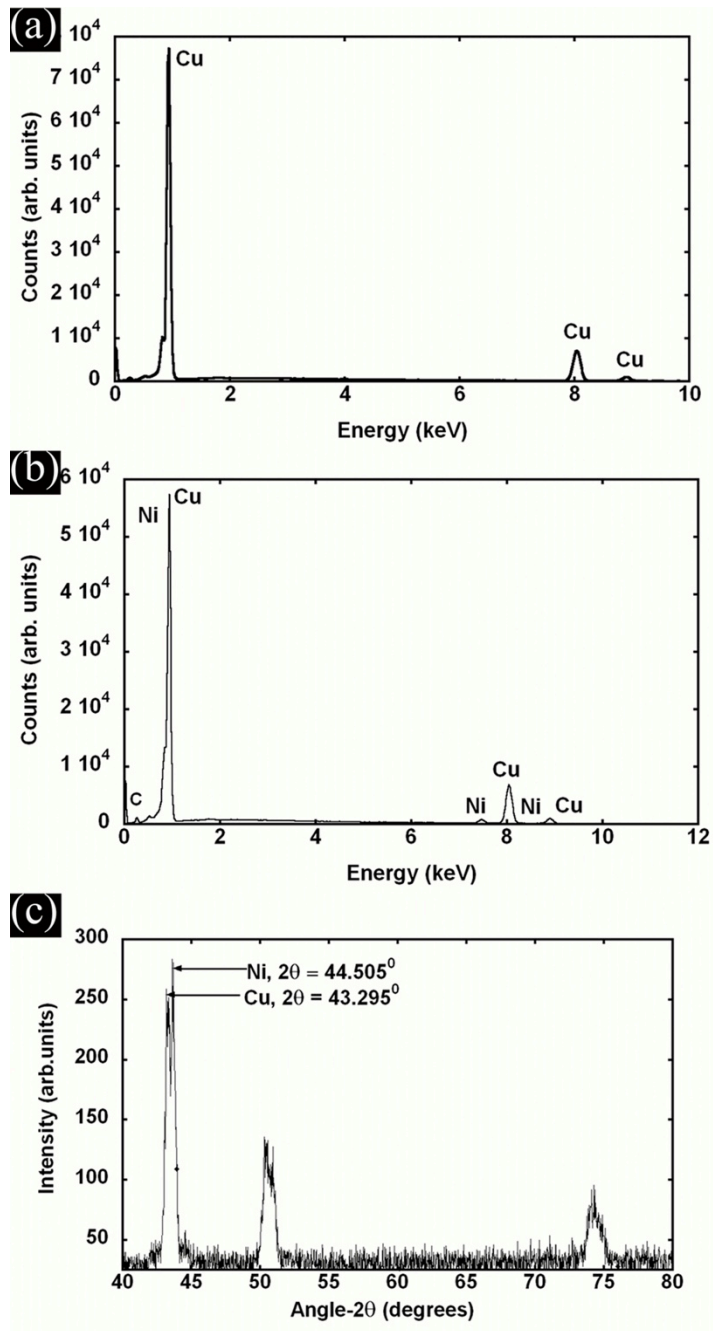
Figure 3.3: (a) EDX spectrum from the bare copper substrate (b) EDX spectrum from the 45 nm Ni film on copper substrate prior to CVD heating. (c) XRD pattern (45 nm Ni film after CVD heating) of the region shown in figure 3.2b.

From the Raman spectrum in figure 3.4 (taken from CNTs grown using the 45 nm Ni film with methane), we report an $I_d/I_g$ ratio of 1.35, which indicates that there are defects in the CNTs grown. The G' peak is indicative of the long-range order[73]. In the case of CNTs grown using the methane source, the G' peak is broad, reflecting the presence of weak long-range order.
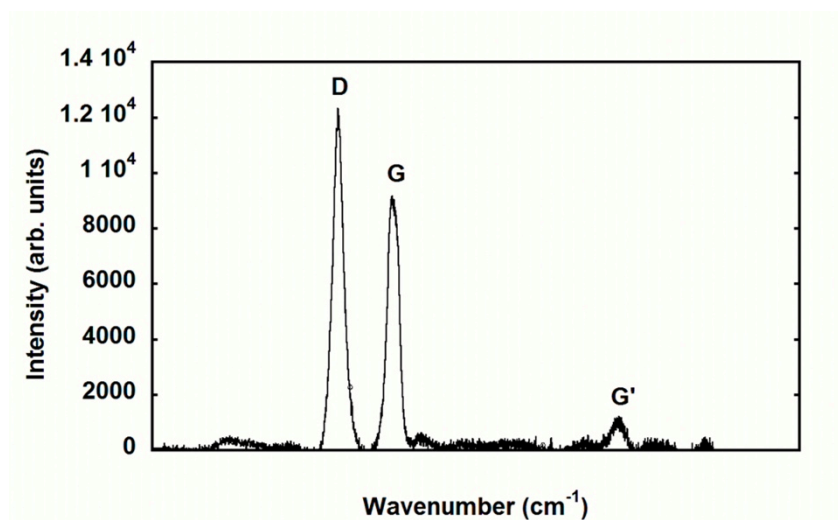


Figure 3.4: Raman spectrum for CNTs grown on the 45 nm Ni film using methane as the carbon feedstock.

**3.2 GROWTH OF CNTS ON A NI CATALYST FILM USING ACETYLENE CARBON FEEDSTOCK**

The same nickel thicknesses were used to study CNT growth with acetylene as the carbon source. Acetylene can be used at a lower working temperature of 650 $^{\circ}$C for carbon decomposition[4]. Sparse CNT growth similar to the methane source (figure 3.1a) was observed for 20 nm Ni films. However for other Ni film thicknesses, dense CNT growth was observed as seen in figure 3.5. Once again the 45 nm Ni film sample yielded the best CNT growth in terms of coverage (~100% coverage) and density. To study the effect of the CVD growth temperature on the Ni film, similar to what was done using the methane source, the 45 Ni film sample was heated in the CVD furnace to 650 $^{\circ}$C at the appropriate Ar and $H_2$ flow rates that were used during the actual CVD growth without the carbon feedstock. From figure 3.6 it is evident that these conditions resulted in the formation of many islands on the copper substrate at the lower growth temperature of 650 $^{\circ}$C. Measurements taken from the SEM image in figure 3.6 show that the islands have a diameter of 200±10 nm, consistent with the diameters of CNTs when grown on these films. We therefore are assuming that it is these islands that are acting as the catalyst for CNT growth. The presence of catalyst islands in figure 3.6 is consistent with the explanation that at the lower temperature of 650 $^{\circ}$C, there is less loss of Ni from the surface of the substrate. This explains the ubiquitous presence of CNTs on the copper surface as observed in figure 3.5b.
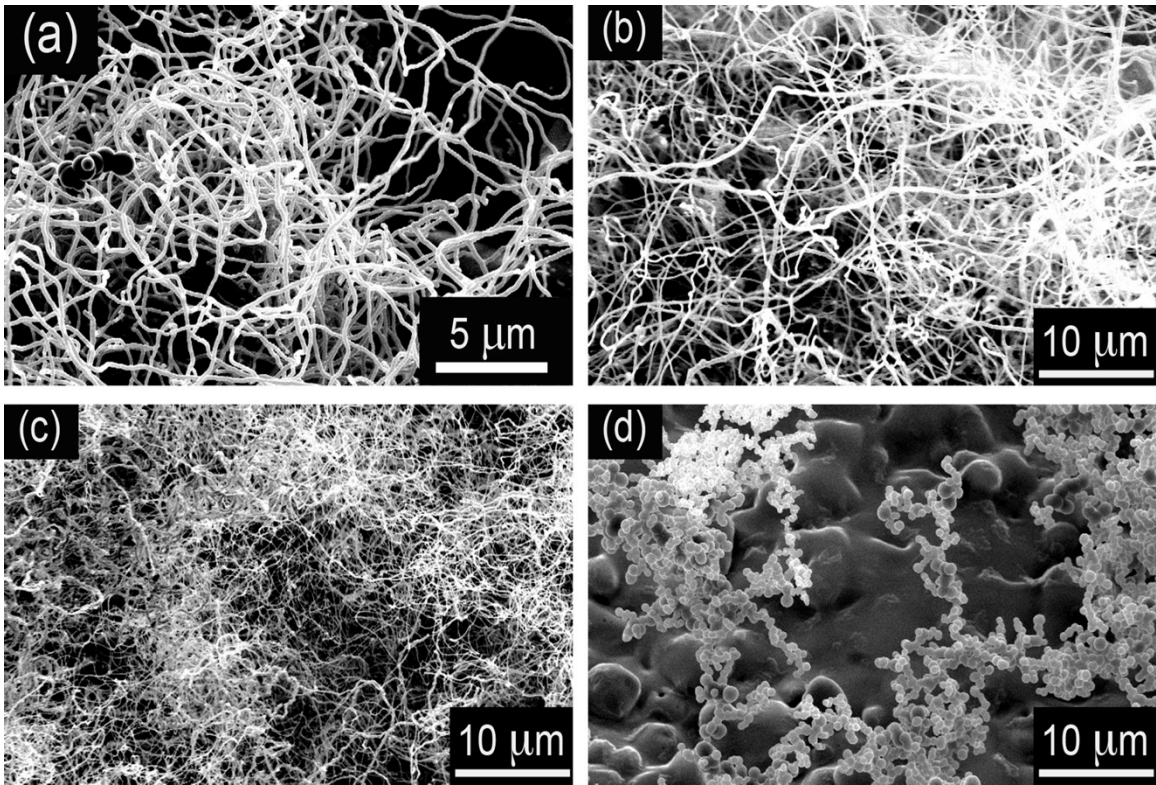
Figure 3.5: SEM images of the CNTs grown using different nickel film thicknesses with acetylene as the carbon source: (a) 30 nm (b) 45 nm (c) 60 nm.

For the 60 nm Ni film (figure 3.5c), the acetylene source yields CNT growth, with better coverage in contrast to the methane source (figure 3.1d) where no CNT growth was observed. The likely explanation for this observation is the temperature driven diffusion process responsible for "island" formation[81]. The average size of the islands shown in figure 3.6 is about $150 \pm 25$ nm. The acetylene source used at 650 $^{\circ}$C may result in the formation of islands that are smaller in size than growth with methane at 900 $^{\circ}$C. This relatively lower temperature used with the acetylene source might be just enough to sufficiently decrease the coarsening kinetics of the thicker film and allow CNT growth to occur.



500 nm
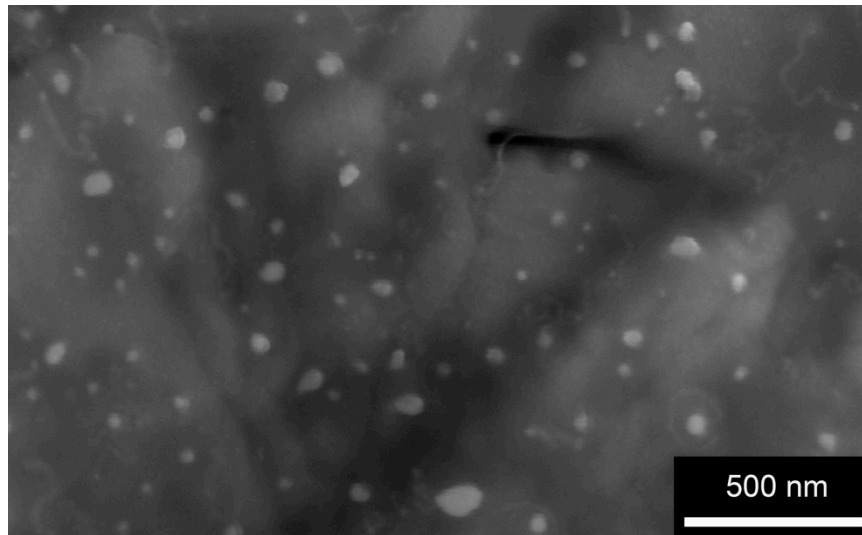
Figure 3.6: SEM image of the 45 nm Ni film on copper substrate post 650 °C anneal showing catalyst islands.

The Raman spectrum in figure 3.7, for the case of the 45 nm Ni film using the acetylene source, also shows a lower $I_d/I_g$ ratio of 0.99. This indicates that the CNTs are less defective in comparison to CNTs grown using the methane source. There is a very sharp G' peak suggesting a very good long range order for the CNTs. Therefore the acetylene source used at 650 $^{\circ}$C, resulted in better CNT growth and denser coverage. This could be due to the presence of islands at the surface to catalyze the CNT growth as opposed to growth using the methane source where an absence of islands may favor amorphous carbon deposition on the substrate surface and hence a larger $I_d/I_g$ ratio and lower purity (figure 3.4).
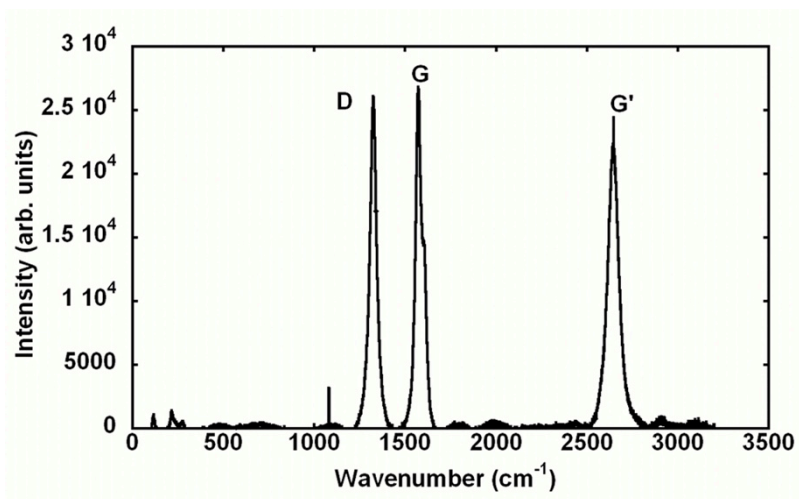


Figure 3.7: Raman spectrum for CNTs grown on the 45 nm Ni film using acetylene as the carbon feedstock.

SEM images (sample image shown in figure 3.8) were used to measure the diameters of the CNTs using the acetylene source. The diameters of the CNTs were averaged over SEM images taken from five different regions on the copper grid. Based on the images obtained and measurements made, it is found that there exists a linear relationship between the thickness of the nickel film and the diameter of the carbon nanotubes (figure 3.9). This is similar to the observation made by Wei et al.[81] on nickel films using dc plasma-enhanced CVD on Si substrates using nickel as a catalyst. They reported that thicker catalyst films tend to form "islands" that are larger in diameter that directly corresponds to the larger diameter of the carbon nanotubes. These "islands" tend to form when the CVD reactor reaches a temperature of 650 $^0$C when the nickel catalyst film breaks up into "islands" on the Si/SiO$_2$ surface[81].
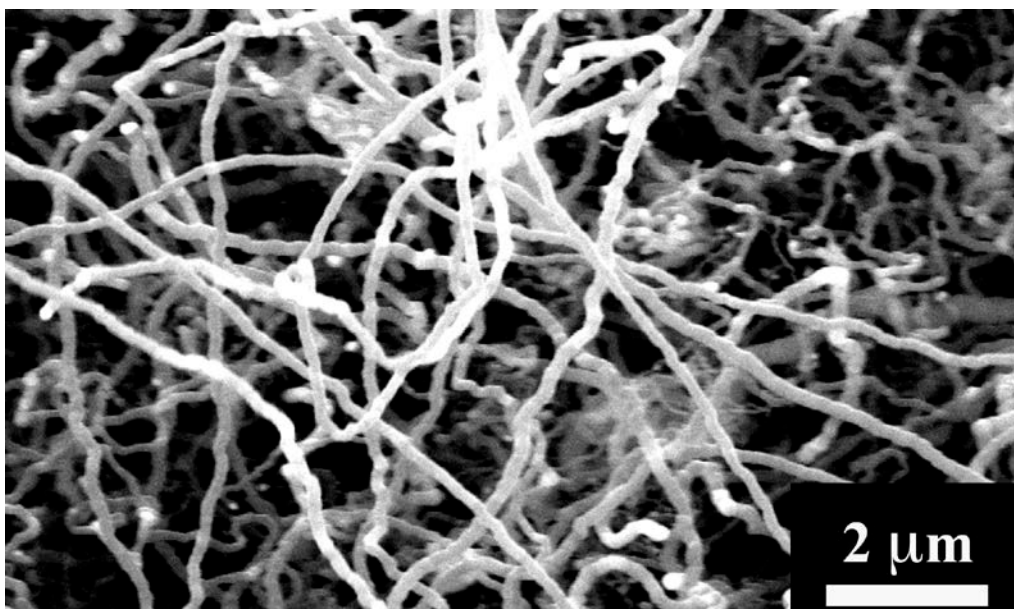
Figure 3.8: Representative SEM image of CNTs grown using 45 nm Ni film with acetylene as the carbon feedstock.

Our results (figure 3.9) show that this linear relationship (for methane and acetylene sources) between CNT diameter and catalyst film thickness may be extended to the thermal CVD technique. We also observe, based on figure 3.9 that lower growth temperatures lead to formation of smaller diameter CNTs for a given Ni film thickness. From this, we infer that the slower surface diffusion at the lower growth temperature is resulting in smaller diameter catalyst islands.
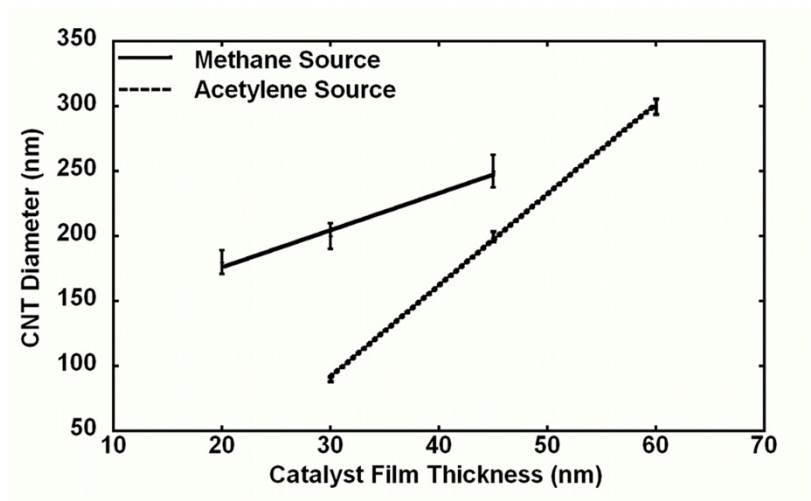
Figure 3.9: CNT diameter vs catalyst film thickness for CNTs grown using methane source and acetylene source (measurements from SEM).

In general, the results in this chapter have shown that random CNT growth was achieved when Ni think films were used with methane or acetylene sources. The primary factor that prevents the CNTs from growing aligned is the lack of greater density of catalyst islands on the copper substrate. An additional catalyst was needed in order to fulfill this criterion. This is addressed in the next chapter.

## 4.0    ALIGNED CNT GROWTH USING NICKEL THIN FILMS AND FERROCENE

### 4.1    INTRODUCTION

As evident from the discussion in the previous section, where CNTs were grown using a nickel thin film, only random CNT growth was possible. This may be due to insufficient catalyst island density, which is needed in order to force the CNTs to grow vertically aligned. Hence an additional catalyst in the form of iron, supplied from the decomposition of ferrocene mixed with the xylene source was tried. m-Xylene (IUPAC: 1,3-Dimethylbenzene) with chemical formula $C_6H_4(CH_3)_2$ was used as   the carbon precursor. Ferrocene (IUPAC: bis ($\eta^5$-cyclopentadienyl) iron) is an organometallic compound with the chemical formula $Fe(C_5H_5)_2$. The results presented below indicate that the presence of an additional catalyst improves catalyst density and consequently the alignment of CNTs. The general processing sequence followed to obtain aligned CNTs using a combination of Ni thin films, xylene and ferrocene mixture is shown in figure 4.1.
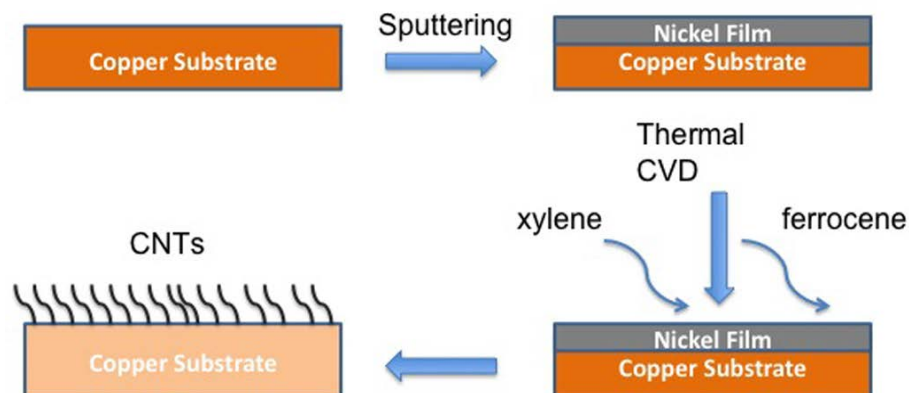
Figure 4.1: Sequence of steps involved in the growth of CNTs using sputtering and thermal chemical vapor deposition.

## 4.2    RESULTS AND DISCUSSION

For all experiments, the thickness of the nickel film was varied between 20 nm and 45 nm to study the effect of film thickness on the quality and alignment of CNTs. Three CVD growth temperatures, 700 $^{\circ}$C, 770 $^{\circ}$C, 850 $^{\circ}$C were investigated, keeping all other parameters constant. CNT growth, in terms of alignment, coverage and density, was poor for 700 $^{\circ}$C and no CNTs were seen at 850 $^{\circ}$C for the three film thicknesses that were tried. Representative images for CNTs grown at 700 $^{\circ}$C and 850 $^{\circ}$C are shown in figure 4.2. It is possible that at 700 $^{\circ}$C, the temperature is not high enough for xylene decomposition and breakdown of ferrocene into iron[71]. The same explanation could possibly hold true for higher values of temperature (in this case 850

$^{\circ}$C) where very little CNT Growth was observed[71]. Eres et al.[71] have proposed that the optimum growth temperature of CNTs grown using ferrocene to be around $760 \pm 20$ $^{\circ}$C on Si (100) wafers. The justification proposed for the optimal growth temperature is that, ferrocene in addition to acting as a catalyst supply in the form of iron, could also be potentially enhancing CNT growth by producing "molecular intermediate decomposition products" in the suggested temperature range. These products could in turn help in active dehydrogenation of the hydrocarbon. Singh et al.[66] also observed a similar optimum (highest CNT yield with least defects) growth temperature of 760 $^{\circ}$C using ferrocene on quartz substrates. In our experiments, the best results in terms of alignment and density were obtained for 770 $^{\circ}$C (figure 4.3). No CNT growth was observed at 700 $^{\circ}$C and 850 $^{\circ}$C. This temperature for optimum CNT growth is also in agreement with Pal et al.[46] who investigated the effect of temperature in terms of growth rate and saturation length of the CNTs. Thinner films appear to work better, as the greatest density and alignment of the CNTs was obtained on the 20 nm thick Ni film as seen in figure 4.3c for CNT growth at 770 °C. The observed linear density for CNTs grown using the 20 nm Ni thin films was about $3 \pm 2$ CNTs/µm
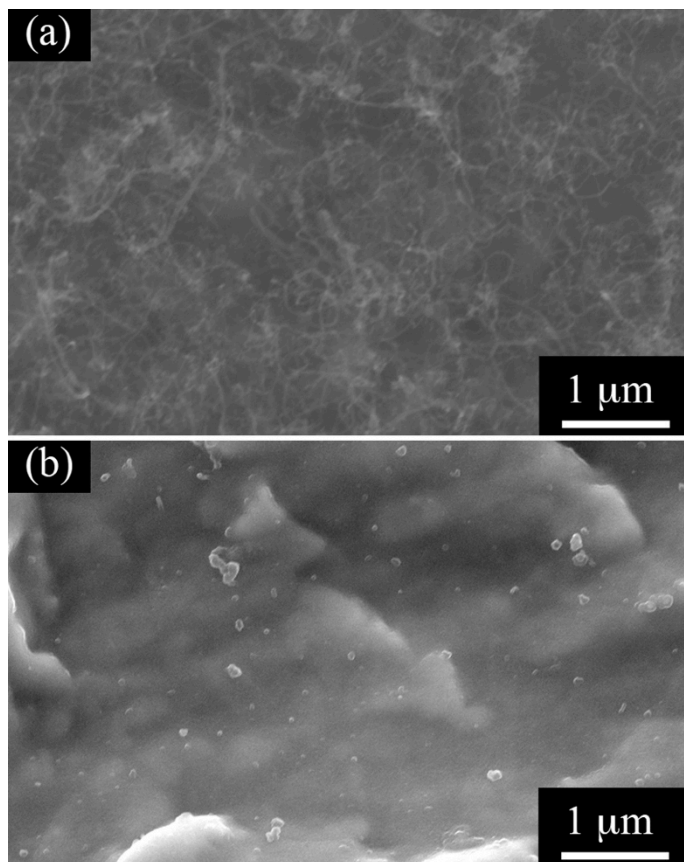
Figure 4.2: Representative SEM images of the samples grown at (a) 700 $^0$C where poor CNT growth and coverage was observed (b) 850 0C where no CNT growth was seen.
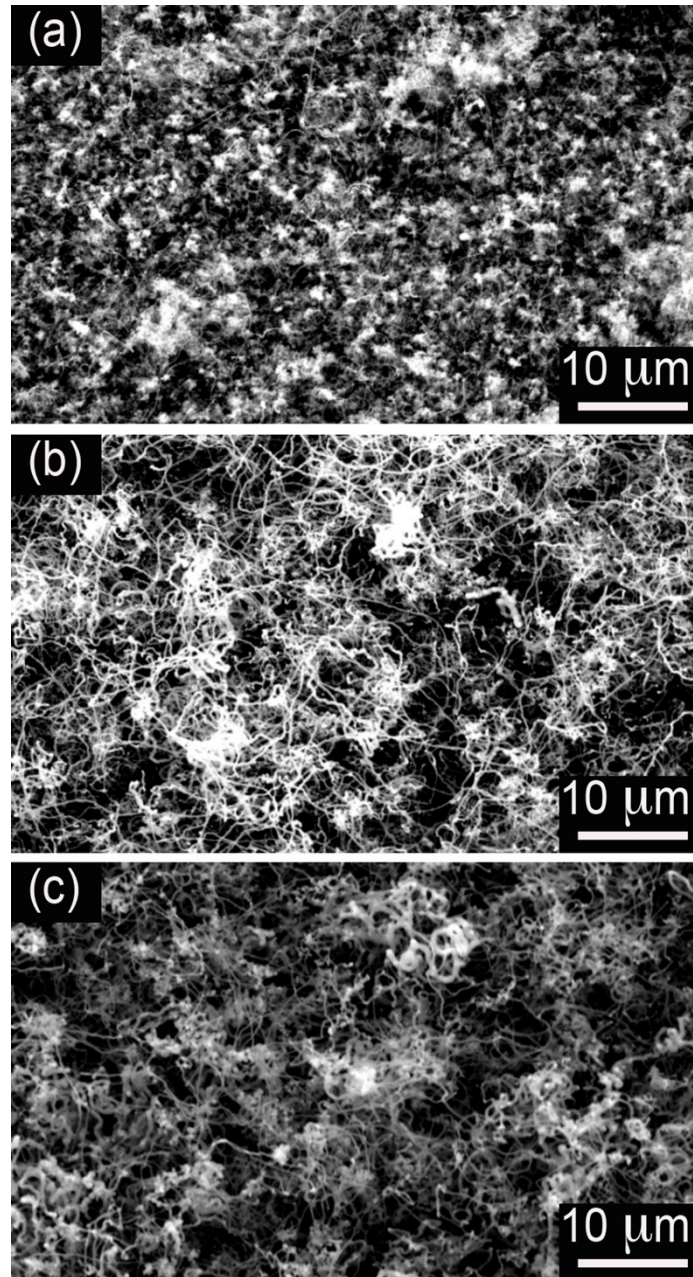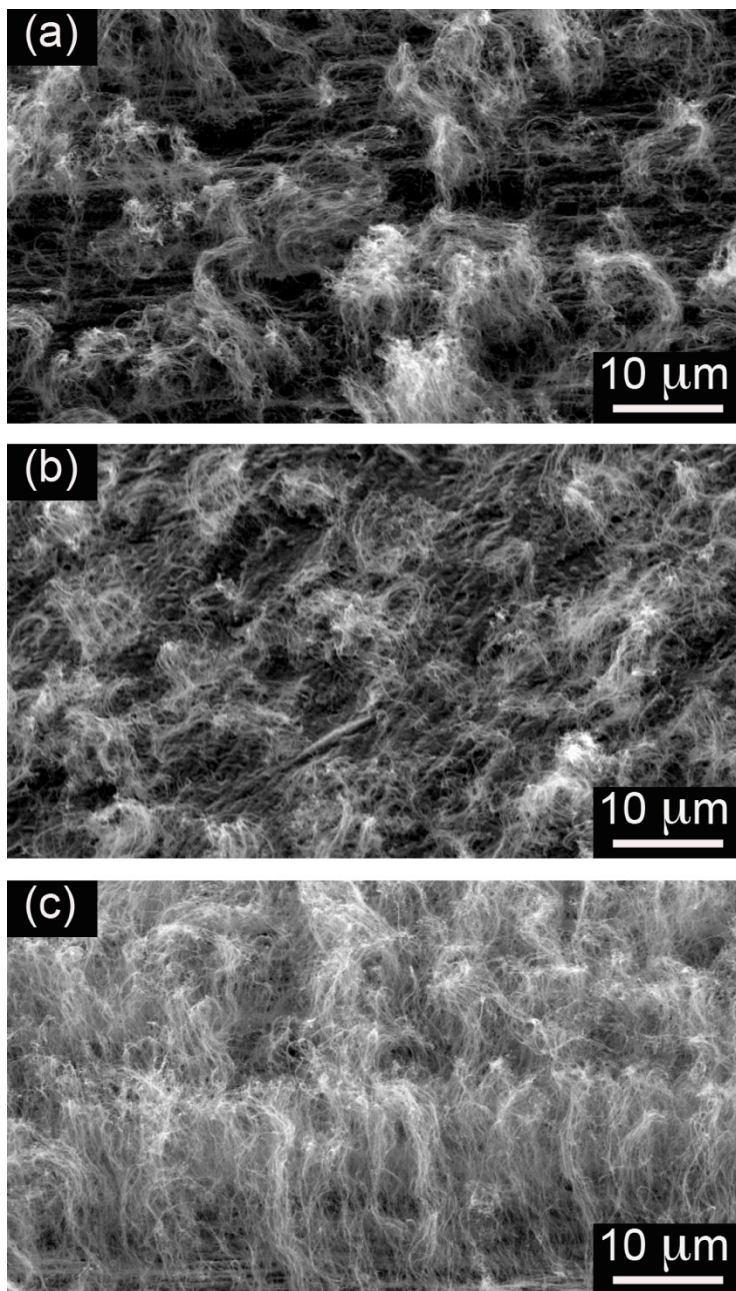
Figure 4.3: SEM images of CNTs grown using different nickel film thicknesses with xylene as the carbon source: (a) 45 nm (b) 30 nm (c) 20 nm.

TEM images reveal that CNTs grown on the 20 nm Ni films are multiwalled and the diameter on average is approximately 40 nm (figure 4.4). From the Raman spectrum in figure 4.5, we report a lower $I_d/I_g$ ratio of 0.72 than the ratios reported by Li et al.[45] There is a sharp G' peak indicating a very good long range order for the CNTs[73,84].
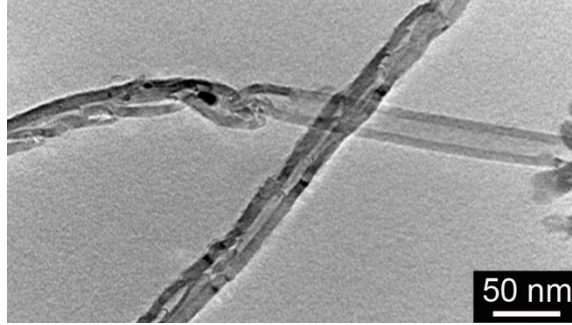
Figure 4.4: TEM image of multiwalled CNTs grown using 20 nm Ni film with xylene as the carbon source.
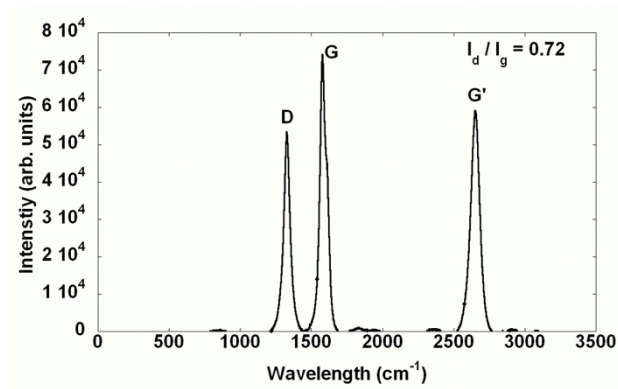


Figure 4.5: Raman spectrum from the CNTs grown using 20 nm Ni film.

CNT growth on the 30 nm and 45 nm Ni films show less vertical alignment. Therefore, there appears to be a critical thickness of around 20 nm for the best possible vertical alignment of

dense CNTs on nickel. One explanation is that the thinner films result in the formation of very small Ni enriched surface sites after heating in the CVD chamber. The thicker nickel may instead result in Ni surface islands that are too large after heating and therefore not as conducive to nanotube growth. This theory is supported by SEM images taken of the surface of the as-deposited Ni film on copper before and after annealing for a time and temperature that replicates the CVD conditions. For a 20 nm Ni film deposited on a copper foil, there is basically no observable change in the surface topography after annealing at 770 $^{\circ}$C for the magnification shown (figure 4.6a, 4.6b). However, for the 45 nm film, islands are visible on the surface (figure 4.6c). The islands have a broad diameter distribution ranging from about 250 nm to 3 µm. It therefore appears that the excessive nickel has the propensity to form into islands on the surface. Since the Ni films are actually deposited on the native copper oxide that is present on the surface of all the copper foils, it is possible that this oxide plays a role in the formation of Ni islands upon heating in the CVD chamber. Copper is known to oxidize rapidly[82,83] on exposure to ambient conditions. It has been proposed that metal oxide layers such as chromium oxide[85] aid in alignment by improving the breakup of catalyst islands. These results also correlate with the diffusion model for CNT growth, which predicts that if the island sizes are larger than the diffusion length of carbon, CNT growth is more difficult[81,86]. The presence of large Ni islands for the thicker film appears to obstruct the efficiency of iron acting as a catalyst since there is poor growth and alignment when thicker Ni films are used (figure 4.3a, 4.3b). Thus thicker nickel films (t > 20 nm in this case) result in the growth of fewer CNTs, which in turn can grow in random directions due to a lack of crowding[87] from other nanotubes. A high density of CNT nucleation and growth is required for preferential vertical CNT growth.
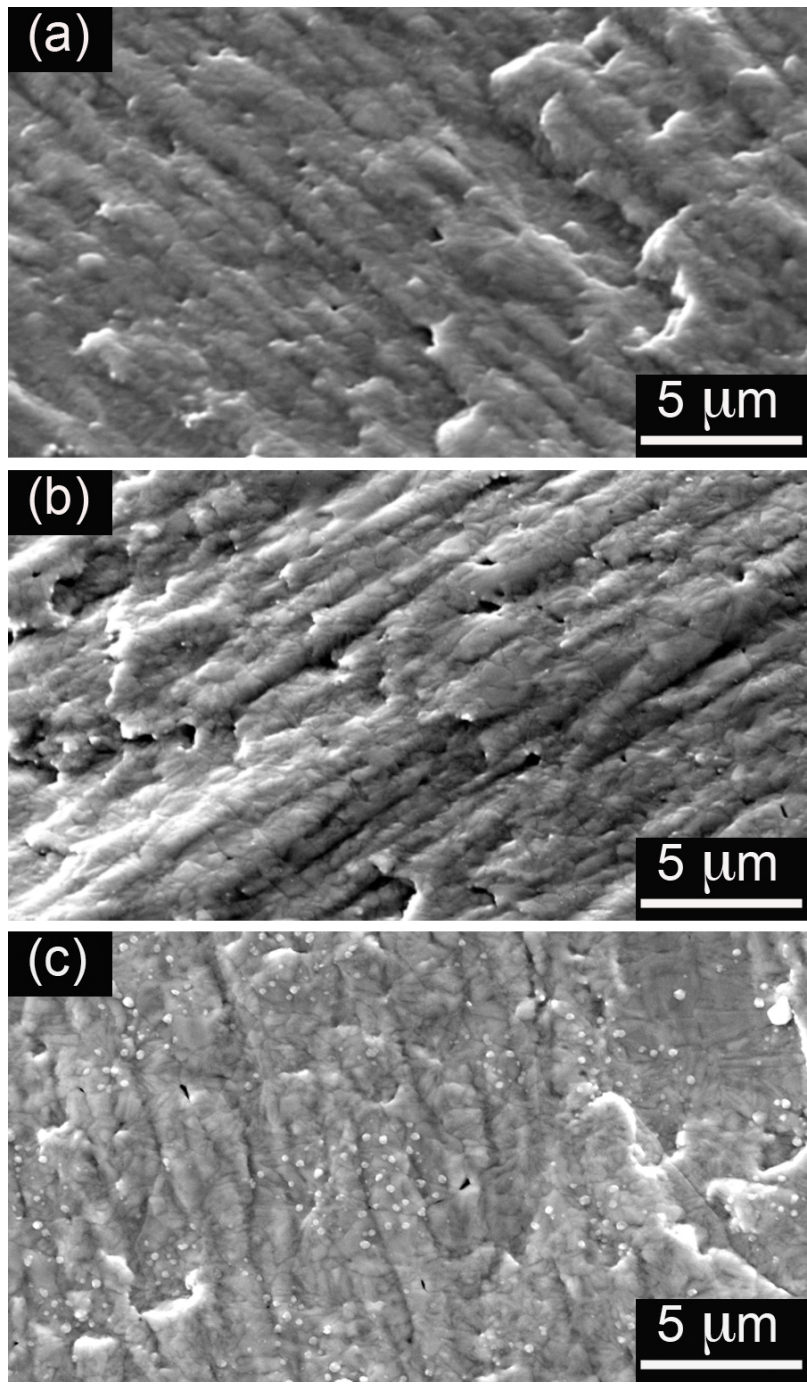
Figure 4.6: SEM images of the surface of the copper substrate with 20 nm Ni film (a) before annealing, (b) after annealing, (c) 45 nm Ni film on copper substrate after annealing.

To determine if the Ni film is still necessary when using the xylene/ferrocene mixture, growth of CNTs on bare copper (no Ni film) was also attempted and random carbonaceous structures with extremely poor coverage and large amorphous carbon chunks were observed as seen in figure 4.7a. We therefore also hypothesize that the nickel film acts as a surface modifier that supports the Fe catalyst from the ferrocene source. The ferrocene therefore is important for obtaining the high density of CNTs that forces the vertical growth to occur, but the presence of the nickel layer is also necessary. This finding can be compared to a study by Miao et al.[86], where it was reported that copper nickel alloy substrates with iron thin films are better than the individual metallic substrates for growing aligned CNTs. On the other hand, CNT growth using just xylene (no ferrocene) on Ni films was also performed and resulted in random CNT growth with poor coverage as seen in figure 4.7b. This finding is consistent with the observation made by Eres et al.[71] who hypothesized that ferrocene has an additional role to providing catalytic iron from its decomposition. The process of ferrocene decomposition could result in intermediate products that are possibly involved in dehydrogenation of the hydrocarbon used as the carbon feedstock. The resulting carbon is involved in CNT growth. Thus it is clear that a 20 nm Ni film with the addition of the iron catalyst (from ferrocene) during CVD growth is the best combination for aligned, dense CNT growth.
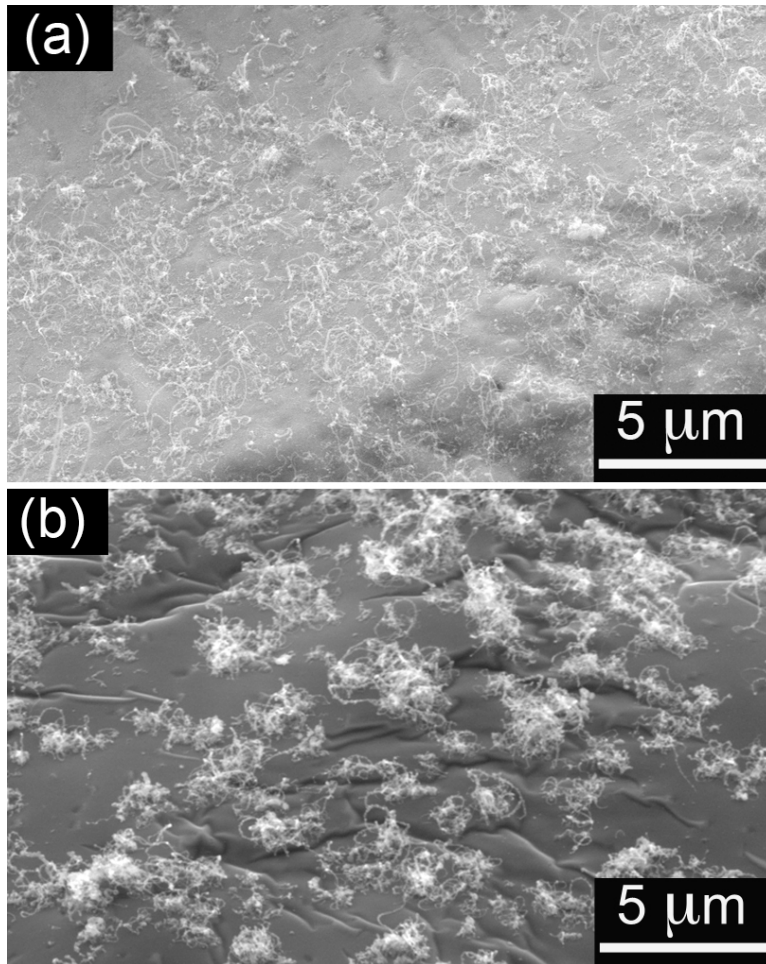
Figure 4.7: SEM images of the surface of the copper substrate with CNTs grown using xylene source with (a) 20 nm Ni film but no ferrocene (b) with ferrocene but no Ni film.

In order to understand the effect of the Ni film better, X-ray Photoelectron Spectroscopy (XPS) was used for qualitative and quantitative surface analysis and chemical state information. A 20 nm nickel film (the thickness that yielded the best nanotube growth, figure 4.3c) was annealed in the CVD chamber under flowing argon and hydrogen at 770 $^{\circ}$C and then removed to analyze the surface composition before nanotube growth using XPS. XPS data in figure 4.8a reveals the presence of copper oxide present on the surface of the substrate in addition to nickel oxide. Quantitative XPS results show that the copper to nickel ratio in terms of atomic percentage to be about 64% on the surface of the copper foil. In addition to acting as a catalyst for nanotube growth, it is possible that the remaining surface Ni will change the surface energy of the substrate. Studies by de los Arcos et al.[88] and Wright et al.[89] state that the contact angle of the catalyst particle on the substrate plays an important role in the wetting of the catalyst particle promoting faster growth and better aligned CNTs. Kanzow and Ding[80] had also proposed that an increased contact angle for the catalyst particle would provide an increased surface area for carbon to precipitate in accordance with the diffusion model for CNT growth. Therefore, a similar effect may be occurring in these experiments. The Ni enrichment of the Cu surface may impact the wetting behavior of the Fe particles on the Cu substrate in a manner that promotes the enhanced formation of CNTs. In addition to the change in the wetting behavior of Fe on Ni enriched Cu substrates, it is also likely that Ni could also be potentially acting as a diffusion barrier to Fe promoting CNT growth[55].

(a)

1.7 E+05

1.5 E+05

1.3 E+05

1.1 E+05

9.0 E+04

7.0 E+04

5.0 E+04

3.0E+04

Counts/s

$Cu2p_{3/2}$
B.E. = 933.1 eV

$Cu\ 2p_{1/2}$
B.E. = 952.9 eV

Binding Energy (eV)

970    960    950    940    930

(b)

4.0 E+04

3.9 E+04

3.8 E+04

3.7 E+04

Counts/s

$Ni\ 2p_{3/2}$
B.E. = 856.4 eV

$Ni\ 2p_{1/2}$
B.E. = 873.8 eV

Binding Energy (eV)

890    880    870    860    850
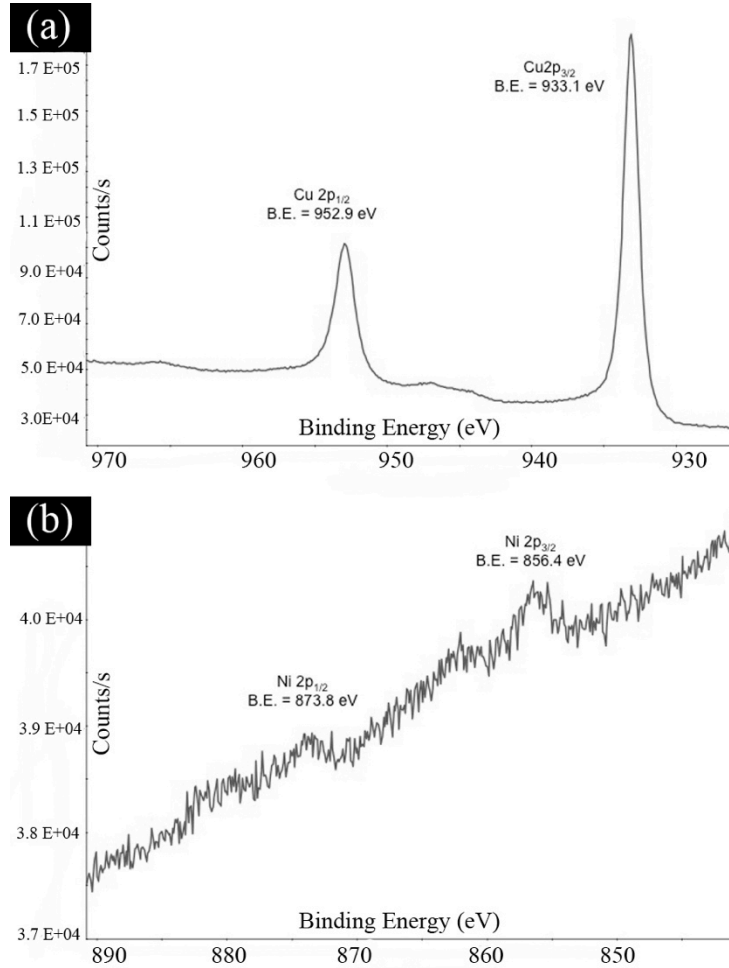
Figure 4.8: Near surface high-resolution XPS spectra of 20 nm Ni sample after annealing for 30 minutes at 770 °C indicating the presence of (a) copper oxide (b) nickel oxide. The oxides of Cu and Ni are formed since the samples were exposed post annealing.

71

In order to ascertain whether iron alone or some nickel-iron compound acts as a catalyst in the CVD growth process, TEM-EDS data from multiple CNTs was analyzed. The analysis revealed that the catalyst particles attached to the nanotubes were composed of only iron from the ferrocene decomposition in the CVD chamber (figure 4.9). No Ni was found.
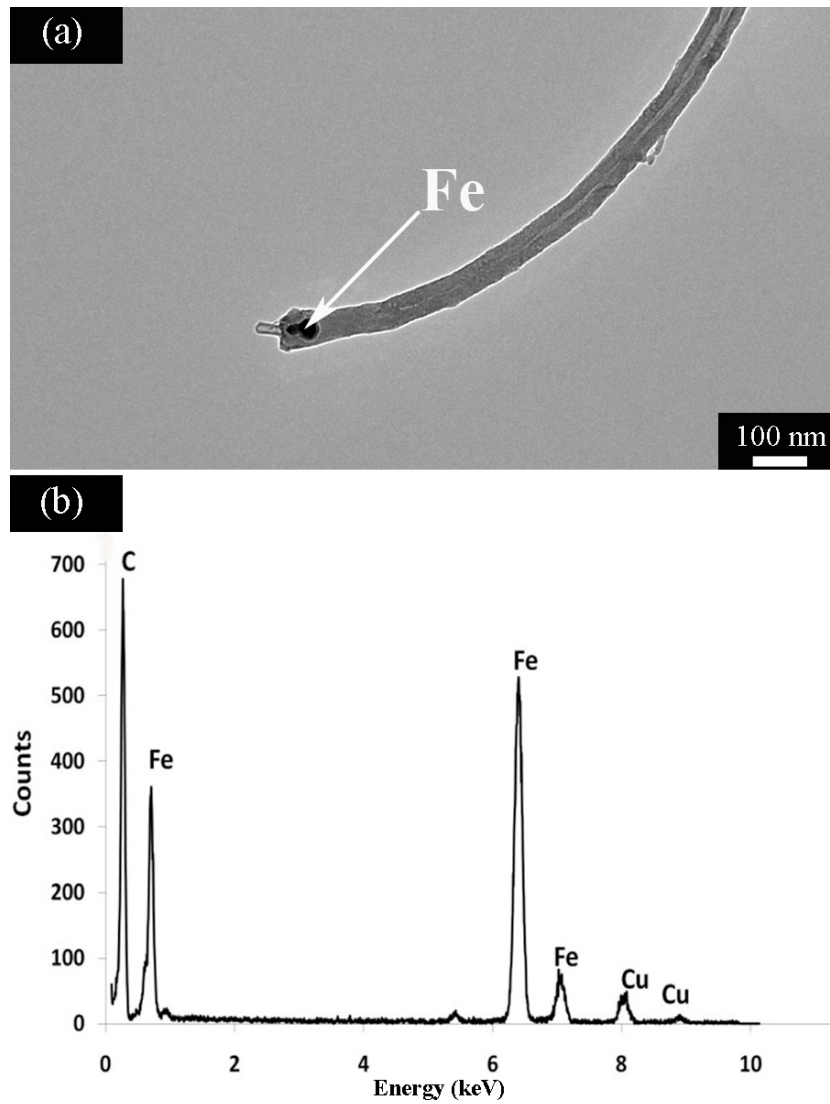
Figure 4.9: (a) Representative TEM image showing CNT with catalyst particle (b) EDS data taken from multiple CNTs indicating the catalyst particle to be iron.

It has been demonstrated that the addition of vapor phase delivered catalyst in the form of iron from ferrocene decomposition causes CNTs to grow aligned on a Ni-enriched Cu surface. However, the break up of the Ni film appears to be non-uniform and this technique leads to alignment in the Ni-enriched areas on the Cu substrate. Hence other thin film catalysts were explored to further improve the alignment and density of CNTs. The use of Inconel thin films in conjunction with ferrocene is examined in the next chapter.

# 5.0    ALIGNED CNT GROWTH USING INCONEL THIN FILMS AND FERROCENE

## 5.1    INTRODUCTION

It has been demonstrated thus far that nickel serves as a good surface modifier for aligned CNTs on copper[90]. However experiments conducted further demonstrate that Inconel 600 (Ni-72%, Cr-14-17%, Fe-6-10%, trace amounts of Si and Carbon (<1%)) is much superior to nickel in that it results in much better alignment and density. The experimental conditions were the same as described in section 4.1 in which the xylene-ferrocene mixture was used for CVD. Inconel film thicknesses in the range of 10-20 nm on copper resulted in the best alignment and density of CNT forests. The general observation made from SEM analysis is the breakup of the Inconel film into numerous islands that act as catalyst sites for CNT growth. The reasons for Inconel films acting as better catalysts in comparison to nickel films will be discussed in this section.

While CNT growth was possible with a simple Inconel film (no ferrocene), vertical growth of the CNTs was not possible, similar to what was observed when using stand-alone nickel films[91] as catalyst (figure 3.5). The reason for this kind of non-aligned spaghetti like CNT growth could be attributed to the lower density of catalyst sites; in other words, there is lesser "crowding" [33] which permits random growth. Hence the presence of an additional catalyst in the

form of iron from ferrocene serves to increase density of the nucleation sites thus forcing the CNTs to grow vertically aligned. The HRTEM image shows that the MWCNTs are similar to the ones grown using nickel (figure 3.8) and have an average of 70-100 walls based on measurements made from ten different regions on the TEM grid.

## 5.2     RESULTS AND DISCUSSION

SEM images of the ferrocene-assisted growth of CNTs on Inconel thin films of various thicknesses deposited on Cu foils are shown in figure 5.1. Inconel film thicknesses in the range of 10-12 nm resulted in the best alignment and density of CNT forests. This critical thickness range can be explained in terms of the diffusion model of Kanzow and Ding[80,92] which postulates that if the size of the catalyst island is larger than the diffusion length of carbon, no CNT growth would occur. If the island size is smaller than the diffusion length of carbon, the strain energy of the carbon nanotube would be too large to support CNT growth.  For Inconel films that are thicker than 15 nm, we assume the majority of islands that form upon heating must be too large to support nanotube growth. Conversely, Inconel films that less than 10 nm thick may not be thick enough to produce the necessary catalyst islands. The importance of the narrow critical thickness range is demonstrated in figure 5.2 where the linear density of the CNTs is plotted as a function of the Inconel film thickness used. The observed linear density for CNTs grown using Ni thin films was about $3 \pm 2$ CNTs/$\mu$m.
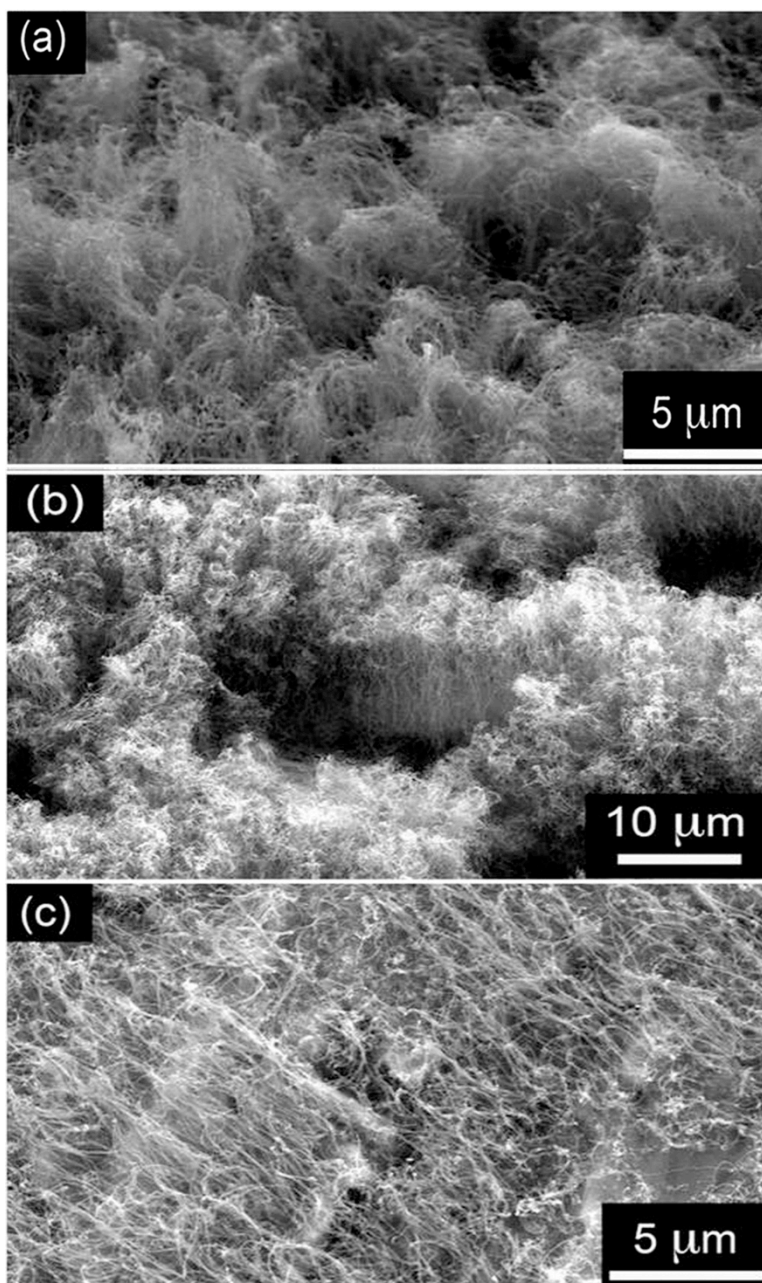
Figure 5.1: SEM images of CNTs on copper using xylene feedstock and ferrocene on various Inconel film thicknesses (a) 8 nm (b) 12 nm (c) 15 nm
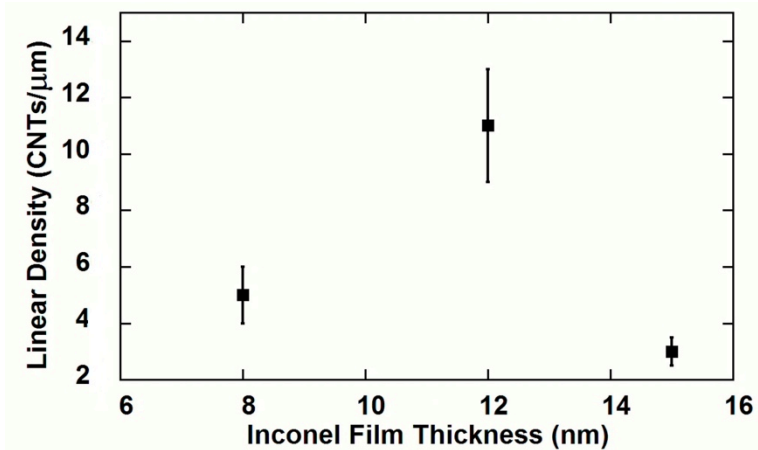
Figure 5.2: A plot of density (linear) of the CNTs as a function of the Inconel film thickness used. The linear density values were calculated form high resolution SEM images.

To understand the individual roles of iron and Inconel, CNT growth was also carried out using only an Inconel film and no ferrocene. The results from using just the Inconel film showed that the CNT growth was random with poor coverage as seen in figure 5.3a. These results are consistent with those previously demonstrated[91] (figure 4.7), which showed that pure nickel thin films alone also resulted in random CNT growth with poor coverage on copper. The reason for the poor CNT density and alignment could be attributed to the low density of catalyst islands that serve as nucleation sites for CNT growth when using only a metal catalyst film and no ferrocene. To observe the island density, an Inconel film on copper was annealed in the CVD chamber at 770 ℃ for 30 minutes under flowing argon and hydrogen gases to mimic the CNT growth conditions without the carbon feedstock. The low island density that results can be seen in figure

5.3b.  This low density explains the low CNT coverage without ferrocene.  It has previously been shown that ferrocene used without a metal catalyst layer on bare copper does not promote dense nanotube growth either[55,90].
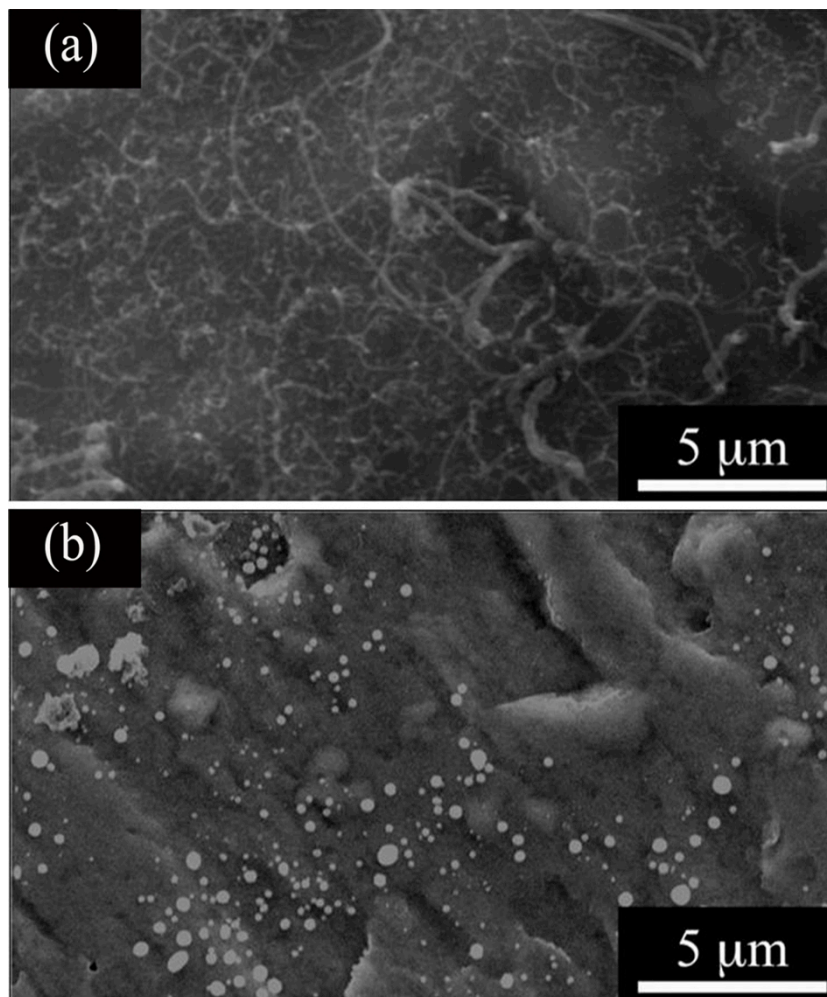
Figure 5.3: SEM images of (a) Random CNT growth from using just the Inconel film (no ferrocene). (b) Low island density post annealing the Inconel film (no ferrocene) at 770 ℃ for 30 minutes (no xylene).

When we heat the Inconel film in the CVD chamber and expose it then to ferrocene alone and no xylene, SEM shows a much greater density of numerous small islands on the surface (figure 5.4) as opposed to without ferrocene (figure 5.3b). These dense catalyst sites lead to the aligned growth of CNTs that was shown in figure 5.1b. Hence the presence of an additional catalyst in the form of iron from ferrocene serves to increase the density of the nucleation sites thus forcing the CNTs to grow upward. The aligned growth in this case is due to the "crowding effect" which forces nanotubes to grow in a vertical direction[33]. Similar results were seen in our previous work when using a Ni thin film and ferrocene[90]. However, the density and relative degree of alignment for the case of Inconel shown here is much greater than that for Ni alone. In addition, the Ni films that produced the highest density of nanotubes were approximately 20 nm[90]. This is much thicker than the 10-12 nm Inconel films which produced the best results seen here. For both of these reasons, Inconel appears to be the better choice to use for this processing method.

Figure 5.4: SEM Image of high island density post annealing the Inconel film with ferrocene at 770 ℃ for 30 minutes (no xylene).

CNTs grown using this method are found to be multiwalled with a diameter of about 60 nm ± 10 nm as seen in TEM images in figure 5.5. From the Raman spectrum in figure 5.6, we report an $I_d/I_g$ ratio of 0.61. There is a sharp G' peak[73] indicating a very good long-range order for the CNTs.
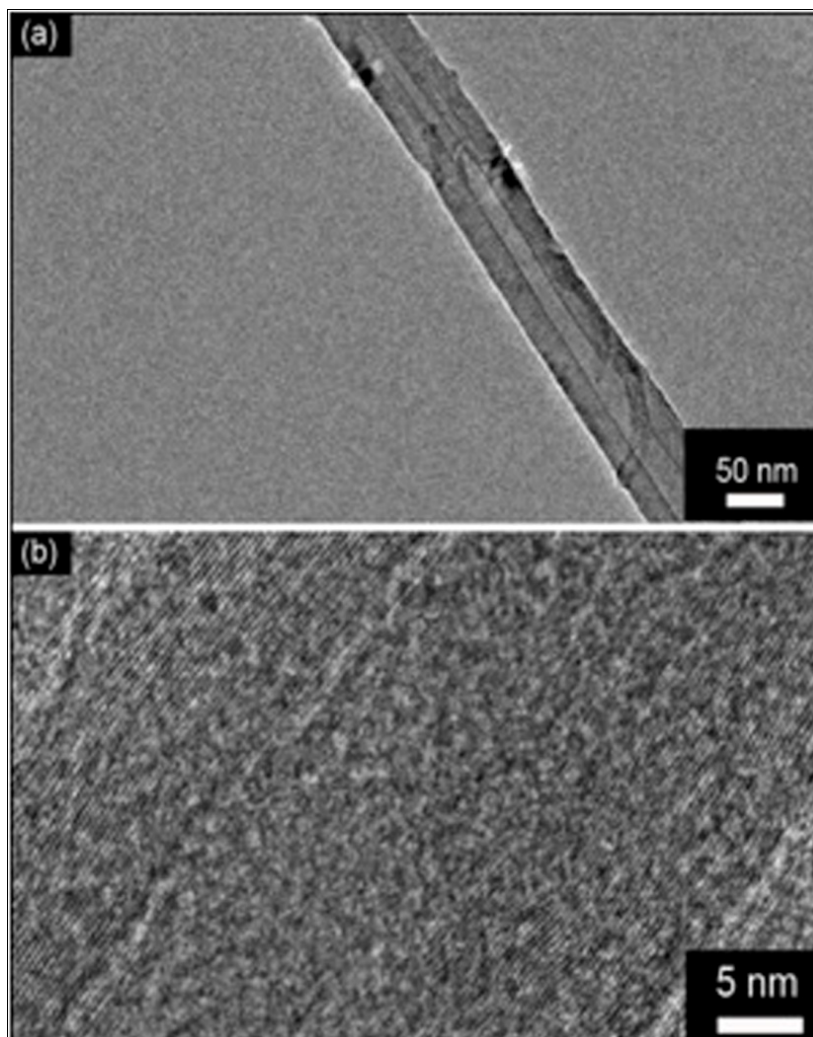
Figure 5.5: (a) TEM image (b) HRTEM image of CNTs grown on copper using Inconel catalyst.
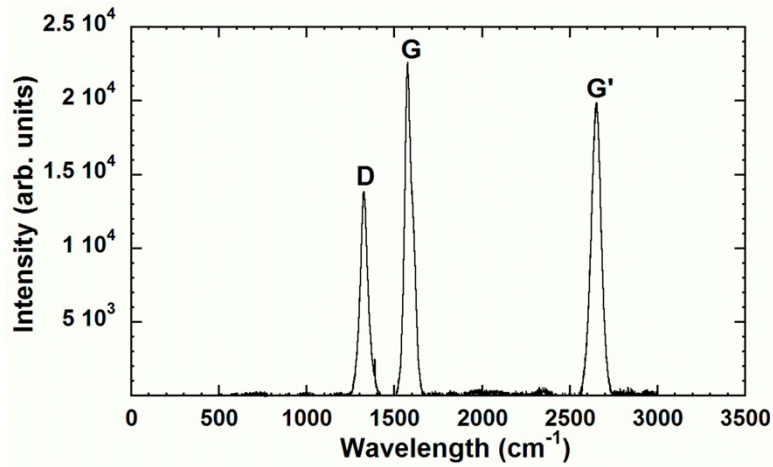
Figure 5.6: Raman spectrum from the CNTs grown using 12 nm Inconel film and ferrocene.

To further understand if both iron and Inconel acted as catalysts for CNT growth, TEM-EDS analysis was done at the tip end of multiple CNTs with catalyst particles. This revealed that the catalyst particles in some cases consisted of just Fe and in other cases were Inconel (figure 5.7). Thus we believe that both iron and Inconel act as catalysts for CNT growth. This is one possible reason that Inconel is a better catalyst than nickel since previous work[90] did not reveal any nickel particles in the CNTs, only Fe. Many research groups have reported Fe[93-95] to be a good catalyst for CNT growth. From a surface energy analysis perspective, Inconel in comparison to nickel[90], could also act as a better catalyst for CNT growth due to the presence of Cr and Fe. Cr and Fe have higher surface energies, 3.5 and 2.2 $J/m^2$ respectively, relative to the copper substrate whose surface energy is 1.9[96]. It has been reported that catalysts with higher surface energies in comparison to the substrates lead to lower Ostwald ripening rates, a phenomenon observed on another low surface energy conducting substrate, cobalt disilicide[41].

84

Since Inconel contains higher surface energy elements (Fe, Cr), it could possibly lead to a lower ripening rate and hence a lower aggregation of the catalyst, resulting in a more even distribution of Inconel islands as compared to nickel[90] during CVD growth at elevated temperatures (770 ℃ in this case) on copper. This would likely lead to an increased density of the nanotubes.
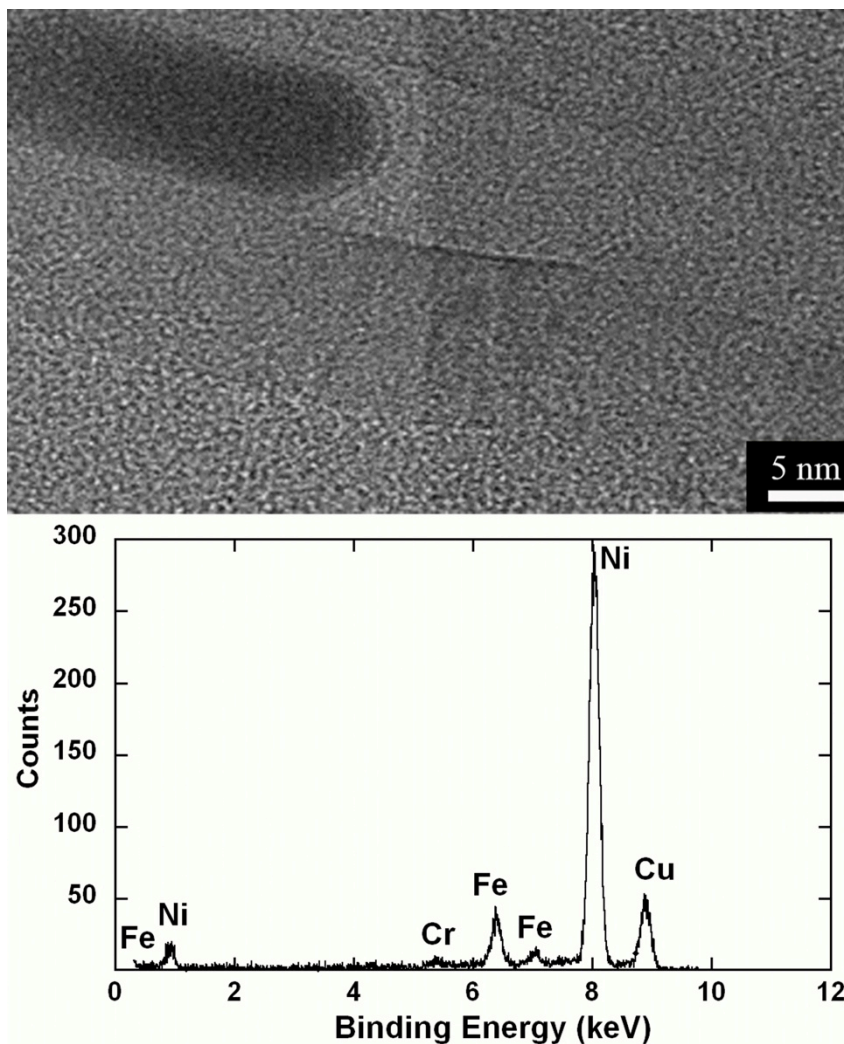
Figure 5.7: TEM-EDS spectrum showing the presence of Inconel catalyst at the tip of a representative carbon nanotube

It has been demonstrated that Inconel is a better choice over Ni, to achieve the degree and density of CNTs that were envisaged at the outset. Since the type of thin film (Inconel) and the carbon source (xylene) have been optimized optimized, further work was warranted in an attempt to improve density and alignment of CNTs by manipulating the substrate properties. At this stage, two specific properties were investigated: the effect of the use of commercial Cu foils in comparison to sputtered Cu and the effect of the native oxides of Cu on the CNT growth. Both the effects are reviewed in detail in the next chapter.

# 6.0　SUBSTRATE: COMMERCIALLY AVAILABLE COPPER FOILS VS SPUTTERED COPPER

## 6.1　EFFECT OF SURFACE ROUGHNESS OF THE COPPER SUBSTRATES

Previous reports have indicated the effect of surface roughness on CNT growth using PECVD on silicon wafers[97] and on nickel substrates[98]. Random CNT growth was reported in these studies. There is limited research of CNT growth on copper and the effect of the surface topography of copper substrates in growing aligned CNT forests. Rougher surfaces tend to cause heterogeneous nucleation of catalyst sites due to possible formation of intermediate layers[45]. The effect of the surface roughness is known to play an important role in alignment and density of CNTs. The copper foils used in all the experiments conducted so far have a surface roughness of ~ 0.4 μm. In order to investigate this surface roughness effect, CNTs were grown on sputtered copper-on-silicon oxide wafers, which should provide a smoother surface. Commercially available $SiO_2$ /Si wafers were used as the supporting substrate for the sputtered copper. To improve adhesion of the copper layer to the underlying $SiO_2$ layer a thin layer of about 20 nm of Inconel was sputtered followed by about 300 nm of copper. AFM measurements were done at this stage that determined the surface RMS roughness of the copper grown via sputtering as opposed to commercially purchased electro polished copper foils with $0.35 \pm 0.5$ μm roughness (figure 6.1) as opposed to $2.5 \pm 0.2$ nm for sputtered copper (figure 6.2).  The actual catalyst layer of Inconel

would then be deposited over this sputtered layer of copper. The sputtered Cu was exposed to the ambient when the surface roughness was estimated using AFM. This was followed by CNT growth in the CVD chamber. The experimental parameters for thin film deposition followed by CVD growth have been discussed in detail in section 2.1 and section 2.2 of the dissertation.
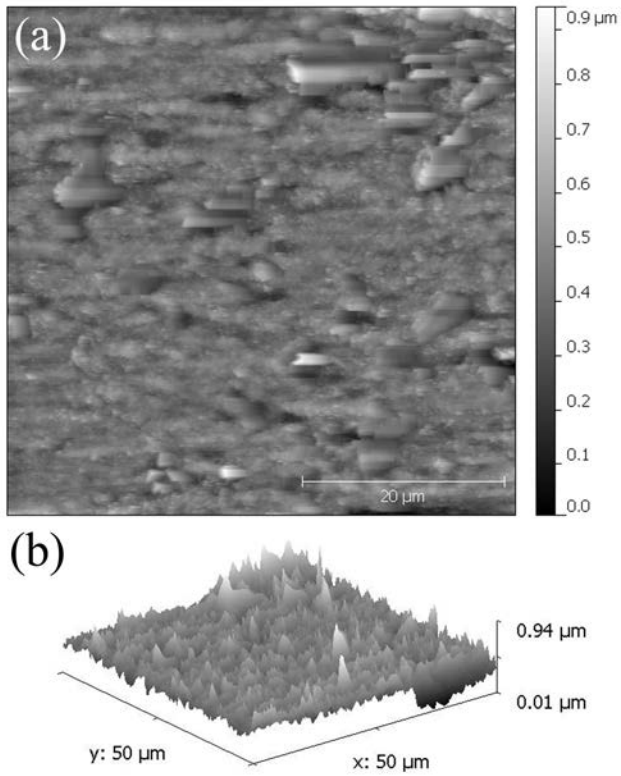
Figure 6.1: (a) AFM image of a plain, commercially purchased copper foil copper (b) 3 D view of the surface of the copper foil with an RMS surface roughness of 0.35 μm
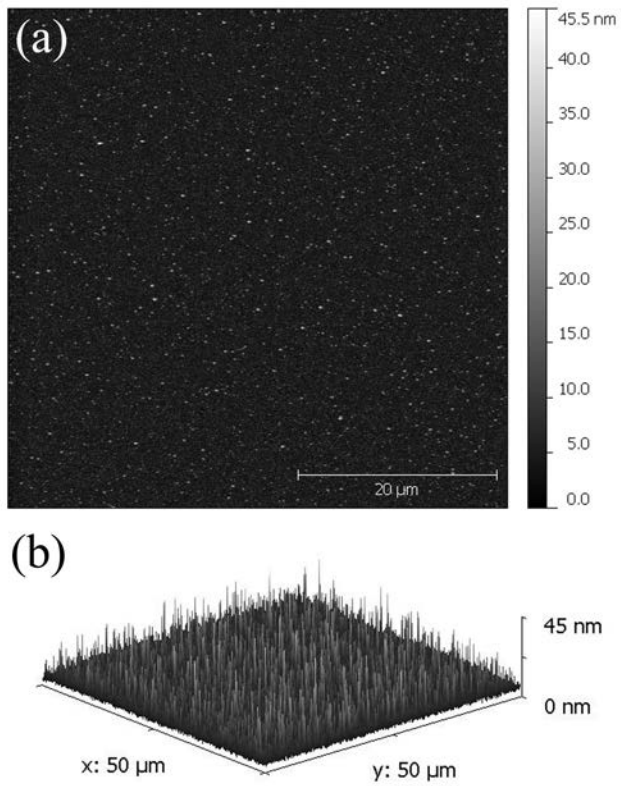
Figure 6.2: (a) AFM image of a plain sputtered copper (b) 3 D view of the surface of sputtered copper with an RMS surface roughness of 2.5 nm.

### 6.1.1 Results and Discussion

The results from the experiments done on the rougher copper foil and the smoother sputtered copper are shown in figure 6.3. For both cases dense nanotube growth is observed. In both the cases, small portions of the carbon nanotubes were removed from the underlying copper substrate using Scotch® tape to observe the density and alignment of the carbon nanotubes. These growth conditions are shown to produce multiwalled nanotubes (figure 6.3c) in both the cases. However, the nanotubes grown on the smooth sputtered copper surface tend to grow as dense vertical bundles while those grown on the foil tend to be more random in terms of growth direction. Therefore, the condition of the copper surface plays a role in the resulting nanotube morphology. One simple explanation for these results is that the serrated surface topography of the copper foil (figure 6.1) is likely to create obstructions affecting the CNT growth during the post nucleation stage as carbon precipitates around the catalyst islands. In addition, since the surface is not flat, nanotubes will grow at various angles to the overall surface normal direction and therefore not be aligned with their neighbors, also resulting in a reduced density. This is consistent with observation made by Reddy et al.[98], that while asperities on the substrate surface promote CNT growth, the density of the CNTs is greatly decreased.
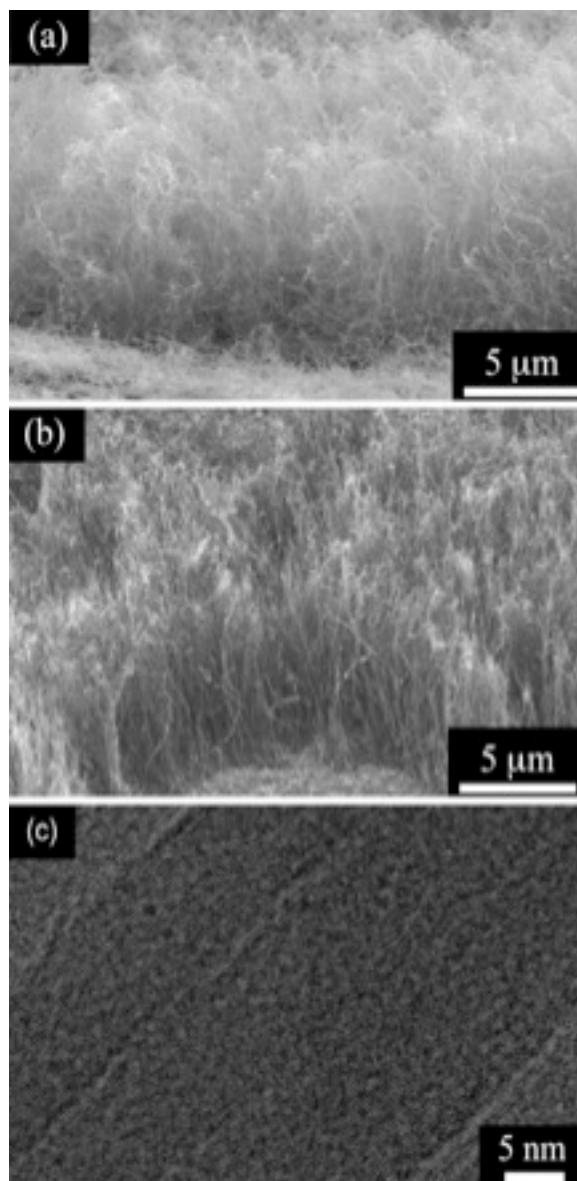
Figure 6.3: (a) SEM image of the CNT growth on the rough copper foil with 12 nm sputtered Inconel layer. (b) SEM image of the denser more aligned CNT growth on the smooth sputtered Cu (with oxide) which were deposited on a silicon oxide/silicon wafer. (c) Representative HRTEM image of the multiwalled carbon nanotubes observed both on the Cu foil and the sputtered Cu.

However, it is also possible that the surface topography may impact the morphology of the deposited catalyst film and the iron nanoparticle distribution (from ferrocene decomposition) during the CVD process. In order to understand better what is happening at the surface of the substrates during CVD growth, a second set of samples were heated in the CVD chamber under flowing Ar and $H_2$ to mimic the CVD growth conditions, but then cooled without growing nanotubes. Figure 6.4a shows the resulting surface morphology on the foil sample. Numerous islands are apparent on the surface, which may act as catalyst sites for the initial stages of CNT growth. This image can be compared to that taken from the sputtered films on the silicon wafer sample, which has a much smoother starting surface before heating. It is observed in figure 6.4b that the island distribution is much denser and more uniform on the smoother surface than for the case of the rough foil. This island morphology would likely lead to denser and more aligned CNT growth as was seen in figure 6.3b. The size distribution of the catalyst islands corresponds to the CNT diameters, which are in the range of $80\pm20$ nm.
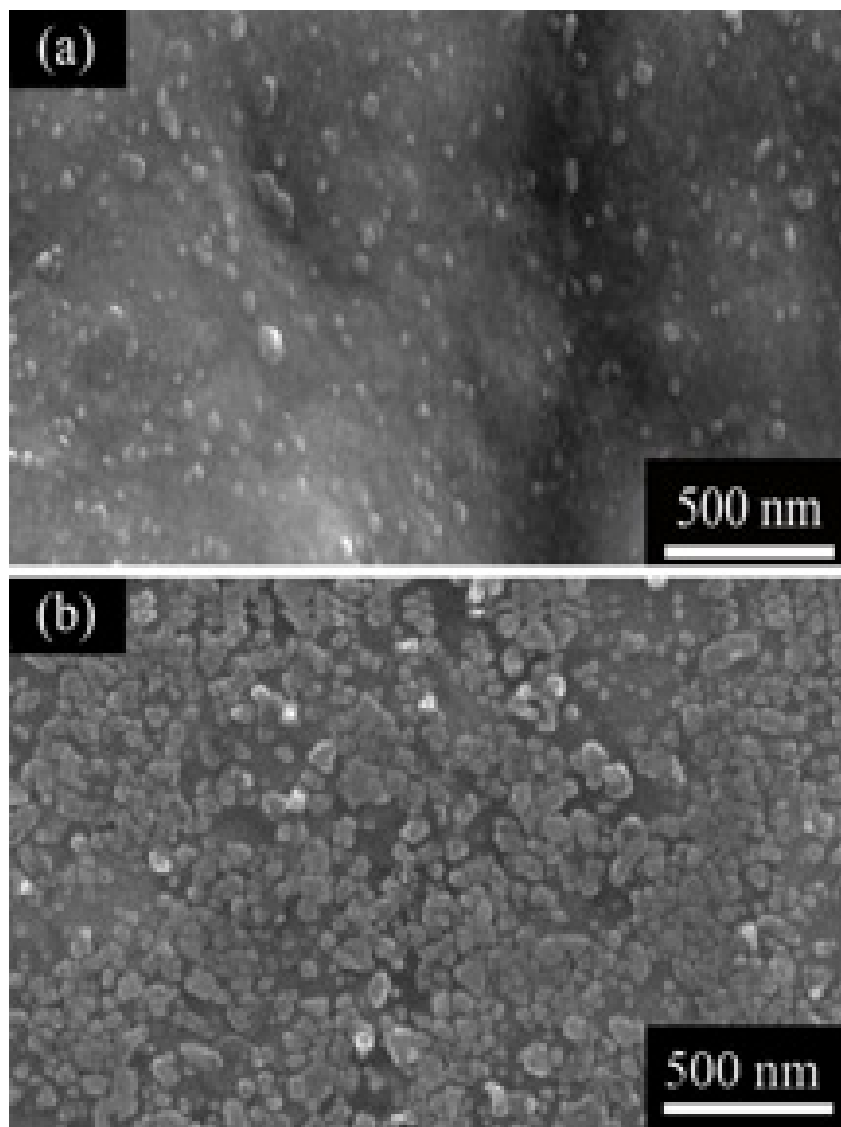
Figure 6.4: SEM image of the island density post annealing the Inconel film at 770 ºC for 30 minutes followed by ferrocene/xylene exposure at low temperature to prevent CNT growth on (a) the rougher copper foil. (b) the smoother, sputtered copper surface.

A semi-quantitative analysis was warranted in order to understand the effect of the catalyst island distribution and CNT density and the ability to duplicate the results obtained. We studied the catalyst island density and the linear density of CNT growth from three experimental rounds of sputtering of a thin film of Inconel followed by CVD growth on the Cu foil and sputtered Cu. The average, statistical number density of the islands per unit micron area on the copper foil (analyzed from ten different regions from each of the three samples) is about $140\pm10$ islands/$\mu$m$^2$ versus a much higher density of $300\pm15$ islands/$\mu$m$^2$ on the smoother, sputtered copper. The linear density of the carbon nanotubes (also analyzed from ten different regions from each of the three samples) is also higher for the CNTs grown on smoother, sputtered copper surface ($12 \pm 3$ CNTs/$\mu$m) as opposed to the CNT growth on the rougher copper foil ($8 \pm 5$ CNTs/$\mu$m). This higher catalyst island density is likely an important factor in obtaining dense CNT bundles, which naturally tend to grow with a higher degree of alignment due to the "crowding effect"[87]. The quantitative analysis of the linear density of the CNTs and the areal density of the catalyst islands are shown in figure 6.5. Our analysis from three different sample data indicates that there is consistency in the areal number density of the catalyst islands as well as the linear CNT density on the two different copper surfaces within a permissible error margin. This consistency in the values is important in the context of reproducibility of the experimental results reported here.
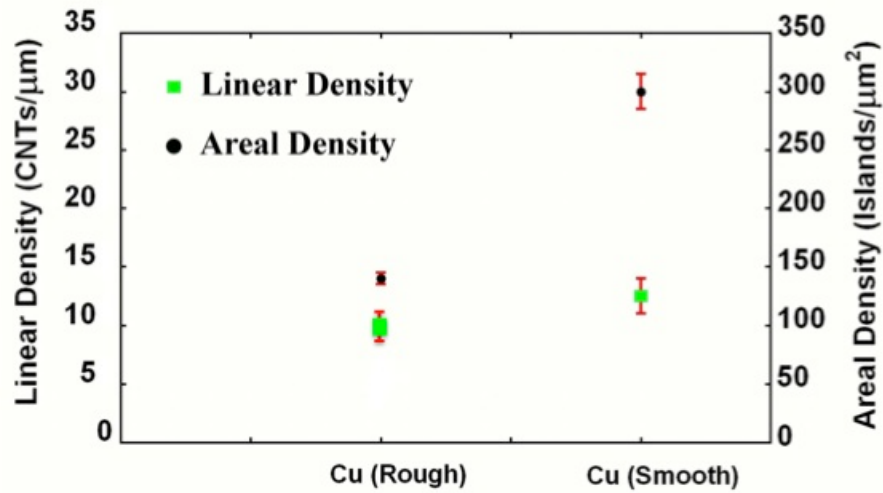
Figure 6.5: A semi-quantitative analysis showing the areal density of the catalyst island and linear density of the CNT growth on rough copper foil and smoother sputtered copper surface. The reported values were taken from three different samples.

Our results demonstrate that the topography of the initial copper surface can have an impact on the resulting morphology and distribution of the islands present on the surface after heating. This in turn will likely impact subsequent CNT density and alignment for the two different copper surfaces. For the case of the rougher Cu foil, ridges and cliff like structures on the surface can lead to an uneven initial coverage of the Inconel and on the rough surface and/or impact local coarsening dynamics during heating. The morphology of the initial surface islands will likely also impact the iron catalyst nanoparticles that result from decomposition of the ferrocene during the CVD process. Another likely possibility is the difference in the grain

microstructure of the copper foils in comparison to sputtered copper. It has been shown that the grain microstructure of the underlying substrate plays an important role in dewetting, diffusion of the catalyst layer used[99].

We believe that the Inconel acts as an additional catalyst, since ferrocene used alone on bare Cu without any catalyst or barrier layer does not support dense nanotube growth[100]. If the Inconel were acting as an additional catalyst, then the most uniform coverage of Inconel on the surface during CVD growth would result in the best CNT growth in terms of density and alignment.

## 6.2    EFFECT OF SURFACE OXIDES ON CNT GROWTH

The experimental results we have obtained so far do not consider the effect of the native copper oxide on the catalyst and hence on CNT growth. Copper is known to have three oxidation states: pristine copper (zero), cuprous (one) oxide $Cu_2O$ and cupric oxide $CuO$ (two). Upon exposure to air, a mixture of copper oxides and copper hydroxide are known to form on the surface[82,83]. To obtain an oxide/hydroxide free Cu surface, the native oxide layer was stripped off the copper foils using acetic acid as proposed by Chavez and Hess[101]. This simple technique involving the use of an organic acid removes the natives copper oxides without reacting with the underlying pure copper and does not affect the surface roughness of the substrate[102]. A thin film of 12 nm

Inconel as catalyst was sputtered on top of the copper layer in-situ under ultra-high vacuum conditions. A thin film of 12 nm Inconel as catalyst was sputtered on top of the copper layer in-situ under ultra-high vacuum conditions. This procedure was done to prevent the oxidation of copper surface before deposition of the Inconel catalyst layer. The sputtering parameters used for the thin film deposition are described in detail in section 2.1 of the dissertation.

CVD process followed the thin film deposition on oxide free copper foils and the CNTs grown using this process were studied to compare if the oxide played any role in the breakup of Inconel film into islands and the iron deposition from ferrocene decomposition onto substrates during CVD growth. This would help in the understanding the oxide effect on CNT growth and alignment. The experimental parameters used to describe the results reported in this section have been discussed in section 2 of the dissertation.

### 6.2.1    Results and Discussion

The results from the oxidized copper foil were compared with the CNT growth on copper foils where there is no oxide layer present. Characterization methods such as SEM, TEM, and Raman spectroscopy were employed to study the CNTs grown under the conditions described above. Figure 6.6 shows SEM images of CNT growth on copper substrates on both oxidized Cu foils (figure 6.6a) and oxide free copper substrates (figure 6.6b). It is observed that the CNT bundles are better aligned in a vertical direction when the native oxides on the copper foils were first removed. The approximate linear density of CNTs on the oxide free Cu substrates is about $11 \pm 3$ CNTs/μm and $6 \pm 3$ CNTs/μm on the substrates with the native oxide layer. The CNTs in both the cases are found to be multiwalled with a diameter of about $60 \pm 15$ nm. Hence we observe a greater linear density of CNTs on the oxide free substrates. A representative high-resolution transmission electron microscopy (TEM) image of the multiwalled CNTs (MWCNT) is shown in figure 6.7.
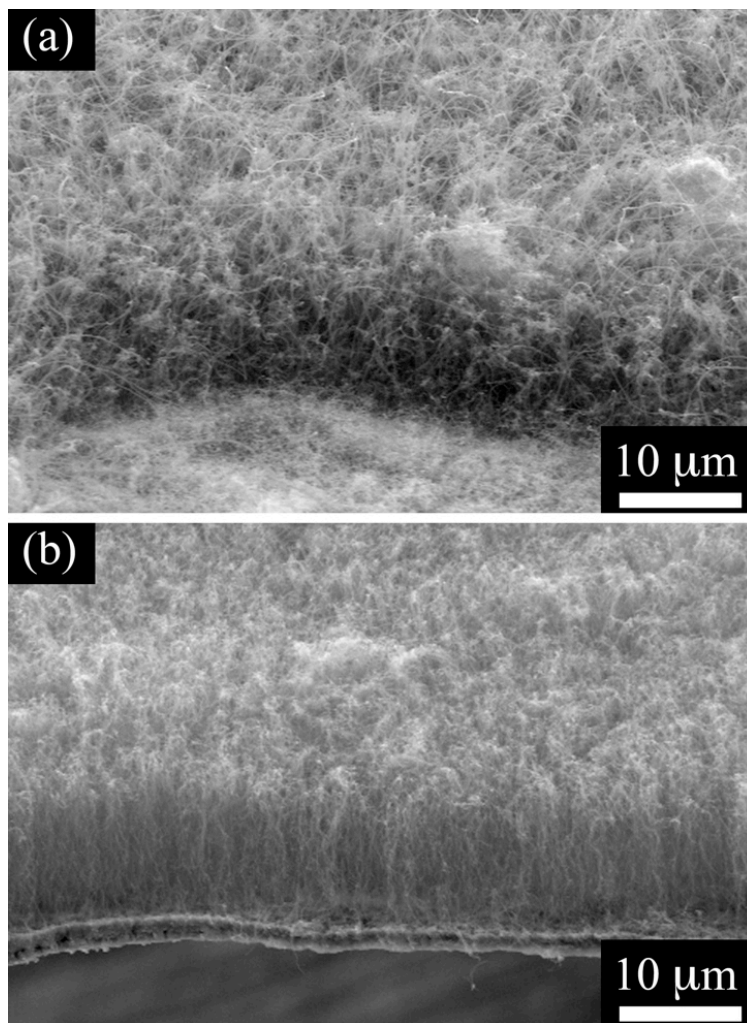
Figure 6.6: SEM images of CNT growth using Inconel and iron catalysts on copper foils with (a) no removal of the Cu native oxide layer before Inconel deposition and (b) removal of the native oxide layer.
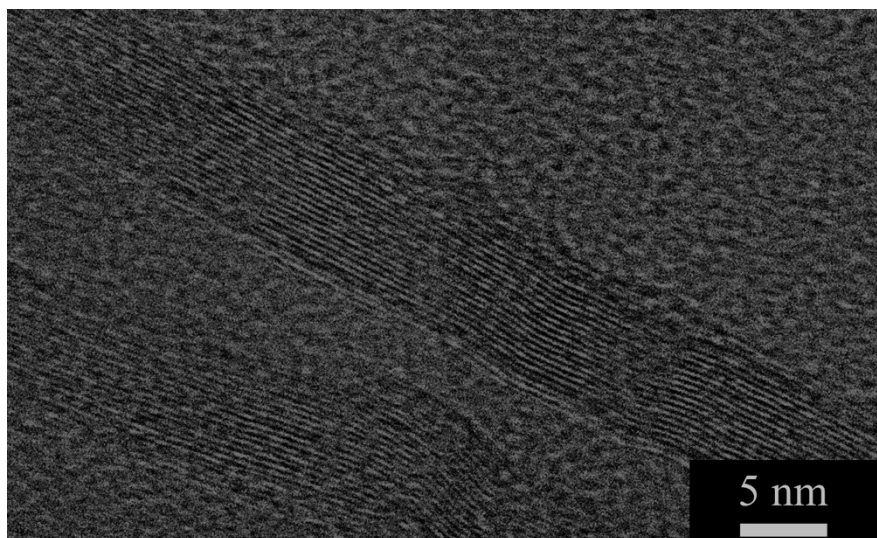
Figure 6.7: Representative HRTEM image of CNTs grown on oxide free copper foil

The Inconel film used in these experiments appears to result in denser CNT growth as opposed to previous results on Ni films[90]. It is difficult at this stage to postulate an exact mechanism that would provide a rigorous explanation for Inconel's behavior leading to the dense, vertical CNT growth on an oxide free substrate. There are three plausible scenarios: a co-catalyst mechanism, the bimetallic catalyst effect, a diffusion barrier effect, and/or the presence of stable chromium oxide at the surface. To explore this further, XPS was used for qualitative and quantitative surface analysis and chemical state information of the copper surface with the oxide layer. A 12 nm Inconel film deposited on copper foil was annealed in the CVD chamber under flowing argon and hydrogen at 770 °C and then removed to analyze the surface composition prior to nanotube growth in the CVD chamber. We observe in figure 6.8a that there are islands on the post-annealed surface. The XPS data (figure 6.8b) obtained from the post-annealed film for the region shown in figure 6.8a reveals the presence of the constituent elements

present in Inconel still on the surface in addition to Cu. Quantitative XPS results show that the Inconel (Ni-Fe-Cr) to copper ratio in terms of atomic percentage is about 67% on the surface of the copper foil. Therefore it is likely that the islands seen in the SEM image are a result of the Inconel breaking up on the surface of the Cu foil, which then exposes some of the underlying copper foil. This data demonstrates that Inconel is still present on the majority of the surface of the copper even after heating in the CVD furnace. Therefore, it is possible that Ni and Fe constituents from the Inconel within these islands can be acting as catalysts in addition to the Fe that is supplied during CVD.

To confirm the catalytic activity of both Inconel and iron, TEM-EDS analysis was carried out on multiple CNTs (obtained from CNTs grown on the oxidized Cu foil) on the copper grid. The TEM-EDS results from CNTs after CVD growth indicate that both Inconel figure 6.9b (inset) and iron nanoparticles [100] (not shown) are found encapsulated at the tips of multiple CNTs. This indicates that both Inconel and iron, from the ferrocene, act as co-catalysts in the CNT growth. Several authors[103,104] have reported models proposing the advantages of using bimetallic catalysts for CNT growth. Deng et al [105] reported that that Ni+Cr and Fe+Cr are very effective as bimetallic catalysts since they energetically favor CNT growth during the nucleation and growth phases in single walled CNTs. They proposed that in a bimetallic catalyst technique, one of the metals would be effective in promoting nucleation of the nanotube while the other metal would aid in the growth of the nanotube. Accordingly, they found that combinations of Ni+Cr and Fe+Cr are very effective bimetallic catalysts. A similar phenomenon could be happening during the CNT growth in the observations reported in here since Inconel is an alloy containing Ni, Cr, and Fe.
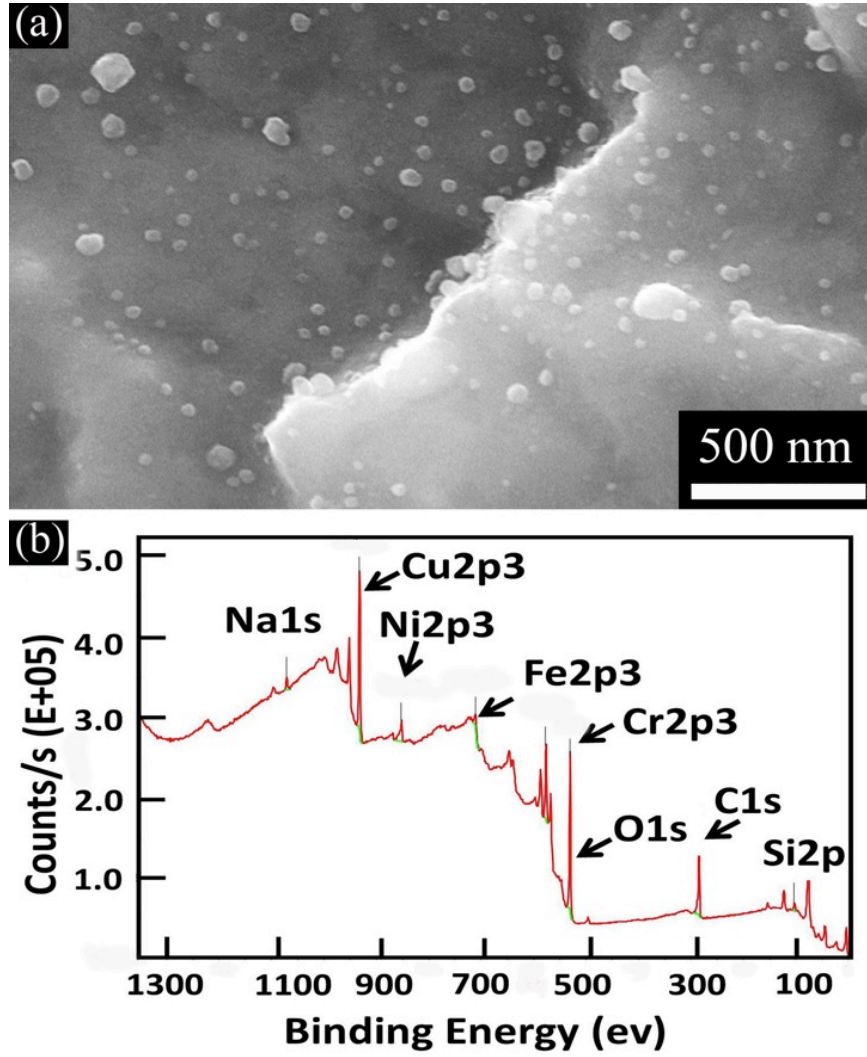
Figure 6.8: (a) SEM image of the surface of copper after annealing a 12 nm thin film of Inconel on the oxidized Cu foil (b) XPS data indicating the presence of constituent elements in Inconel.

The third likely mechanism is that some fraction of the constituent elements of Inconel could potentially act as a diffusion barrier for iron nanoparticles and prevents them from diffusing into the underlying Cu substrate. The presence of such diffusion barriers assists the catalytic activity of iron for CNT growth[55]. Garcia et al.[55] have proposed the use of TiN barrier layer on Cu to prevent the diffusion of Fe at a growth temperature 750 ℃. A similar effect as that of TiN could be happening with the use of Inconel thin films (in addition to their catalytic effect) in the CNT growth reported here if the diffusion of Fe in Cu is lesser due to the presence of a barrier layer[55]. In addition to acting as a barrier to diffusion, the Inconel layer may lead to the formation of stable chromium oxide at the surface.

These results also indicate that a copper oxide surface is not necessary in order to cause the Inconel to "break-up" into the nanoparticles needed for catalyzing nanotube growth. It has been proposed by a number of research groups that the presence of stable non-conductive oxide layers on substrates such as silicon, aid in the formation of metal nanoclusters that act as catalyst sites for CNT growth. Recently, Ajayan's research group[85] has demonstrated the oxide effect on bulk Inconel where chromium oxide aids the growth of aligned nanotubes. In this particular case, the presence of chromium oxide in bulk Inconel assists in the formation of iron nanoclusters that then catalyze CNT growth.

However, based on our results, we believe that the thin film can act as a supporting catalyst even without an oxide layer present underneath. One explanation for this could be the relative difference in surface energies of the substrate and catalyst. From the standpoint of relative surface energies, the elemental components of Inconel (Cr, Fe in particular), could also

play a key role in catalyzing CNT growth[106]. This has been discussed in section 5.2. The surface energy theory is to some extent supported by the XPS data (figure 6.8) which showed that this Inconel may not fully cover the copper surface after heating and instead form small Inconel rich islands or surface patches.

The type of thin film, the carbon precursor along with the effects of surface roughness and native oxides has been tackled to achieve the optimized density and alignment of CNTs. At this stage, the application of the CNT-Cu system in the context of energy storage was critical to explore. The use of such a system for potential use in capacitors is addressed in the next chapter.

# 7.0 ELECTROCHEMICAL CHARACTERIZATION OF CNTS FOR SUPERCAPACITOR APPLICATIONS

## 7.1 INTRODUCTION

In order to observe the potential for use in practical applications such as supercapacitors, we tested the CNT-Cu samples as double layer capacitors (DLC) using the "Swagelok" type arrangement discussed in section 2.4 of the dissertation. This section contains the results for CNTs tested as double layer capacitors using Inconel and Ni thin films. The power density and specific capacitance values are also reported for CNTs grown on oxidized Cu foils and oxide free copper substrates. It is observed from our results that there is a vast improvement in the charge storage capacity of the CNTs when grown on oxide free Cu substrates using Inconel thin films.

## 7.2    RESULTS AND DISCUSSION

### 7.2.1    CNTs grown using Ni thin films on oxidized Cu substrates

In the first set of experiments involving the use of Ni thin films, a 20 nm Ni film was first deposited on the copper foil followed by CVD growth. The CNT growth using the Ni thin film is shown in figure 7.1a. We observe in figure 7.1a that the CNTs preferentially grow in a vertical direction but the density of the CNTs is relatively low. There are also regions on the copper substrate where no CNT growth is observed. We believe that localized CNT growth using Ni thin films on copper occurs due to changes in the chemical composition of the copper surface and that Ni itself may not be acting as an actual catalyst for CNT growth [90]. In this case, the Ni is instead acting as a support for the iron catalyst particles that are formed from ferrocene and that lead to nanotube growth. The change in the surface composition of copper due to the Ni thin film is likely not even and hence not conducive for uniform catalytic activity on this surface from the iron nanoparticles [90]. This is possibly the reason we see less dense, non-uniform CNT growth when using Ni thin films.

The CV measurements made using a CHI potentiostat at 1000 mVs$^{-1}$ on the CNTs using the Ni film are shown in figure 7.1b. The power density value reported using this technique is 0.01 kWkg$^{-1}$. The low power density could be due to lower CNT yield per unit area of the substrate, in other words, insufficient CNT (electrode) coverage on the copper substrate leads to

lower charge storage capacity. The nearly linear region that we observe in figure 7.1b could simply be the resistance from the copper substrate itself where there is no CNT growth. Thus CNT growth using Ni thin films may not be the best choice for use in capacitors due to low CNT density unless ways can found to make the surface composition more uniform. In an effort to improve upon the power density values, aligned CNTs grown using Inconel thin films were tested.
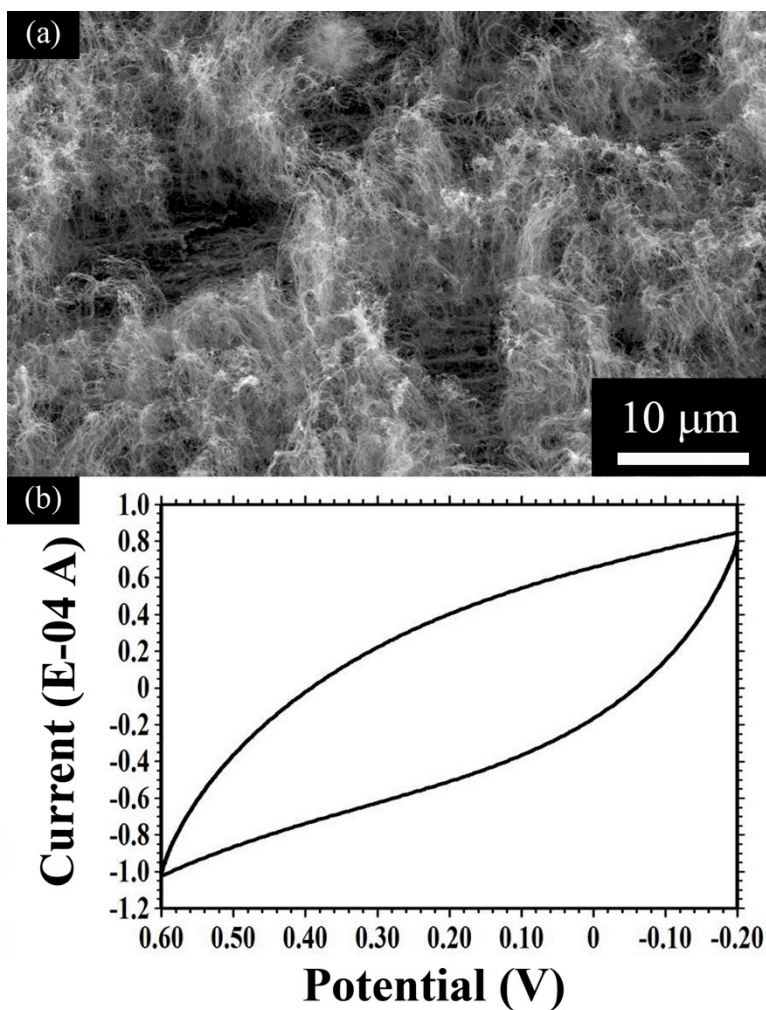
Figure 7.1 (a): CNT growth on copper foil using 20 nm thick Ni film and iron from ferrocene (b): CV measurement from the CNTs grown on Cu foil using Ni thin film at a scan rate of 1000 mVs-1.

### 7.2.2   CNTs grown using Inconel thin films on oxidized Cu substrates

The second set of experiments was carried out using Inconel thin films (~12 nm thick) on copper foil followed by CVD growth of nanotubes. The CNT growth using the Inconel thin film is shown in figure 7.2a. We observe longer, denser and better-aligned CNTs in comparison to the CNT growth observed using Ni thin films. In addition, the CNTs appear to be growing in configurations that resemble dense bundles. The greater density of CNTs and better coverage seen with Inconel has been discussed in section 5.2 of the dissertation.

When the CNTs grown using Inconel thin films on copper were tested for capacitive behavior, we observed rectangular shaped CV curves at very high scan rates (1000 mVs$^{-1}$) in figure 7.2b. The rectangular shape of the CV curves is typical of ideal capacitive behavior [63,76] and suggests low contact resistance between the as-grown CNTs and the underlying copper substrates. The power density for the DLC tested using this method is calculated to be 3.5 kWkg$^{-1}$ and is comparable to the values reported in the literature where testing was done using binders [63]. This value of power density is much higher then the value obtained from using Ni thin films due to the longer, better aligned, denser bundles of CNTs that lead to higher charge storage capacity. For supercapacitor applications, the growth of aligned, high density CNTs directly on copper substrates is very advantageous. Traditionally CNTs grown on non-conductive substrates (quartz, $SiO_2$/Si) are transferred onto copper that involves the use of binders and solvents [63]. In the process, the surface morphology and the alignment of CNTs are altered thus affecting their charge storage capabilities. We also observe another impressive property in that, the CNT-Cu

system remains robust even after 500 cycles at a scan rate of 1000 mVs$^{-1}$ thus ideally suited for rapid charge and discharge applications at high scan rates.
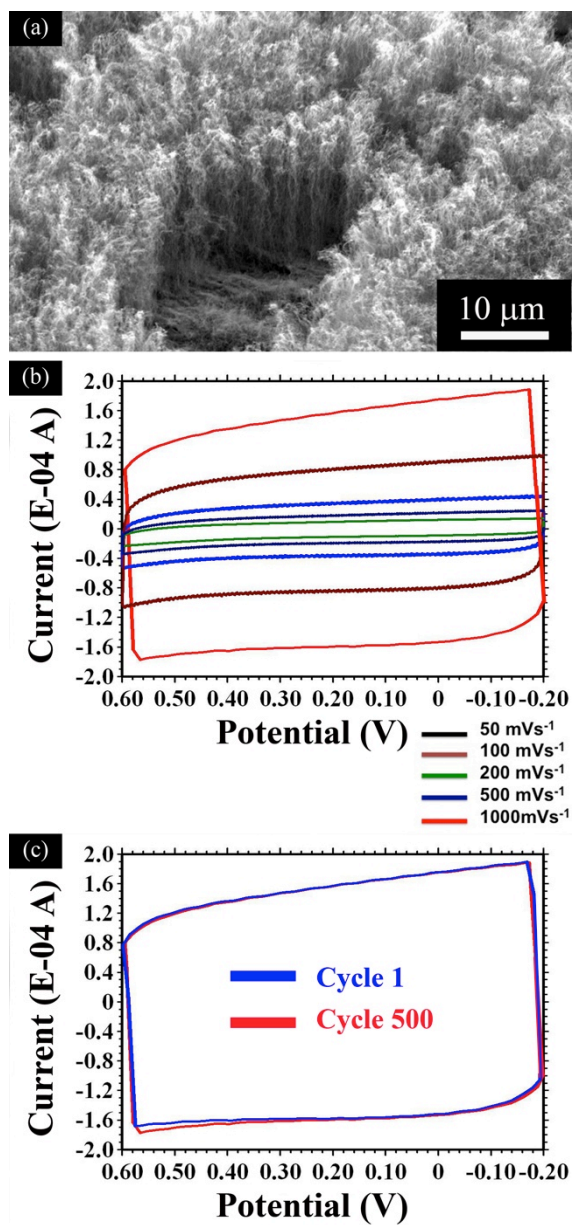
Figure 7.2: (a) CNT growth on copper foil using 12 nm Inconel thin film (b) CV measurements of the CNTs on copper at five different scan rates (c) CV measurement at a scan rate of 1000 mVs-1 for cycle 1 and cycle 500.

## 7.3    CNTS GROWN USING INCONEL THIN FILMS ON OXIDE FREE CU SUBSTRATES

In order to improve the power density and test the specific capacitance values of the CNTs grown on oxidized copper foils, electrochemical testing was done on oxide free Cu substrates. From the experimental results described in section 6.2.1, CNTs were grown on oxide free Cu substrates using $Si/SiO_2$ support substrates.  However, the copper films on Si wafers cannot be tested using this method.  Therefore, it was necessary to make a new set of substrates in which the native oxide was removed from a copper foil before depositing Inconel and growing nanotubes. Several studies have been conducted in the semiconductor industry to prevent surface oxidation of copper, as the presence of oxides will induce an added resistance. Studies conducted have proposed passivating the surface by self-assembled monolayers of n-Alkanethiolates[107,108]. More recent studies[101] have indicated the use of organic acids such as oxalic acid and acetic acid. The use of organic acids as opposed to inorganic acids has been shown to have the least effect on surface roughness during the removal of oxides by chemical etching. For experiments that were conducted to compare the growth of CNTs on pristine Cu foils, the native oxides were stripped off using the method proposed by Chavez and Hess[101]. The technique employs copper foils dipped in glacial acetic acid (99.8% pure) in Pyrex beakers using stir bar rotated at 500 rpm at room temperature for a period of about 10 minutes. Acetic acid reacts effectively removes the oxides of copper without reacting with the underlying pure metallic copper.  Upon removal of oxides, the copper foils were transferred immediately to the load lock of the sputtering system to pump down to $10^{-6}$ Torr. It is therefore possible to remove the oxide from the surface of the copper before depositing the catalyst film in order to determine the effect it has on the catalyst

layer. This technique removes the natives copper oxides without reacting with the underlying pure copper and does not affect the surface roughness of the substrate. Sputtering an additional 300 nm copper onto the foil surface and then the 12 nm Inconel layer before the CVD growth followed the removal of the oxide layer.

For an applied voltage range between -0.2 V and +0.6 V, we observed rectangular shaped CV curves at a scan rate of 1000 mVs$^{-1}$ in figures 7.3a and 7.3b for both sets of samples. The power density for the CNTs grown using this method on unoxidized copper surface is reported as 4.48 kWkg$^{-1}$. As before, the CNT-Cu system remains robust even after 500 cycles at a scan rate of 1000 mVs$^{-1}$. From figure 7.3b, we observe a higher power density value for the CNTs grown on copper without the oxide layer. This could be due to a greater packing density of the CNTs (figure 6.6b) allowing for greater charge storage. Figure 7.3c shows the CV curves for the DLC on oxide free copper surface tested at various scan rates. The reported electrochemical results were obtained for growth time of 30 minutes.
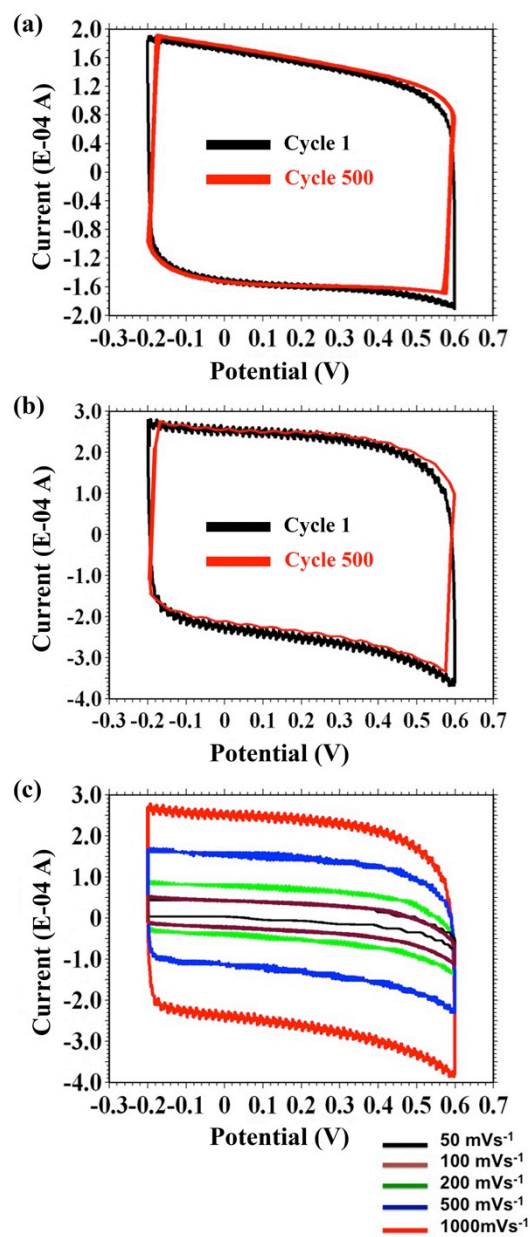
Figure 7.3: (a) CV curve for CNTs on oxidized copper foil at 1000 mVs-1 for cycle 1 (black) and

cycle 500 (red) (b) CV curve for CNTs on oxide free copper surface at 1000 mVs-1 for cycle 1

(black) and cycle 500 (red) (c) CV curve for CNTs on oxide free copper surface at different scan

rates.

Specific capacitance testing in the galvanostatic mode was also done on the CNT electrodes grown on oxide free Cu substrates using the formula described in section 2.4. A constant current of 1 mA was applied for the charge discharge process. Based on the slope of the curve in figure 7.4, the specific capacitance value was calculated to be 30 $Fg^{-1}$. This value is higher than those reported for CNTs grown directly on Inconel[47].
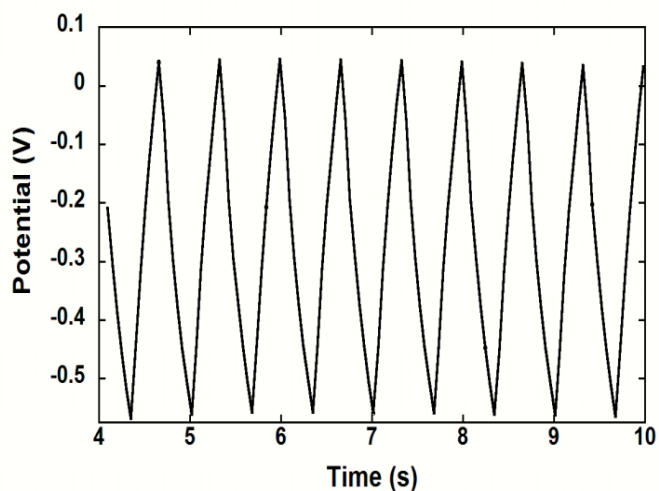


Figure 7.4: Charge–discharge cycle data obtained at a constant current of 1 mA. The discharge slope was used to calculate the specific capacitance of the device.

Raman analysis was done to check the graphitic crystallinity of the CNTs grown using Inconel films. The presence of long range ordered crystalline graphite as opposed to amorphous carbon promotes charge storage capacity. From the Raman spectrum in figure 7.5, we report an $I_d/I_g$ ratio of 1.07, which indicates that there are some defects (broken sp2 bonds, amorphous carbon) in the CNTs grown. We observe a sharp G' peak in figure 4 indicating that is very good long range order in the CNTs grown using Inconel films on copper. In addition, Dileo et al. [84] reported that a higher G'/G peaks ratio is indicative of greater "average purity" (crystallinity) of the CNTs. For the CNTs grown on Inconel films, the G'/G ratio is 0.86 and for the CNTs grown using Ni thin films, it is 0.79. Thus Inconel films also yield better quality (higher purity) CNTs.
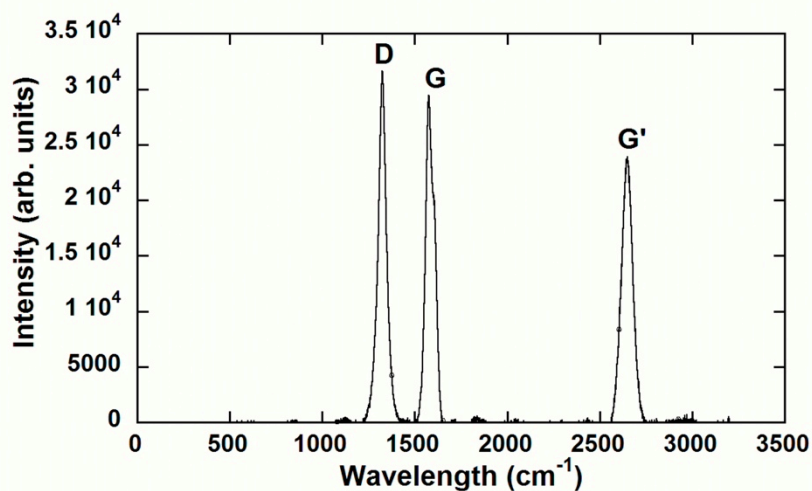


Figure 7.5: Raman spectrum for the CNTs grown using Inconel thin films and iron (from ferrocene) on copper.

The growth time was increased to observe its effect on power density and specific capacitance values. CNT growth was carried out from 30, 45, 60, 75 and 90 minutes. It was found that the optimal growth time for the highest values for power density (~ 12 kWkg$^{-1}$) and specific capacitance (~80 Fg$^{-1}$) were obtained for growth time of 45 minutes (figure 7.6). The CNT growth was carried out on copper foils with the oxide layer that was removed using acetic acid as described in section 6.2.
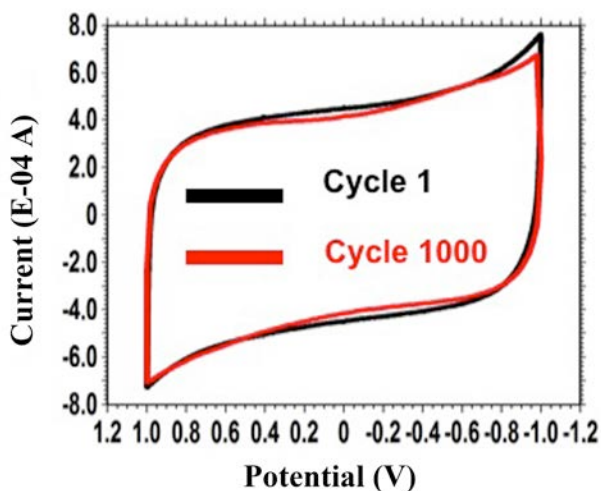


Figure 7.6: CV curve for CNTs on oxide free copper foil at 1000 mVs-1 for cycle 1 (black) and cycle 1000 (red) for a growth time of 45 minutes.

A comparison of results from the electrochemical testing results is presented in table 7.1. Based on the values obtained in table 7.1, it is observed that the Inconel thin films in combination with ferrocene with optimized CNT length provide the maximum values of power density (~10-12 kWkg$^{-1}$) and specific capacitance (~70-80 Fg$^{-1}$).

Table 7.1: Tabulated values of results from electrochemical testing of CNTs on Cu

| Capacitor Type | Power Density (kWkg$^{-1}$) | Specific Capacitance (Fg$^{-1}$) |
|---|---|---|
| Ni thin films, oxidized Cu substrates | 0.01 | 5 |
| Inconel thin films, oxidized Cu Substrates | 2.5 | 20 |
| Inconel thin films, oxide free Cu Substrates | 4.4 | 35 |
| Inconel thin films, oxide free Cu substrates, optimized growth time | 8-10 | 65-80 |
| Commercial capacitors | 10 | 120[60] |

# 8.0    SUMMARY AND FUTURE WORK

## 8.1    SUMMARY OF RESULTS AND CONCLUSIONS

The use of dense and aligned CNT forests on conductive copper substrates may provide a new platform for the development of novel and high-energy storage systems such as batteries and supercapacitors. In order to exercise control on the storage capacity and the lifetime of such potential devices, a fundamental understating of the growth and synthesis of CNT electrodes is necessary. The optimization of the various growth conditions with respect to the catalyst and the substrate to achieve the greatest possible density and alignment has been demonstrated by the experimental results discussed in the dissertation.

CNTs grown on Ni catalyst films using methane at 900 $^{\circ}$C show poor coverage that could likely be due to the non-formation of nickel islands on the copper surface needed to catalyze the CNT growth. The diameters of the CNTs grown using the methane source are larger than those grown at lower temperatures using acetylene source. CNTs grown using acetylene at 650 $^{\circ}$C also show better coverage and are smaller in diameter. Raman data also indicates that the quality of CNTs is better using the acetylene source at 650 $^{\circ}$C. Hence acetylene is a better choice for large-scale synthesis of multiwalled CNTs on copper using a Ni catalyst film. The concept of linear relationship between the diameter of CNTs and the thickness of the Ni metal catalyst for a

thermal CVD technique is also demonstrated. It is believed that the effects of decreased diffusion on the Ni film using lower growth temperature can explain these results.

The results from a Ni enriched Cu surface show that it is beneficial in obtaining dense vertically aligned CNT growth on bulk copper foil substrates when using a thermal CVD method with additional Fe catalyst supplied during growth. The results are comparable to what has previously been reported for PECVD growth of CNTs. The method proposed here, using a single thin Ni layer, is relatively simple in comparison to others that use multiple barrier films of different thicknesses that would also add to the contact resistance. To obtain these results, the xylene/ferrocene mixture is critical, as CNTs grown using only a nickel film or only iron, from ferrocene, as the catalyst show poor coverage and alignment. For the case of the xylene/ferrocene growth, the Ni enriched surface acts as a support for the Fe catalyst that results in densely aligned CNT growth. It is believed that thinner nickel films result in better alignment due to compositional modification of the surface of the Cu on a smaller scale, as opposed to thicker films where the nickel can form large surface islands, which may hinder CNT growth due to their size.

In an effort to improve the alignment and length of CNTs obtained using Ni thin films, the growth of aligned CNTs on copper using an Inconel thin film catalyst and iron, from ferrocene decomposition during CVD proved to be a better option. Since only a single thin film of Inconel is required, this eliminates the need for additional barrier layers that could lead to higher contact resistance between the substrate and the carbon nanotubes. An Inconel thin film in conjunction with iron particles appears to work together as excellent catalysts in promoting

dense and aligned CNT growth on copper. Particularly, this combination on a smooth, oxide free copper surface could be the synergetic combination that promotes dense, aligned CNT growth using a simple thermal CVD nanotube growth chamber and also results in good contact between the nanotubes and the underlying conductive Cu substrate. This direct CNT growth mechanism described here and their potential application for energy storage offers new insights into aligned CNT growth studies on bulk metals devoid of native oxides.

The length of the CNT vs the growth time (using Inconel films) is shown in figure 8.1. It is widely known that the growth of CNTs in a thermal CVD abruptly terminates once it reaches a maximum due to catalytic deactivation[32,109]. Meshot and Hart[109] also observed that in addition to an abrupt termination of CNT growth, there is also a loss of alignment of CNTs that begins with a slow decay of growth. These results are consistent with the observations made from our experiments (using optimized Inconel thin film thickness with xylene and ferrocene combination) where there was loss of alignment of CNTs beyond a growth time of 45 minutes. Based on our results, the optimized CNT growth time range and length are 30-45 minutes and 20 μm respectively.
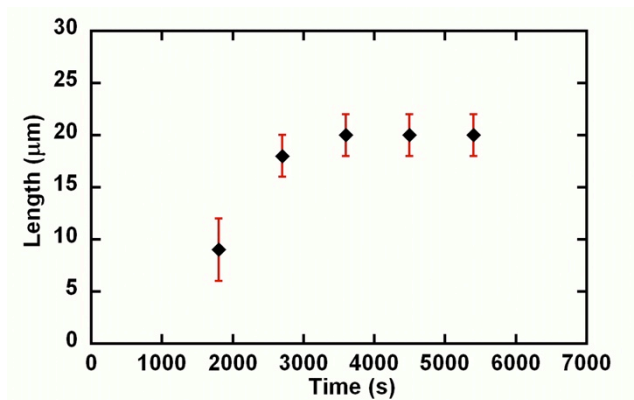
Figure 8.1: CNT length vs growth time for optimized Inconel film thickness using xylene source and ferrocene.

The comparative growth, alignment and the electrochemical properties of the CNTs grown on copper using Ni and Inconel thin films have also been discussed. CNTs grown on copper using Inconel thin films prove to be superior in terms of alignment and density thus making them better suited for potential charge storage applications such as supercapacitors. It is worthwhile to note that the as fabricated CNT electrodes on copper using Inconel thin films remain robust even after 1000 cycles at high scan rates of 1000 $mVs^{-1}$.

In conclusion, table 8.1 summarizes the various growth parameters and results obtained using nickel and Inconel thin films on copper. It is observed from table 8.1 that CNT growth using Inconel thin films are superior in terms of the actual CNT growth and their application as double layer capacitors.

Table 8.1: A comparison of optimized values for CNT growth using nickel and Inconel thin films using thermal CVD growth technique

| Catalyst Film Type | Optimal Thickness of Film (nm) | Carbon Precursor | Linear Density of CNTs CNTs/µm | Power Density (kWkg$^{-1}$) | Specific Capacitance (Fg$^{-1}$) | G'/G (no units) |
|---|---|---|---|---|---|---|
| Nickel | 20 | Xylene | $3 \pm 2$ | 0.01 | ~5 | 0.79 |
| Inconel | 10-15 | Xylene | $12 \pm 3$ | 10-12 | ~70-80 | 0.86 |

## 8.2    FUTURE WORK

### 8.2.1    Cross Sectional TEM investigation of CNTs

A set of experiments will be required to determine if CNT growth follows root or tip mode during the CVD process. From the TEM images we have obtained thus far, we observe that the innermost wall MWCNTs are filled with catalyst material. We also observe catalyst material at the tip of the MWCNTs. This could mean that the CNT growth is likely to be tip mode. Sonicating the CNT containing substrates in acetone for about 10 minutes followed by casting the resulting solution on a copper grid makes TEM samples for CNTs. However, this technique could cause the catalyst (if present at the base of the CNTs) to peel off the root of CNTs during the sonication procedure. In order to confirm the actual mode of CNT growth, cross sectional samples of CNT forest will need to be done using the Seiko Dual Beam FIB in the Nano Fabrication and Characterization Facility (NFCF) at the University of Pittsburgh. The procedure involves growth of CNTs on sputtered Cu on $SiO_2$/Si substrates as described in section 6.2 of the dissertation. The growth of CNTs on a supporting $SiO_2$/Si wafer makes it suitable to mill portions of the substrate containing CNTs. This will be followed by lifting off the milled portion and anchoring it on to copper grid. This process will facilitate the observation of the sample using TEM to determine the precise location of the catalyst particle.

### 8.2.2   Quantification of CNT alignment and density.

In section 6.1, an attempt to quantify the CNT density was demonstrated. However a more detailed analysis is necessary to draw valid conclusions about the observed alignment of CNTs in relation to the catalyst density. It has been proposed that the nanoparticle diameter (D) scales with the average film thickness $(d_f)$[110,111] as

D ~ 6 $d_f$. So the nanoparticle density $(N_p)$ varies as

$$N_p = \frac{1}{30\ d_f^2}$$

Esconjauregui et al.[110] proposed that the method to quantify CNT alignment and density by way of counting using TEM and SEM data could potentially lead to an overestimate in the CNT density. So the alternative technique that could lead to more accurate results is utilize the weight gain method. In this method, the areal CNT density (CNTs/cm$^2$) can be derived from sample weight post growth, divided by the average CNT height and the nanotube mass per unit length calculated from its diameter, number of nanotube walls measured using TEM[110]. Calculations made using this technique could provide insights into quantifying CNT density thus lending credibility to the usage of the misnomer "vertically aligned CNTs".

### 8.2.3 Effect of the thickness of catalyst thin films

It has been proposed in chapter 4 of the dissertation that the critical thickness of the Ni thin film for the best possible CNT growth to be around 20 nm as opposed to 12 nm for Inconel thin films. Further growth studies are warranted to observe the effect of decreasing the Ni film thickness to understand if the chemical composition of the surface (Ni enriched Cu) would still support CNT growth.  In the experimental results discussed in the dissertation, Ni and Inconel thin films in conjunction with ferrocene proved to be the best combination. Ni films work by modifying the Cu surface composition (chapter 4). Inconel thin films work by acting as co-catalysts along with iron from ferrocene decomposition (chapter 5 and chapter 6). Inconel alloy films also prove to be superior due to the presence of high surface energy elements present (Cr, Fe and Ni). It would be worthwhile to observe the resulting CNT growth when Fe thin films in conjunction with ferrocene were used. It has been observed that stand alone Fe thin films103 do not result in aligned CNT growth. Fe has a higher surface energy[96] in relation to copper and could potentially work with additional catalyst support from ferrocene decomposition.  Similar to the work done using Ni and Inconel thin films, a critical film thickness for Fe would have to be calculated to tailor the resulting CNT growth for alignment and density.  The use of a single high surface energy Fe (which is also a component of Inconel) film could also help in understanding the validity of the bimetallic catalyst effect that has been postulated for the effectiveness of Inconel alloy films.

### 8.2.4   CVD growth parameters: hydrogen gas and addition of water vapor, air oxidation

A number of parameters such as growth temperature, catalyst film composition, catalyst film thickness were explored in this dissertation in an effort to understand and improve CNT growth, density and alignment. One other important CVD growth parameter namely the timing and the duration of hydrogen introduction into the CVD chamber, needs to be studied in greater detail to gain better understanding of the mechanism of catalyst role in the CNT growth. It has been proposed that CNT growth via thermal CVD involves two important steps: reduction of catalyst particle and the nucleation and growth of CNTs from the catalyst particle[113]. It is generally assumed that CNT growth begins once the catalyst has been activated, in other words, the catalyst needs to be deoxidized to promote CNT growth. A number of workers[37,114] have proposed that a particle is catalytically active if it is in its metallic (devoid of oxides) state. Nessim et al.[113] have conducted extensive studies to study the effect of the amount, duration of hydrogen exposure on CNT growth on $SiO_2$/Si substrates with Fe catalyst. They concluded that hydrogen exposure (~30 minutes), ~ 12 minutes after the introduction of the carbon precursor greatly increases the areal density of CNTs in a thermal CVD technique. A similar study on the effect of hydrogen on the thin film catalysts (Ni and Inconel) and iron nanoparticles could provide some insight into controlling the areal density of the CNTs using the technique described in the dissertation (chapter 5 and chapter 6). It would also be interesting to study the effect of hydrogen on the iron atoms decomposing from ferrocene. Hydrogen is known to aid iron's catalytic activity by reducing it to the zero oxidation state. The zero oxidation state iron adatoms become mobile on the substrate surface leading to the formation of nanoparticles that catalyze CNT growth.

Other workers[35] have suggested that the slight addition of water vapor leads to a dramatic increase in the length of aligned SWCNTs (millimeters long SWCNTS have been reported). The presence of the water vapor has been shown to etch amorphous carbon from catalyst particle surface, prolonging the catalytic life of the particle. It would be instructive to see if a similar effect can be observed in the case of MWCNTs on copper.

In an effort to reduce the amount of amorphous carbon that was present in the samples, air oxidation of the CNT samples was carried out. This was done post CNT growth at 450 ℃ for about 60 minutes. Air oxidation of CNTs was carried out in an effort to increase the power density and specific capacitance of the CNTs. The electrochemical testing results post air oxidation (growth time 30 minutes) did not result in substantial increase in the values for power density ($\sim$6 kWkg$^{-1}$) and specific capacitance (35 Fg$^{-1}$). This was not explored in detail (varying the other growth parameters such as growth time, xylene/ferrocene concentration) and is worth exploring as part of experiments to be conducted in the future.

### 8.2.5 Support structures for Si based anodes for batteries

There have been a number of efforts in recent years to use aligned CNTs grown on quartz as conductive support structures for Si based anodes on $SiO_2$/Si substrates[44] for batteries. The use of amorphous Si obtained via silane decomposition (at 500 °C) in a thermal CVD chamber results in high specific capacitances of about 4200 mAhg$^{-1}$. The drawbacks in using this method include

the growth of CNTs on non-conductive substrates such as quartz. The CNT-Si material on quartz is scraped off and using binders and solvents, it is coated as slurry on copper followed by battery testing. The potential loss of CNT alignment and change in the surface chemical composition of CNTs due to the binder used could be mitigated if CNTs were grown directly on copper. This scenario has been discussed in chapter 7 of the dissertation, in the context of capacitor testing. In addition, using CVD silane decomposition[44] method for amorphous Si deposition on the CNTs at 500 °C is a disadvantage due to the formation of copper silicides[115] at 300 °C. Silicide formations lead to copper substrate embrittlement causing a complete breakdown of the CNT-Cu system. This could be overcome by using sputtered Si at room temperature, post CNT growth and testing the resulting CNT-Si system on copper as a battery.

### 8.2.6   Support structures for photovoltaic applications

Carbon nanotube superstructures have large active surfaces suitable for photon absorption and harvesting solar energy for photovoltaic applications. An individual single walled carbon nanotube (SWCNT) which can act as a p-n junction has been shown to produce photocurrent[116,117]. Freitag et al.[117] have determined the mechanism of photocurrent generation involves the resonant excitation of the second exciton state of the semiconducting nanotube, which then decays to produce electron hole pairs [117]. Unaligned films of SWCNTs have also been shown to produce a photocurrent, with efficiencies reported from 0.15%[118,119]. MWCNTs have also been shown to generate a large photocurrent with an efficiency of about 7% in the visible and ultra violet spectral range[120]. MWCNTs (due to conduction form the multiple

walls)[121] have potential advantages over SWCNTs since the latter is known to have lesser conductivity. Statistically only of ~ 35% of SWCNTs on a given substrate are known to directly contribute to conduction[113].

The dispersion of metal nanoparticles on random MWCNTs has been shown to increase the photoconversion efficiency as compared to undecorated CNTs[122]. Metal nanoparticles of nickel [123-125], iron[126] and copper[127,128] have shown promising results. The photoactive metal nanoparticles serve to enhance the intrinsic ability of MWCNTs to behave as efficient low dimensional media for generating electron hole pairs[127,128]. The electrical and photoelectrical effects of depositing metallic nanoparticles on aligned MWCNTs could have more benefits due to access to greater CNT surface area. This could help in enhancing the fundamental interactions between the nanoparticles and the CNTs.

The efficiency of solar cells has always been a contentious issue with maximum attainable (practical) efficiencies at about 10% for dye sensitized solar cells (DSSC)[129]. We propose using MWCNTs with sputtered metallic nanoparticles to improve the efficiencies of solar cells. In traditional DSSCs (without CNTs), the electrons rely on their mean free path for current generation. The use of CNTs gives the electrons a direct path to the current collecting electrode with very low resistivity. Growing CNTs on a transparent, conducting electrode is necessary for photocurrent generation. Fluorine doped tin oxide (FTO) substrates are a viable option. However, currently CNTs grown on non-conducting quartz substrates are scraped off and cast onto FTO substrates. In the process the CNT alignment and potential photoconversion efficiency is lost[130]. It would be useful to study if the current recipe of using an extremely thin

sputtered layer of Inconel on FTO and iron from ferrocene decomposition can be used to obtain

the desired aligned CNTs and test them for improved photoconversion efficiency.

# REFERENCES

[1] S. Iijima, Nature **354**, 56-58 (1991).

[2] P.C. Eklund, G. Dresselhaus, and M.S. Dresselhaus, *Science of Fullerenes and Carbon Nanotubes* (Academic Press, New York, USA, 1996).

[3] P. Harris, *Carbon Nanotubes and Related Structures* (Cambridge University Press, Cambridge, UK, 1999).

[4] Fan, Chapline, Franklin, Tombler, Cassell, and Dai, Science **283**, 512-514 (1999).

[5] W.Z. Li, S.S. Xie, L.X. Qian, B.H. Chang, B.S. Zou, W.Y. Zhou, R.A. Zhao, and G. Wang, Science **274**, 1701-1703 (1996).

[6] T.W. Ebbesen and P.M. Ajayan, Nature **358**, 220-222 (1992).

[7] C. Niu, E.K. Sichel, R. Hoch, D. Moy, and H. Tennent, Appl. Phys. Lett. **70**, 1480 (1997).

[8] Y. Soneda and M. Makino, Carbon **38**, 478-480 (2000).

[9] D. Park, Y. Hoon Kim, and J. Kee Lee, Carbon **41**, 1025-1029 (2003).

[10] L. Yuan, K. Saito, W. Hu, and Z. Chen, Chemical Physics Letters **346**, 23-28 (2001).

[11] Y.J. Jung, S. Kar, S. Talapatra, C. Soldano, G. Viswanathan, X. Li, Z. Yao, F.S. Ou, A. Avadhanula, R. Vajtai, S. Curran, O. Nalamasu, and P.M. Ajayan, Nano Letters **6**, 413-418 (2006).

[12] C. Du, J. Yeh, and N. Pan, Nanotechnology **16**, 350-353 (2005).

[13] S.J. Tans, A.R.M. Verschueren, and C. Dekker, Nature **393**, 49-52 (1998).

[14] Y. Tang, G.P. Kotchey, H. Vedala, and A. Star, Electroanalysis **23**, 870-877 (2011).

[15] D.R. Kauffman, C.M. Shade, H. Uh, S. Petoud, and A. Star, Nature Chem **1**, 500-506 (2009).

[16] D.R. Kauffman, D.C. Sorescu, D.P. Schofield, B.L. Allen, K.D. Jordan, and A. Star, Nano Lett. **10**, 958-963 (2010).

[17] D.R. Kauffman and A. Star, Angew. Chem. Int. Ed. **47**, 6550-6570 (2008).

[18] Y. Wang, Z. Luo, B. Li, P.S. Ho, Z. Yao, L. Shi, E.N. Bryan, and R.J. Nemanich, J. Appl. Phys. **101**, 124310 (2007).

[19] T. de los Arcos, F. Vonau, M.G. Garnier, V. Thommen, H.-G. Boyen, P. Oelhafen, M. Düggelin, D. Mathis, and R. Guggenheim, Appl. Phys. Lett. **80**, 2383 (2002).

[20] G.G. Tibbetts, Journal of Crystal Growth **66**, 632–638 (1984).

[21] J.H. Hafner, M.J. Bronikowski, B.R. Azamian, P. Nikolaev, A.G. Rinzler, D.T. Colbert, K.A. Smith, and R.E. Smalley, Chemical Physics Letters **296**, 195–202 (1998).

[22] R.T.K. Baker, P.S. Harris, R.B. Thomas, and R.J. Waite, Journal of Catalysis **30**, 86-95 (1973).

[23] H. Dai, A.G. Rinzler, P. Nikolaev, A. Thess, D.T. Colbert, and R.E. Smalley, Chemical Physics Letters **260**, 471–475 (1996).

<sup>24</sup> J.W.G. Wildoer, L.C. Venema, A.G. Rinzler, R.E. Smalley, and C. Dekker, Nature **391**, 59–62 (1998).

<sup>25</sup> E.G. Gamaly and T.W. Ebbesen, Physical Review B **52**, 2083 (1995).

<sup>26</sup> T. Guo, P. Nikolaev, A. Thess, D.T. Colbert, and R.E. Smalley, Chemical Physics Letters **243**, 49–54 (1995).

<sup>27</sup> M. Endo, K. Takeuchi, S. Igarashi, K. Kobori, M. Shiraishi, and H. Kroto, Journal of Physics and Chemistry of Solids **54**, 1841-1848 (1993).

<sup>28</sup> Z.P. Huang, D.Z. Wang, J.G. Wen, M. Sennett, H. Gibson, and Z.F. Ren, Applied Physics A: Materials Science & Processing **74**, 387-391 (2002).

<sup>29</sup> M. Meyyappan, L. Delzeit, A. Cassell, and D. Hash, Plasma Sources Sci. Technol. **12**, 205-216 (2003).

<sup>30</sup> C. Bower, W. Zhu, S. Jin, and O. Zhou, Appl. Phys. Lett. **77**, 830 (2000).

<sup>31</sup> P. Poncharal, Z.L. Wang, D. Ugarte, and W.A. de Heer, Science **283**, 1513 -1516 (1999).

<sup>32</sup> G.D. Nessim, Nanoscale **2**, 1306 (2010).

<sup>33</sup> T. Nozaki, K. Ohnishi, K. Okazaki, and U. Kortshagen, Carbon **45**, 364-374 (2007).

<sup>34</sup> M. Cantoro, S. Hofmann, S. Pisana, V. Scardaci, A. Parvez, C. Ducati, A.C. Ferrari, A.M. Blackburn, K.-Y. Wang, and J. Robertson, Nano Letters **6**, 1107-1112 (2006).

<sup>35</sup> K. Hata, D.N. Futaba, K. Mizuno, T. Namai, M. Yumura, and S. Iijima, Science **306**, 1362 - 1364 (2004).

[36] G. Zhang, D. Mann, L. Zhang, A. Javey, Y. Li, E. Yenilmez, Q. Wang, J.P. McVittie, Y. Nishi, J. Gibbons, and H. Dai, Proceedings of the National Academy of Sciences of the United States of America **102**, 16141 -16145 (2005).

[37] S. Hofmann, R. Sharma, C. Ducati, G. Du, C. Mattevi, C. Cepek, M. Cantoro, S. Pisana, A. Parvez, F. Cervantes-Sodi, A.C. Ferrari, R. Dunin-Borkowski, S. Lizzit, L. Petaccia, A. Goldoni, and J. Robertson, Nano Letters **7**, 602-608 (2007).

[38] A.J. Hart and A.H. Slocum, J. Phys. Chem. B **110**, 8250-8257 (2006).

[39] S. Hofmann, G. Csányi, A.C. Ferrari, M.C. Payne, and J. Robertson, Phys. Rev. Lett. **95**, 036101 (2005).

[40] L. Delzeit, C.V. Nguyen, B. Chen, R. Stevens, A. Cassell, J. Han, and M. Meyyappan, J. Phys. Chem. B **106**, 5629-5635 (2002).

[41] C. Zhang, F. Yan, C.S. Allen, B.C. Bayer, S. Hofmann, B.J. Hickey, D. Cott, G. Zhong, and J. Robertson, J. Appl. Phys. **108**, 024311 (2010).

[42] L. Gao, A. Peng, Z. Wang, H. Zhang, Z. Shi, Z. Gu, G. Cao, and B. Ding, Solid State Communications **146**, 380-383 (2008).

[43] S. Esconjauregui, C.M. Whelan, and K. Maex, Carbon **47**, 659-669 (2009).

[44] W. Wang and P.N. Kumta, ACS Nano **4**, 2233-2241 (2010).

[45] G. Li, S. Chakrabarti, M. Schulz, and V. Shanov, Journal of Materials Research **24**, 2813-2820 (2009).

[46] S.K. Pal, S. Talapatra, S. Kar, L. Ci, R. Vajtai, T. Borca-Tasciuc, L.S. Schadler, and P.M. Ajayan, Nanotechnology **19**, 045610 (2008).

[47] S. Talapatra, S. Kar, S.K. Pal, R. Vajtai, L. Ci, P. Victor, M.M. Shaijumon, S. Kaur, O. Nalamasu, and P.M. Ajayan, Nature Nanotech **1**, 112-116 (2006).

[48] C. Deck and K. Vecchio, Carbon **44**, 267-275 (2006).

[49] D. Takagi, Y. Homma, H. Hibino, S. Suzuki, and Y. Kobayashi, Nano Lett. **6**, 2642-2645 (2006).

[50] W. Zhou, Z. Han, J. Wang, Y. Zhang, Z. Jin, X. Sun, Y. Zhang, C. Yan, and Y. Li, Nano Lett. **6**, 2987-2990 (2006).

[51] S. Sinharoy and L.L. Levenson, Thin Solid Films **53**, 31-36 (1978).

[52] S. Sinharoy, M.A. Smith, and L.L. Levenson, Surface Science **72**, 710-718 (1978).

[53] P.K. de Bokx, A.J.H.M. Kock, E. Boellaard, W. Klop, and J.W. Geus, Journal of Catalysis **96**, 454-467 (1985).

[54] F. Bonnet, F. Ropital, Y. Berthier, and P. Marcus, Materials and Corrosion **54**, 870-880 (2003).

[55] J. García-Céspedes, S. Thomasson, K.B.K. Teo, I.A. Kinloch, W.I. Milne, E. Pascual, and E. Bertran, Carbon **47**, 613-621 (2009).

[56] H. Wang, J. Feng, X. Hu, and K.M. Ng, The Journal of Physical Chemistry C **111**, 12617-12624 (2007).

[57] W. Liang, M. Bockrath, D. Bozovic, J.H. Hafner, M. Tinkham, and H. Park, Nature **411**, 665-669 (2001).

[58] S. Frank, P. Poncharal, Z.L. Wang, and W.A. de Heer, Science **280**, 1744 -1746 (1998).

[59] R.H. Baughman, Science **297**, 787-792 (2002).

[60] P. Simon and Y. Gogotsi, Nat Mater **7**, 845-854 (2008).

[61] K.H. An, W.S. Kim, Y.S. Park, Y.C. Choi, S.M. Lee, D.C. Chung, D.J. Bae, S.C. Lim, and Y.H. Lee, Advanced Materials **13**, 497-500 (2001).

[62] R.H. Baughman, C. Cui, A.A. Zakhidov, Z. Iqbal, J.N. Barisci, G.M. Spinks, G.G. Wallace, A. Mazzoldi, D. De Rossi, A.G. Rinzler, O. Jaschinski, S. Roth, and M. Kertesz, Science **284**, 1340-1344 (1999).

[63] A. Burke, Journal of Power Sources **91**, 37-50 (2000).

[64] M. Ohring, *Materials Science of Thin Films : Deposition and Structure*, 2nd ed. (Academic Press, San Diego CA, 2002).

[65] P.D. Davidse, Vacuum **17**, 139-145 (1967).

[66] C. Singh, M.S.P. Shaffer, and A.H. Windle, Carbon **41**, 359-368 (2003).

[67] B.C. Satishkumar, A. Govindaraj, and C.N.R. Rao, Chemical Physics Letters **307**, 158-162 (1999).

[68] H.M. Cheng, F. Li, G. Su, H.Y. Pan, L.L. He, X. Sun, and M.S. Dresselhaus, Appl. Phys. Lett. **72**, 3282 (1998).

[69] R. Sen, A. Govindaraj, and C.N.R. Rao, Chemical Physics Letters **267**, 276-280 (1997).

[70] H. Hou, A.K. Schaper, F. Weller, and A. Greiner, Chemistry of Materials **14**, 3990-3994 (2002).

[71] G. Eres, A.A. Puretzky, D.B. Geohegan, and H. Cui, Appl. Phys. Lett. **84**, 1759 (2004).

[72] D.B. Geohegan, A.A. Puretzky, I.N. Ivanov, S. Jesse, G. Eres, and J.Y. Howe, Appl. Phys. Lett. **83**, 1851 (2003).

[73] P.C. Eklund, J. Holden, and R. Jishi, Carbon **33**, 959-972 (1995).

[74] R.A. DiLeo, B.J. Landi, and R.P. Raffaelle, J. Appl. Phys. **101**, 064307 (2007).

[75] A.C. Ferrari, J.C. Meyer, V. Scardaci, C. Casiraghi, M. Lazzeri, F. Mauri, S. Piscanec, D. Jiang, K.S. Novoselov, S. Roth, and A.K. Geim, Phys. Rev. Lett. **97**, (2006).

[76] C. Du, J. Yeh, and N. Pan, Nanotechnology **16**, 350 (2005).

[77] J. Robertson, Materials Today **10**, 36-43 (January).

[78] N.M. Rodriguez, Journal of Materials Research **8**, 3233-3250 (1993).

[79] R.T.K. Baker, Carbon **27**, 315-323 (1989).

[80] H. Kanzow and A. Ding, Phys. Rev. B **60**, 11180-11186 (1999).

[81] Y.Y. Wei, G. Eres, V.I. Merkulov, and D.H. Lowndes, Appl. Phys. Lett. **78**, 1394 (2001).

[82] H.G. Tompkins and D.L. Allara, Journal of Colloid and Interface Science **49**, 410-421 (1974).

[83] N.S. McIntyre, D.G. Zetaruk, and D. Owen, Applications of Surface Science **2**, 55-73 (1978).

[84] R.A. DiLeo, B.J. Landi, and R.P. Raffaelle, J. Appl. Phys. **101**, 064307 (2007).

[85] J.B. Bult, W.G. Sawyer, P.M. Ajayan, and L.S. Schadler, Nanotechnology **20**, 085302 (2009).

[86] H.Y. Miao, J.T. Lue, S.Y. Chen, S.K. Chen, and M.S. Ouyang, Thin Solid Films **484**, 58-63 (2005).

[87] T. Nozaki, K. Ohnishi, K. Okazaki, and U. Kortshagen, Carbon **45**, 364-374 (2007).

[88] T. de los Arcos, F. Vonau, M.G. Garnier, V. Thommen, H.-G. Boyen, P. Oelhafen, M. Düggelin, D. Mathis, and R. Guggenheim, Appl. Phys. Lett. **80**, 2383 (2002).

[89] A.C. Wright, Y. Xiong, N. Maung, S.J. Eichhorn, and R.J. Young, Materials Science and Engineering: C **23**, 279–283 (2003).

[90] G. Atthipalli, R. Epur, P.N. Kumta, M. Yang, J.K. Lee, and J.L. Gray, J. Phys. Chem. C **115**, 56–58 (2011).

[91] G. Atthipalli, R. Epur, P.N. Kumta, B.L. Allen, Y. Tang, A. Star, and J.L. Gray, Thin Solid Films **519**, 5371-5375 (2011).

[92] H. Kanzow, C. Lenski, and A. Ding, Phys. Rev. B **63**, 125402 (2001).

[93] P.B. Amama, C.L. Pint, S.M. Kim, L. McJilton, K.G. Eyink, E.A. Stach, R.H. Hauge, and B. Maruyama, ACS Nano **4**, 895-904 (2010).

[94] T. de los Arcos, M.G. Garnier, J.W. Seo, P. Oelhafen, V. Thommen, and D. Mathys, J. Phys. Chem. B **108**, 7728-7734 (2004).

[95] C. Mattevi, C.T. Wirth, S. Hofmann, R. Blume, M. Cantoro, C. Ducati, C. Cepek, A. Knop-Gericke, S. Milne, C. Castellarin-Cudia, S. Dolafi, A. Goldoni, R. Schloegl, and J. Robertson, The Journal of Physical Chemistry C **112**, 12207-12213 (2008).

[96] W.R. Tyson and W.A. Miller, Surface Science **62**, 267-276 (1977).

[97] I.K. Song, W.J. Yu, Y.S. Cho, G.S. Choi, and D. Kim, Nanotechnology **15**, S590 (2004).

[98] N.K. Reddy, J.L. Meunier, and S. Coulombe, Materials Letters **60**, 3761–3765 (2006).

[99] G.D. Nessim, D. Acquaviva, M. Seita, K.P. O'Brien, and C.V. Thompson, Advanced Functional Materials **20**, 1306-1312 (2010).

[100] G. Atthipalli, R. Epur, P. Kumta, and J.L. Gray, J. Vac. Sci. Technol. B **29**, (2011).

[101] K.L. Chavez and D.W. Hess, J. Electrochem. Soc. **148**, G640 (2001).

[102] C. Pernel, J. Farkas, and D. Louis, J. Vac. Sci. Technol. B **24**, 2467 (2006).

[103] A.N. Andriotis, M. Menon, and G. Froudakis, Physical Review Letters **85**, 3193–3196 (2000).

[104] C.H. Kiang and W.A. Goddard III, Physical Review Letters **76**, 2515–2518 (1996).

[105] W.-Q. Deng, X. Xu, and W.A. Goddard, Nano Lett. **4**, 2331-2335 (2004).

[106] L. Vitos, A.V. Ruban, H.L. Skriver, and J. Kollar, Surface Science **411**, 186–202 (1998).

[107] P.E. Laibinis and G.M. Whitesides, Journal of the American Chemical Society **114**, 9022-9028 (1992).

[108] Y.T. Tao, Journal of the American Chemical Society **115**, 4350-4358 (1993).

[109] E.R. Meshot and A.J. Hart, Appl. Phys. Lett. **92**, 113107 (2008).

[110] D. Kim, A.L. Giermann, and C.V. Thompson, Applied Physics Letters **95**, 251903–251903 (2009).

[111] S. Hofmann, M. Cantoro, B. Kleinsorge, C. Casiraghi, A. Parvez, J. Robertson, and C. Ducati, J. Appl. Phys. **98**, 034308 (2005).

[112] S. Esconjauregui, M. Fouquet, B.C. Bayer, C. Ducati, R. Smajda, S. Hofmann, and J. Robertson, ACS Nano **4**, 7431-7436 (2010).

[113] G.D. Nessim, A.J. Hart, J.S. Kim, D. Acquaviva, J. Oh, C.D. Morgan, M. Seita, J.S. Leib, and C.V. Thompson, Nano Letters **8**, 3587-3593 (2008).

[114] I. Sushumna and E. Ruckenstein, Journal of Catalysis **94**, 239-288 (1985).

[115] M. Setton, J. Van der Spiegel, and B. Rothman, Appl. Phys. Lett. **57**, 357 (1990).

[116] J.U. Lee, Appl. Phys. Lett. **87**, 073101 (2005).

[117] M. Freitag, Y. Martin, J.A. Misewich, R. Martel, and P. Avouris, Nano Lett. **3**, 1067-1071 (2003).

[118] S. Barazzouk, S. Hotchandani, K. Vinodgopal, and P.V. Kamat, J. Phys. Chem. B **108**, 17015-17018 (2004).

[119] S. Lu and B. Panchapakesan, Nanotechnology **17**, 1843 (2006).

[120] P. Castrucci, F. Tombolini, M. Scarselli, E. Speiser, S. Del Gobbo, W. Richter, M. De Crescenzi, M. Diociaiuti, E. Gatto, and M. Venanzi, Appl. Phys. Lett. **89**, 253107 (2006).

[121] H.J. Li, W.G. Lu, J.J. Li, X.D. Bai, and C.Z. Gu, Phys. Rev. Lett **95**, 086601 (2005).

[122] G.M.A. Rahman, D.M. Guldi, E. Zambon, L. Pasquato, N. Tagmatarchis, and M. Prato, Small **1**, 527–530 (2005).

[123] C. Bittencourt, A. Felten, B. Douhard, J.F. Colomer, G. Van Tendeloo, W. Drube, J. Ghijsen, and J.J. Pireaux, Surface Science **601**, 2800–2804 (2007).

[124] C. Bittencourt, A. Felten, J. Ghijsen, J.J. Pireaux, W. Drube, R. Erni, and G. Van Tendeloo, Chemical Physics Letters **436**, 368–372 (2007).

[125] J.Y. Hwang, A.R.P. Singh, M. Chaudhari, J. Tiley, Y. Zhu, J. Du, and R. Banerjee, J. Phys. Chem. C **114**, 10424-10429 (2010).

[126] Z. Yong, Z. Zhu, Z. Wang, J. Hu, and Q. Pan, Nanotechnology **18**, 105602 (2007).

[127] M. Scarselli, P. Castrucci, L. Camilli, S.D. Gobbo, S. Casciardi, F. Tombolini, E. Gatto, M. Venanzi, and M.D. Crescenzi, Nanotechnology **22**, 035701 (2011).

[128] M. Scarselli, C. Scilletta, F. Tombolini, P. Castrucci, M. Diociaiuti, S. Casciardi, E. Gatto, M. Venanzi, and M. De Crescenzi, J. Phys. Chem. C **113**, 5860-5864 (2009).

[129] C. Pietro, C. Giuseppe, S. Alessandro, and G. Pietro Giuseppe, International Journal of Photoenergy **2010**, (2010).

[130] S. Uk Lee, W. Seok Choi, and B. Hong, Solar Energy Materials and Solar Cells **94**, 680–685 (2010).